



THE UNIVERSITY OF  
**WAIKATO**  
*Te Whare Wānanga o Waikato*

Research Commons

<http://researchcommons.waikato.ac.nz/>

## Research Commons at the University of Waikato

### Copyright Statement:

The digital copy of this thesis is protected by the Copyright Act 1994 (New Zealand).

The thesis may be consulted by you, provided you comply with the provisions of the Act and the following conditions of use:

- Any use you make of these documents or images must be for research or private study purposes only, and you may not make them available to any other person.
- Authors control the copyright of their thesis. You will recognise the author's right to be identified as the author of the thesis, and due acknowledgement will be made to the author where appropriate.
- You will obtain the author's permission before publishing any material from the thesis.

**Investigation of respiratory  
Surfactant A protein  
in middle ear epithelium**

A thesis  
submitted in fulfilment  
of the requirements for the degree  
of  
**Master of Philosophy in Biological Sciences**  
at  
**The University of Waikato**  
by  
**Anthony Andrew Cecire**



THE UNIVERSITY OF  
**WAIKATO**  
*Te Whare Wānanga o Waikato*

**2020**

# Abstract

---

**Introduction:** The middle ear of mammals is an air-chamber required for sound transmission. It is lined by an epithelium which is variable but which resembles that of the lungs. Lung function depends upon surfactant which is a family of surfactant proteins which have an important role in breathing as well as infection control. Given that both the middle ear and the lungs can suffer collapse as well as infection, it is worth exploring whether surfactant protein is expressed throughout the middle ear in any manner analogous to that in the lung.

**Materials and methods:** Our study has used simple histological stains to study cell and tissue morphology of the rodent middle ear. We used immunohistochemistry and protein electrophoresis to identify surfactant A protein as well as four cytokeratins expressed in lung cells.

**Results:** We have demonstrated that surfactant protein A is indeed expressed in the middle ear and that there are cells which have a protein cytokeratin expression consistent with surfactant production and other cells whose cytokeratin expression reflects a likely role in gas exchange. Our research has also confirmed the presence of surfactant in the bone marrow spaces adjacent to the middle ear as well as other tissues reflecting its diverse roles. This also suggests a role in local and innate immunity. A novel finding was the presence of communications between the marrow spaces and the mouse middle ear cavity.

**Conclusion:** These results suggest that there is a need for further work to assess the anatomical and topographical distribution of surfactant A protein throughout the variety of cell types within the middle ear. This will help to understand better the interaction of the various cell types in regard to the local and innate immunity of the middle ear as well as its gas exchange function.

# Acknowledgements

---

Undertaking an M Phil thesis in biological science has been a wonderful educational experience for someone from a medical background. I would like to thank the following persons associated with the Molecular Genetics Lab:

Dr Linda Peters, my chief supervisor, for her ready advice and availability, constant enthusiasm and patient explanation of everything from troubleshooting lab methods to painstaking histological processing to understanding scientific principles.

Dr Ray Cursons who encouraged me to undertake a higher degree and for technical advice and revision of thesis.

Dr Steve Bird for frequent advice, discussion and input along the path.

Dr Gregory Jacobson for much technical assistance and practical advice (the “go-to-guy” in the lab).

Dr Barry O’Brien who introduced me to the art of fluorescence microscopy.

Dr Sari Karppinen for technical assistance in the lab and photo-editing.

Dr Grant Smolenski from MS3 Solutions Ltd for technical assistance with the western blotting.

Olivia Patty for lab inductions, technical assistance, instructions on gel-making and on endless minor tasks in the lab.

Ric Broadhurst and Bobby Smith from Agresearch and Bruce Patty from University of Waikato for assistance with care of rodents.

Dr Judith Burrows for technical assistance and lab induction training.

Cheryl Ward for her librarian assistance.

# Table of Contents

---

Abstract .....	2
Acknowledgements .....	3
Table of Contents .....	4
List of Figures .....	7
List of Tables .....	16
List of Abbreviations .....	17
1 Chapter 1 .....	19
Literature Review .....	19
1.1 Introduction .....	19
1.2 Middle ear infection in New Zealand .....	20
1.3 The anatomy of the mammalian middle ear .....	21
1.4 The lung and respiratory tracts: glossary and terminology .....	22
1.5 Micro-anatomy of the lung .....	23
1.6 The lung and middle ear: similarities .....	25
1.7 Surfactant proteins: history, biochemical structure, functions and genetics .....	28
1.7.1 Surfactant protein biochemistry .....	29
1.7.2 Surfactant proteins: functional roles .....	32
1.7.3 Surfactant proteins: history and genetics .....	32
1.8 Surfactant protein within the middle ear .....	33
1.9 Surfactant protein A antibody: a tool to identify the type II alveolocyte .....	34
1.10 Cytokeratins: tools to distinguish type I and type II alveolocytes .....	35
1.11 Data from research using cytokeratins in human middle ear .....	36
1.12 Data from research using cytokeratins in rat middle ear .....	38
1.13 Data from research using cytokeratins in mouse middle ear .....	38
1.14 Strategy for using SP-A and cytokeratins together in the middle ear .....	39
1.15 Surfactant and type II alveolocytes .....	39
1.16 Beyond lung and middle ear: Surfactant protein A in body tissues .....	41
1.17 Aim and objectives of the thesis .....	41
2 Chapter 2 .....	42
Materials and Methods .....	42
2.1 Materials .....	42

2.2	Animal ethics.....	42
2.3	Histology .....	43
2.3.1	Fixation, decalcification and embedding of rodent temporal bones.....	46
2.3.2	Sectioning.....	46
2.3.3	Haematoxylin and eosin (H&E) staining.....	47
2.4	Immunohistochemistry.....	49
2.5	Western blotting.....	51
2.5.1	Preliminary Bradford assay of lung tissue.....	52
2.5.2	Coomassie blue staining of electrophoresed protein lysates on PAGE gel .....	52
2.5.3	Western blotting analysis.....	54
3	Chapter 3 .....	56
	Bioinformatics .....	56
4	Chapter 4 .....	67
	Results .....	67
4.1	Histology, IHC and western blotting.....	67
4.1.1	Histology of rat lung .....	67
4.1.2	Histology of mouse lung.....	68
4.1.3	Histology of mouse middle ear epithelium.....	70
4.1.4	An unexpected finding in mouse middle ear: communications with bone marrow .....	77
4.2	Immunohistochemistry.....	86
4.2.1	Rat lung antibody to SP-A .....	86
4.2.2	Rat lung antibody to CK18.....	89
4.2.3	Rat lung antibody to CK19.....	91
4.2.4	Rat lung antibody to CK7 and CK8.....	93
4.2.5	Rat middle ear: SP-A and cytokeratins.....	93
4.2.6	Mouse lung.....	94
4.2.7	SP-A in mouse lung.....	95
4.2.8	SP-A in mouse middle ear .....	98
4.2.9	SP-A in bone marrow nests above mouse middle ear .....	100
4.2.10	SP-A signal in the mouse Eustachian tube .....	102
4.2.11	Cytokeratins in mouse middle ear .....	106
4.3	Western blotting.....	107
4.3.1	Protein concentrations using the Bradford assay.....	107

4.3.2 Protein yield and quality using a Coomassie blue stained polyacrylamide gel .....	107
4.3.3 Western blot for lung .....	110
4.3.4 Signals for middle ear .....	115
5 Chapter 5 .....	116
Discussion.....	116
5.1 Introduction .....	116
5.2 Extrapolating data from lung to middle ear .....	117
5.2.1 H&E staining .....	117
5.2.2 H&E reveals communications from the middle ear cavity to the bone marrow.....	118
5.3 Immunohistochemistry.....	119
5.4 Antibody validation.....	121
5.5 Future directions.....	122
References.....	124
Appendices.....	133

# List of Figures

---

Figure 1.1. Anatomy of the mammalian auditory system. Source: Poster Cecire, Cursons, Barnett, Epithelial turnover in the Middle Ear, Frontiers in Otolaryngology Conference 2014, Garnett-Passe and Rodney Williams Foundation, Melbourne. ....	21
Figure 1.2. Anatomy of the human lung. Adapted from Wheater’s Functional Histology (Young, 2014). ....	22
Figure 1.3. Diagram showing variation in height of cells composing the simple epithelium of the respiratory tract (Source: Kotton, 2008). The dark blue cell is a type 2 alveolocyte and it is adjacent to the very large, flat, pale blue type I alveolocytes. The red cells are Clara cells which also secrete SP-A; green cells are basal cells; grey cells are neuro-endocrine cells; tall pale blue cells are typical ciliated cells. Some Clara cells at the bronchiolo-alveolar junction are thought to have regenerative potential (variant-Clara cells, yellow). These have been found to give rise to standard tall ciliated cells and secretory Clara cells.....	23
Figure 1.4. Section of lung alveoli showing type I alveolocyte (pale cells, purple nuclei) and type II alveolocytes (green cytoplasm). Note macrophages (blue cells with ruffled cell membranes. Adapted from <a href="http://www.antranik.org">www.antranik.org</a> , Articles and Tutorials, Science Index, Human Anatomy series, The Respiratory System © 2010.....	24
Figure 1.5. Schematic of middle ear with oblique line dividing 2 functional compartments of the middle ear into postero-superior gas exchange and antero-inferior ciliated and mucus-secreting cells. ....	27
Figure 1.6. Quaternary structure of SP-A and SP-D. Both are hydrophilic proteins with an N-terminal collagen-like domain and carbohydrate recognition domain (Sano and Kuroki, 2005).....	30
Figure 1.7. Diagram of outer and middle ear showing distribution of cytokeratins (based on Broekaert, 1988).....	37
Figure 2.1. Microscope slide showing two H&E stained sections derived from one paraffin-embedded block containing a decalcified mouse head. The processed paraffin block is shown underneath the slide. ....	44
Figure 2.2. Mouse thorax and ribs viewed from behind with lungs showing in front.....	45
Figure 2.3. Inflation of a rat lung <i>in vitro</i> using a 5ml syringe and 18G blunt needle.....	45

Figure 3.1. Comparative Genomics of Human Alternative Transcripts of *STFPA1*. Shown are the six reported human *STFPA1* transcripts in the sense direction on chromosome 10 (Table 3.1). The number and size of exons (blue rectangle) differs between the mRNA transcripts. The green peaks show high homology with the coding exons when compared against 30 mammals including mouse. In addition, high nucleotide identity between mouse and human *STFPA1* (bottom bar - black vertical lines) ..... 58

Figure 3.2. CLUSTAL Alignment of the Six Human SFTPA1 Protein Isoform Sequences. Listed on the left are the Protein GenBank Accession numbers (Table 3.1). \* = amino acid identity; : = conservative substitutions; . = semiconservative substitutions. .... 59

Figure 3.3. CLUSTAL Alignment of the Six Human SFTPA1 Protein Isoform Sequences and Mouse Sfta1. Listed on the left are the Protein GenBank Accession numbers. \* = amino acid identity; : = conservative substitutions; . = semiconservative substitutions. NP\_075623.2 = mouse. Human Isoform 1 = NP\_005402.3, NP\_001158116.1 and NP\_001158119.1. .... 60

Figure 3.4. CLUSTAL Alignment of Human SFTPA1 Protein Isoform 1 (generated from mRNA transcript 1) and Mouse Sfta1. Listed on the left are the Protein Genbank Accession numbers. \* = amino acid identity; : = conservative substitutions; . = semiconservative substitutions; blue line = ab115791 peptide sequence: WNDKGCLQYRLAICEF. Mouse = NP\_075623.2; Human Isoform 1 = NP\_005402.3, NP\_001158116.1 and NP\_001158119.1. .... 61

Figure 3.5. Summary of BLASTp alignment of Human SFTPA1 Protein Isoform (generated from mRNA transcript 6, Query) and Mouse Sfta1 (Sbject). .... 62

Figure 3.6. CLUSTAL Alignment of the Mouse and Rat Sftpa1 Protein Sequences. Listed on the left are the Protein GenBank Accession numbers (Table 3.1). \* = amino acid identity; : = conservative substitutions; . = semiconservative substitutions; blue line = ab115791 peptide sequence: WNDKGCLQYRLAICEF. Mouse = NP\_075623.2; Rat Isoform 1 = NP\_001257574, Rat Isoform 2 = NP\_059025.2 and Rat isoform 3 = NP\_001257576. .... 63

Figure 3.7. CLUSTAL Alignment of the Mouse Surfactant Protein Sequences. Listed on the left are the Protein GenBank Accession numbers. \* = identities; : = conservative substitutions; . = semiconservative substitutions; blue line = ab115791 peptide sequence: WNDKGCLQYRLAICEF. NP\_075623.2 = pulmonary surfactant-associated protein A precursor; AAB34846.2 = surfactant protein B; AAA40010.1 = pulmonary surfactant protein SP-C; AAA92021.1 = surfactant protein D. .... 64

Figure 3.8. CLUSTAL Alignment of the ab115791 Peptide Sequence Against Mouse Surfactant A and B Protein Sequences. Listed on the left are the Protein GenBank Accession numbers. * = amino acid identity; : = amino acid similarity; SP-A = NP_075623.2 = pulmonary surfactant-associated protein A precursor; SP-D = AAA92021.1 = surfactant protein D. ....	65
Figure 3.9. SmartBLAST of the ab115791 Peptide Sequence. ....	66
Figure 4.1. Initial results for H&E of rat lung. Shown are expanded alveoli (a), adjacent blood vessels (b) and engorged capillaries (ca). ....	68
Figure 4.2. H&E stained sections showing distribution of Clara cells with their strong pink cytoplasm and their histological features. Fig 4.2A shows alveolar ducts leading to alveoli. Fig 4.1 A is X20, Fig 4.2 B, and Fig 4.2D are X40 and Fig 4.2C is X100 magnification. ....	69
Figure 4.3. Oil immersion image X100 showing alveoli containing very thin, flat type I cells (1), cuboidal type II cells and large foamy macrophages (m). Capillaries are evident by their enucleate red blood cells.....	70
Figure 4.4. Coronal cross-sections of nasopharynx and Eustachian tubes in BALBc mice using H&E staining. A. Panoramic view of nasopharynx (n) and a complete Eustachian tube orifice on the right side (r). The right tube extends into the middle ear cavity (tympanum) via a narrowing (cartilaginous isthmus). Both Eustachian tubes show adjacent mucous glands. Magnification X2.5. B. Closer view showing pharyngeal openings of Eustachian tube with mucus and some cellular debris in the nasopharynx. Magnification X5. C. View of the roof of the nasopharynx showing epithelium which is pseudostratified, simple, columnar. Supporting connective tissue contains lymphoid tissue and mucous gland elements. D. Opening of pharyngeal end of right Eustachian tube with some mucus and cellular debris.....	71
Figure 4.5. Coronal cross-sections of BALBc mice upper Eustachian tube adjacent to middle ear using H&E staining. Image A and B are X10 magnification; image C is X20, D is X40. A. Junction of right Eustachian tube with middle ear cavity (cartilaginous isthmus) showing simple epithelium with slight stratification sometimes referred to as transitional epithelium. B. Middle ear (tympanic) opening of right Eustachian tube showing change from transitional stratified epithelium to simple ciliated, low cuboidal epithelium. C. Lateral right Eustachian tube lumen showing mainly pseudostratified, low columnar, ciliated epithelium. D. Tympanic opening of Eustachian tube: Cartilaginous isthmus of lateral right Eustachian tube lumen showing mainly low cuboidal ciliated epithelium with Goblet cells.....	72

- Figure 4.6. Coronal cross-sections of BALBc mice middle ear at the superomedial level using H&E staining. Images A, B and C are X10 and D is X 40 magnification. A. Roof of right middle ear cavity showing the transition from cuboidal, ciliated epithelium on cartilage (c) to flatter epithelium over the tensor tympani muscle (m). B. Roof of right middle ear cavity showing flatter epithelium overlying tensor tympani muscle. C. Roof of right middle ear cavity showing flatter epithelium overlying tensor tympani muscle undergoing transition to ciliated cuboidal epithelium (c). D. Closer view of roof of right middle ear cavity showing flatter epithelium overlying tensor tympani muscle undergoing transition with cuboidal epithelium some of which is ciliated..... 73
- Figure 4.7. Coronal cross-sections of BALBc mice middle ear using H&E staining. A. Roof of right middle ear cavity showing flatter epithelium with areas of cuboidal, ciliated epithelium. B. Closer view of roof of right middle ear cavity showing mostly cuboidal ciliated epithelium..... 74
- Figure 4.8. Coronal cross-sections of BALBc mouse middle ear. A. Panoramic view of middle ear ossicles: malleus (m); incus (i); stapes(s); also seen is stapedial artery (sa); facial nerve (fn); bone marrow (bm) and tympanic membrane in two layers (tm). B. Closer view of stapes bone with its incomplete arch and stapedial artery (sa). C. Junction of stapes footplate (s) and oval window of cochlea (c) with intervening stapedial ligament (arrow). Note very thin flattened epithelium lining bony structures. D. Closer view of roof of right tympanic membrane showing a bilayered structure of modified outer squamous epithelium (oe) separated from flat middle ear epithelium (me). .... 75
- Figure 4.9. Coronal cross-sections of BALBc mice floor of middle ear using H&E staining. A. View of inferior tympanic membrane (tm) attached to connective tissue annulus (a) adjacent to the floor of the middle ear (me); the bilayered structure of the tm is still evident by the two layers of nuclei. B. Closer view of thin flattened epithelium lining bony floor of middle ear still within the postero-superior zone of the middle ear. C. Transition (arrow) from thin flattened epithelium lining bony floor of middle ear to the ciliated cuboidal epithelium. D. Closer view of ciliated epithelium of the middle ear (me) as it ascends to reach the mouth of the tympanic end of the Eustachian tube (et) which is supported by a cartilaginous framework. .... 76
- Figure 4.10. Axial cross-section of C57/B6 (17.2.17) mouse middle ear magnification X2.5. Note malleus bone (m), the incus (i), facial nerve (f), stapedius muscle (s), cochlea (c) and bone marrow nests (\*). There are no communicating passages in this image. .... 77

Figure 4.11. Axial cross-section of BALBc mouse middle ear (magnification X2.5). Note malleus bone (m), the cochlea (c) anterior to the middle ear space and a bone marrow nest. Communicating passage shown by arrow. ....	78
Figure 4.12. Axial cross-section of BALBc mouse middle ear magnification X10. Note malleus bone (m), the cochlea (c) anterior to the middle ear space and a bone marrow nest (bm). Communicating passage with smooth margins shown by arrow. ....	79
Figure 4.13. Axial cross-section of second BALBc mouse middle ear (me) magnification X10. Note malleus bone (m) medial to external auditory meatus (eam), the cochlea (c) and an adjacent semi-circular canal (scc) opposite a bone marrow nest (bm). Communicating passage shown by arrow. ....	80
Figure 4.14. Axial cross-section of second BALBc mouse middle ear (me) at magnification X40. Note red blood cells (rbc) within a capillary within the bone communication. Flat endothelial cells line the capillary. ....	81
Figure 4.15. Axial cross-section of C57/B6 mouse bone communication (arrow) magnification X2.5. There are cells filling the communication between middle ear space (me) and the bone marrow nest. ....	82
Figure 4.16. Axial cross-section of C57/B6 mouse bone communication (box). By comparison a breach in bone (thin arrow) with no intervening cells represents a sectioning artefact. There are cells filling the communication between middle ear space (me) and the bone marrow nest (bm). Note free cellular debris (cd). Magnification X2.5. ....	83
Figure 4.17. Higher magnification of Figure 4.16 showing a capillary (c) with red blood cells (rbc). There are cells filling the communication between middle ear space (me) and the bone marrow nest (bm). Magnification X40. ....	83
Figure 4.18. Axial cross-section of C57/B6 mouse bone communication. A. There are cells filling the communication (box) between middle ear space (me) and the bone marrow (bm) nest. Note location adjacent to cochlea (c). Magnification X2.5. B. At X40 magnification, there are cells filling the communication between me and bm. Note ciliated middle ear epithelium (arrows). ....	84
Figure 4.19. Axial cross-section of C57/B6 mouse communication at magnification X40. Closer view shows presence of a double layer of cells (yellow arrows) lining the wall of the communication between middle ear space and the bone marrow nest (bm). There is also a capillary present close to the	

communication containing red blood cells (rbc). Amongst cellular debris in the middle ear are some large cells with eccentric nuclei (blue arrow) which probably represent macrophages analogous to the “free” pulmonary macrophages seen in lung spaces..... 85

Figure 4.20. IHC of Rat lung with SP-A 1:500 signal visible at 10X magnification. A. Shows apple-green 1:500 A SP-A signal above background. B is nuclear DAPI stain. C. Composite image shows discoloration of primary antibody signal. D. Control image from non-contiguous section of same paraffin block showing no fluorescence signal. Scale bar = 200  $\mu$ M..... 87

Figure 4.21. IHC of Rat lung with SP-A 1:500. A. signal clearly visible at 20X magnification (arrow) located at corner or margin of lung alveolus. B is nuclear DAPI stain. C. Composite merged image still shows significant discoloration of primary antibody signal (arrow). D is control image from non-contiguous section of same paraffin block showing background signal only. Scale bar = 100  $\mu$ M. .... 88

Figure 4.22. Rat lung with CK18 antibody at 10X magnification. This shows signal in primary (A) and, to lesser extent, in the composite images (C). A. the signal is much more continuous in the larger airways (asterisk) where it corresponds to Clara cells than in the alveolar walls (arrows) where it corresponds to type II alveolocytes. B. DAPI nuclear stain. D. control from a non-contiguous slide omitting primary antibody. Scale bar = 200  $\mu$ M. .... 89

Figure 4.23. IHC of Rat lung alveoli with CK18 antibody at X40 magnification. This shows signal in primary (A) and composite merged images (C). B. DAPI nuclear stain. D. control omitting primary antibody. Scale bar = 50  $\mu$ M..... 90

Figure 4.24. IHC Rat lung with CK19 antibody (1:500). A. positive signal in CK19 primary with magnification 10X revealing signal in continuity along alveolar walls. C. a composite image in which the signal is less evident and requires further magnification. D. negative control from a non-contiguous section from the same paraffin block. Scale bar = 200  $\mu$ M. .... 91

Figure 4.25. IHC of rat lung with CK19 antibody (1:500) showing signal in primary (A) and (C) composite images. B. DAPI nuclear stain. The associated nuclei are relatively flat compared to nuclei of type II cells. Magnification 20X. D. negative control from a non-contiguous section from the same paraffin block. Scale bar = 100  $\mu$ M..... 92

- Figure 4.26. H&E stain of a Mouse lung A. Shown is relatively collapsed alveolar sacs. Magnification 10X; Scale bar = 200  $\mu$ m. B. Adjacent H&E image at 40X shows well expanded alveoli with various cell types as seen in Figure 4.3. Scale bar = 20  $\mu$ m. .... 94
- Figure 4.27. IHC Mouse lung with labelled SP-A with secondary at 1:2000. A. SPA antibody (1:500) B. DAPI stain. C. Merged composite. D. Control image from non-contiguous section omitting primary antibody and using secondary at 1:4000. Magnification 10X; scale bar = 200  $\mu$ m. .... 95
- Figure 4.28. IHC of Mouse lung. A. SP-A primary Ab (1:500) and secondary Ab applied at 1:4000. B. DAPI nuclear stain. C. Merged. D. shows a non-contiguous control section with omitted primary antibody. Magnification X20. Scale bar = 100  $\mu$ m. .... 96
- Figure 4.29. IHC of Mouse lung with SP-A. A. positive signal for SP-A at 1:500 with mainly extracellular distribution. B. DAPI stain. C Merged composite. No control section was available. Magnification 100X, scale bar omitted. .... 97
- Figure 4.30. IHC of Mouse Ear. (A) This figure shows the epithelium of the superomedial middle ear with SP-A antibody (1:50) at the highest concentration visible at 20X magnification. (C) Control images with primary antibody omitted showing no signal in primary or (D) composite image (20X magnification). Scale bar = 100  $\mu$ m. .... 98
- Figure 4.31. IHC of Mouse Ear. This figure shows epithelium of the inferomedial middle ear where there are some ciliated, low cuboidal cells with SP-A antibody (A) at the lower concentration 1:500 visible at 100X magnification with (B) DAPI stain, (C) composite image and (D) adjacent H&E section. The H&E shows that, in the middle ear, even flat cells may be ciliated. Some of the SP-A signal is accumulated on the cell surface (large arrow) and a tiny amount is seen in a perinuclear, intracellular location (small arrow). No control image available. Scale bar = 20  $\mu$ m. .... 99
- Figure 4.32. IHC of Mouse Ear. This figure shows ciliated, low cuboidal epithelium of the medial wall of middle ear with SP-A antibody (A) at the lower concentration 1:500. The SP-A signal is visible at 100X magnification with (B) DAPI stain in the composite image (C) although the signal is mainly situated in the ciliary layer of epithelium rather than intracellular. D. Adjacent H&E section shows typical ciliated, low cuboidal epithelium of middle ear adjacent to Eustachian tube. Scale bar = 20  $\mu$ m. .... 100
- Figure 4.33. IHC of Mouse Ear. Figure A shows bone marrow cells labelled with SP-A in a bone marrow nest above the roof of the middle ear. It shows apple-green SP-A signal above background, B. is a

DAPI stain and C. is a merged image which results in significant discoloration of primary antibody signal. The merging program gives an enhanced intensity to background fluorescence. D. shows control bone marrow cells without primary antibody giving diffuse background signal in cell cytoplasm. Scale bar = 100µm. .... 101

Figure 4.34. IHC of Mouse Ear. This figure shows bone marrow cells labelled with SP-A in a bone marrow collection above the roof of the middle ear. A. apple-green signal above background, B. DAPI stain and C. is a merged image which results in significant discoloration of primary antibody signal. D. control bone marrow from non-contiguous section of same specimen showing no signal. Scale bar = 100 µM. .... 102

Figure 4.35. Panoramic view of middle ear space and adjacent Eustachian tube cartilage (et), bone marrow niche (bm) and middle ear space (me). Magnification 2.5X. Scale bar =2 mm. .... 103

Figure 4.36. IHC of mouse coronal section of left Eustachian tube (nasopharyngeal end) adjacent to its supporting cartilage. A. Primary SP-A at 1:50 showing signal in apical areas of epithelium as well as some chondrocytes of the Eustachian tube. B. DAPI stain. C. Merged. D. Control image. Magnification 40X. Scale bar = 100 µM. E. H&E of similar segment of Eustachian tube at 20X showing surrounding cartilage. F. H&E showing variation in epithelium from tall ciliated to flat squamous. Magnification 40X, scale bar omitted. .... 104

Figure 4.37. IHC of Rat Coronal section of left Eustachian tube (tympanic end) adjacent to its supporting cartilage. A. Primary SP-A at 1:500 showing speckled signal in free cellular debris within middle ear space. There is also some intracellular perinuclear speckling within ciliated epithelium (arrow). B. DAPI stain. C. Merged. D. control image - omitting primary antibody. Magnification 40X. Scale bar = 100 µM. .... 105

Figure 4.38. Coomassie blue stained 12% polyacrylamide gel of mouse lung protein lysates. Lane 1: PAGE ladder (P). Lanes 2-7: Four partial mouse lungs from animal 1, animal 2, animal 3 (3, 3A), and animal 4 (4, 4A). Lane 8: BSA (1 mg/mL). Lanes 9-14: replicate loading samples as reported in Lanes 2-7. .... 108

Figure 4.39. Coomassie blue stained 12% polyacrylamide gel of gradient mouse lung protein lysates (a-f) from animals 1 and 3A. Lane 1: PAGE ladder. Lanes 2-7: increasing concentration of mouse lung lysate from animal 3A (a-f). Lanes 8-14: increasing concentration of mouse lung lysate from animal 1. Lanes 7 and 14 represent the maximum protein concentration (f) available to add to the 4X Laemmli dye. .... 109

Figure 4.40. Coomassie blue stained 16% polyacrylamide gel of mouse protein lysates from six mouse organs. Lane 1: PAGE ladder (P). Lane 2: brain 1, Lane 3: brain 2, Lane 4: kidney, Lane 5: liver, Lane 6: lung (1f and 4f), Lane 7: spleen, Lane 8: paired middle ears 1, 2, 3, 4. ....	110
Figure 4.41. Western blot of 12% polyacrylamide gel of gradient mouse lung protein lysates from Animals 1 and 4 using SP-A antibody at 1:500 concentration. Lane 1: PAGE ladder. Lanes 2-7: increasing concentration of mouse lung lysate from animal 1. Lane 8: Western Ladder. Lanes 9-14: increasing concentration of mouse lung lysate from animal 4. Faint bands are visible at increased concentrations better seen in animal 1 (arrow). SP-A antibody = 1:500. ....	111
Figure 4.42. Western blot of 12% polyacrylamide gel of gradient mouse lung protein lysates from animals 1 and 4 using three antibodies. Lane 1: PAGE ladder. Lanes 2-7: increasing concentration of mouse lung lysate from animal 2 (BALBc). GAPDH at 36 kDa; CK19 at 44 kDa; surfactant A (SP-A) at 35 kDa and CK18 at 47 kDa. ....	112
Figure 4.43. Coomassie blue stained 12% gel showing retention of mouse protein from middle ear (Lanes 2, 12), lung (Lanes 6, 7, 14, 15) and kidney (Lanes 7, 8, 16, 17). L = Ladder. ....	113
Figure 4.44. PVDF membrane showing SP-A signal in mouse kidney and corresponding faint bands in mouse middle ear and lung. SP-A 1:1000; Middle ear (Lane 2), lung (Lane 6, 7) and kidney (Lanes 7, 8). SP-A 1:5000; Middle ear (Lane 12), lung (Lanes 14, 15) and kidney (Lanes 16, 17).....	114
Figure 4.45. Western blot showing bands at approximately 35 kDa consistent with SP-A protein. Lung 1 is a fresh lung sample, Lung 2 is stored sample. Kidney is negative possibly due to deterioration in storage. Middle ear 1 is 5 $\mu$ L load and Middle ear 2 is 20 $\mu$ L. SP-A = 1:1000. ....	115

## List of Tables

---

Table 1.1. Comparison of mouse lung and human lung (Kotton, 2008).....	25
Table 1.2. Summary of amino acid sequence of SP-A peptide showing sequence carbohydrate recognition domain which complements the antibody (data from Abcam ab115791). ....	31
Table 1.3. Cytokeratins expressed in human outer ear canal, tympanic membrane (lateral and medial surfaces) and middle ear cavity (data from Broekaert, 1988). ....	36
Table 1.4. Cytokeratin Profile in Type 1 and Type II cells. ....	38
Table 1.5. Cytokeratin and SP-A Profile in Type I and Type II cells.....	39
Table 2.1. Summary of the advantages and disadvantages using two different rodent models for histological purposes. ....	43
Table 2.2. Dehydration, clearing and infiltration of tissue. ....	47
Table 2.3. List of antibodies used. WB = western blot, IHC = immunohistochemistry, ab = Abcam, GTX = GeneTex.....	50
Table 3.1. Comparison of the Mammalian Surfactant A1 at the Molecular Level. Source: gene cards and NCBI. GenBank accession numbers are provided for the mRNA and protein sequences.....	57
Table 3.2. Official name of the protein isoforms generated by alternative mRNA splicing of <i>SFTPA1</i> . The six <i>SFTPA1</i> mRNA transcripts results in four different isoforms of the surfactant A1 protein. ....	57

## List of Abbreviations

---

AA	Amino acids
AOM	Acute Otitis Media
bm	Bone marrow
Bp	Base pairs
BSA	Bovine serum albumen
°C	Degrees Celsius
c	Cochlea
ca	Capillaries
cd	Cellular debris
ci	Ciliated cuboidal epithelium
CRD	Carbohydrate recognition domains
CK	Cytokeratin
dd	Double deionised H <sub>2</sub> O
DAPI	4',6-diamidino-2-phenylindole
DPPC	Dipalmitoylphosphatidylcholine
eam	External auditory meatus
EDTA	Ethylenediaminetetraacetic acid
ETOH	Ethanol
ET	Eustachian tube
FITC	Fluorescein Isothiocyanate
fn	Facial nerve
g	Relative Centrifugal Force
GAPDH	Glyceraldehyde 3-phosphate dehydrogenase
H&E	Haematoxylin and eosin
IHC	Immunohistochemistry
i	Incus
kb	Kilobase(s)
kDa	Kilodalton
LPS	Lipopolysaccharide
OM	Otitis media
m	Malleus
M	Molar
mA	milli-Ampere

MES buffer	2-(N-morpholino) ethanesulfonic acid
min	Minutes
MOPS buffer	3-(N-morpholino) propanesulfonic acid
mQH2O	Double distilled deionised water
me	Middle ear epithelium
NCBI	National Centre for Biotechnology Information
NZ	New Zealand
oe	Outer squamous epithelium
PAGE	Polyacrylamide Gel Electrophoresis
PBS	Phosphate Buffered Saline
PVDF	Polyvinylidene Difluoride
rbc	Red blood cells
rpm	Revolutions per minute
RT	Room temperature
s	Stapes
sa	Stapedial artery
SD	Sprague-Dawley
SDS	Sodium Dodecyl Sulphate
Sec	Seconds
SP-A	Surfactant A protein
TBS	Tris Buffered Saline
TBST	Tris Buffered Saline with Tween 20
Tm	Tympanic membrane
Tris	Tris (hydroxymethyl) amino-methane
Tween 20	Polyoxyethylene (20) Sorbitan Monolaurate
µg	Microgram
µL	Microlitre
WB	Western blot

# 1 Chapter 1

## Literature Review

---

### 1.1 Introduction

The mammalian middle ear is an air-containing chamber which is a frequent site of infectious disease in children and adults. Both the middle ear and the lungs are air-containing systems which are subject to infection and to collapse. Infection and collapse can occur in the lung as it is a network of pliable air chambers. Collapse in the middle ear is limited to its outer wall - the eardrum - which can collapse when pressure drops within the middle ear.

Some important proteins found in the lung which help prevent lung collapse are the family of surfactant proteins. They are called SP-A, SP-B, SP-C and SP-D. In the lung, the cells which line the lung's air sacs (alveoli) are called alveolocytes. Some of these cells make surfactant proteins and are called type II alveolocytes. Most of the cells lining lung alveoli are air-exchanging cells called type I alveolocytes. Surfactant proteins also coat bacteria by opsonisation allowing phagocytosis by macrophages. These proteins are also important for the innate immunity of the lung (Sano, 2005). Surfactant proteins are also present in the middle ear, although it is not known exactly which cells in the middle ear make them.

My hypothesis is that the lining of the middle ear should possess cells similar to the alveolocytes of the lung including those which make surfactant proteins as well as those which exchange air. The aim of this study was to determine the distribution and expression of the most abundant surfactant protein (SP-A) within middle ear cells. This can give an insight as to whether SP-A in the middle ear has a role similar to that in the lung i.e., preventing infection and preventing collapse. The distribution of cells producing SP-A may also help to understand how these cells can be damaged during middle ear infection and how this influences treatment and recovery.

The next section will introduce the importance of middle ear infection with a particular focus on the New Zealand population, followed by the anatomy of the mammalian ear and lung, general data about surfactant proteins as the functional proteins of respiratory epithelium and their usefulness in distinguishing respiratory cells as well as the need for other markers such as cytokeratins (CKs).

## **1.2 Middle ear infection in New Zealand**

Otitis media (OM) is one of the most common childhood diseases and is responsible for the majority of doctor's visits, antibiotic treatment, and related procedures for children in developed countries (Mills et al., 2014). Evidence of serous or mucoid fluid in the middle ear, without acute symptoms, is characteristic of otitis media with effusion (New Zealand District Health Board 2004; Barnett, 2007). The incidence of acute otitis media in New Zealand children under five years of age in the primary care setting ( $n=19,146$ ) was estimated to be 27% (Gribben et al., 2012). Of interest, fluid from human middle ear infections has been aspirated from 20 ears in 18 children between ages 4-8 years old (Grace, 1987). Phospho-lipids, the major components of pulmonary surfactant, were identified in appreciable quantities using two-dimensional thin-layer chromatography.

Studies on middle ear infection often focus on the bacteria and viruses responsible. One consequence of middle ear infection is persistence of a sticky fluid within the middle ear, a condition termed otitis media with effusion, commonly called "glue ear". The fluid from glue ear can be apparently sterile using routine culture methods although molecular techniques such as PCR or DNA sequencing yield a great diversity of bacteria. The stickiness of the fluid is due to the interaction of biofilms with the middle ear epithelium through various stages of inflammation as well as neutrophil extracellular traps (Thornton, 2013).

Like all epithelia, lung alveolocytes have features to resist infection. Type II alveolocytes have an important role in replacing the epithelium which adds to the cellular debris which accumulates during and after lung infection. It is important to identify whether there are cells like alveolocytes, both type I and type II cells within the middle ear.

### 1.3 The anatomy of the mammalian middle ear

Figure 1.1 shows the anatomy of mammalian ear which consists of three auditory systems: outer, middle and inner ear. The outer ear includes the ear canal which leads to the eardrum (tympanic membrane).

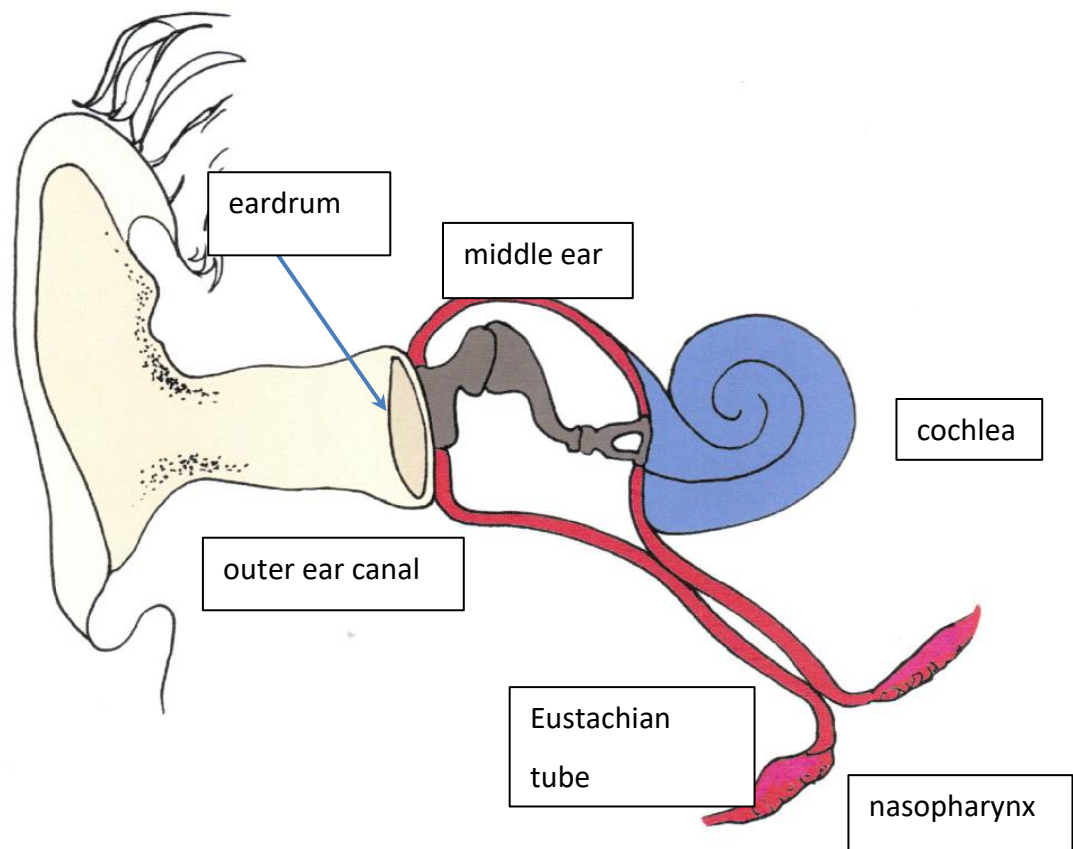


**Figure 1.1. Anatomy of the mammalian auditory system. Source: Poster Cecire, Cursons, Barnett, Epithelial turnover in the Middle Ear, Frontiers in Otolaryngology Conference 2014, Garnett-Passe and Rodney Williams Foundation, Melbourne.**

Beyond the eardrum is a complex air chamber called the middle ear which receives air from the back of the nose (nasopharynx) via the Eustachian tube passage. Strictly speaking, the middle ear comprises Eustachian tube, middle ear space (tympanic cavity) and the mastoid air cell system in humans and larger mammals. The inner ear is the hearing organ and includes the cochlea and balance channels.

#### 1.4 The lung and respiratory tracts: glossary and terminology

The respiratory system of mammals is comprised of two anatomical parts: the upper, conducting zone that transports the air to the lungs and the lower, respiratory zone responsible for gas exchange. Figure 1.2 highlights the main features of the respiratory tract.

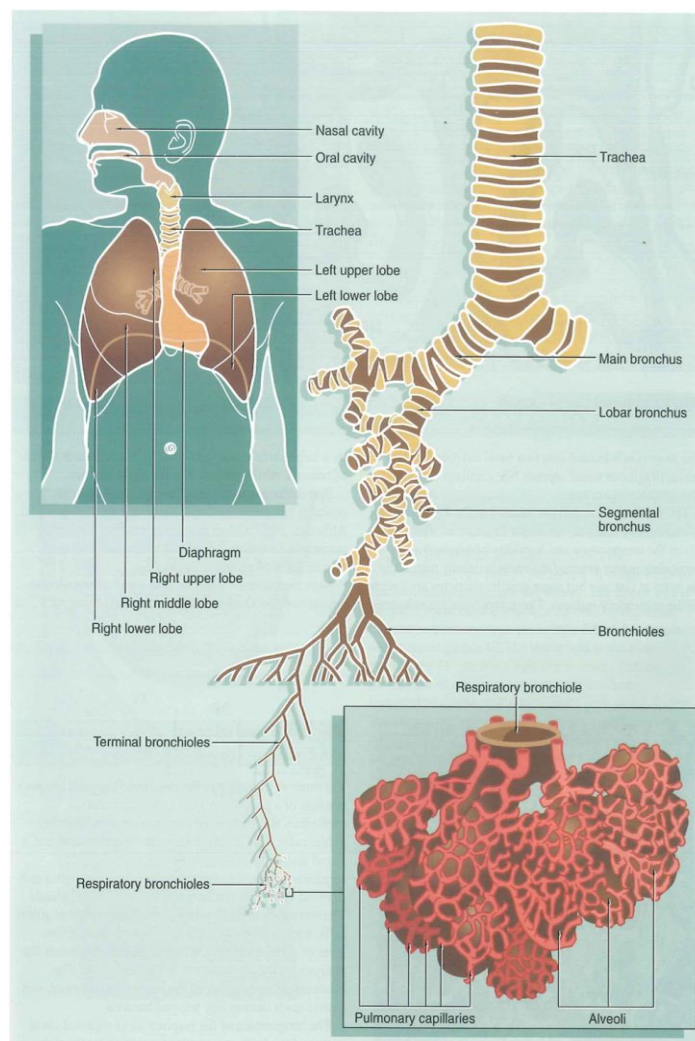
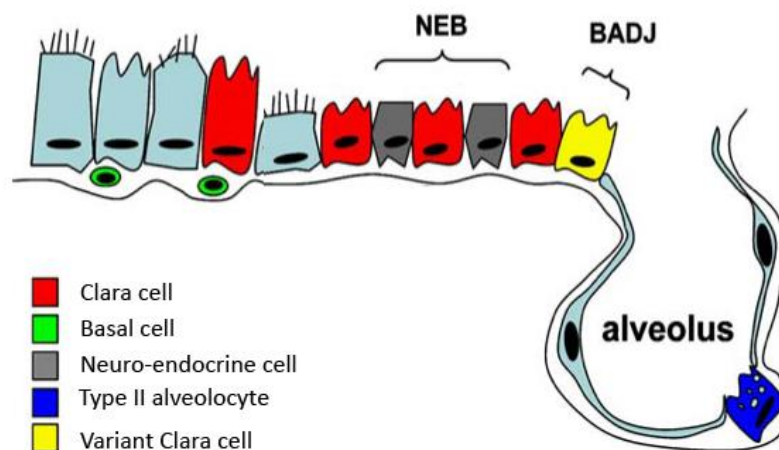


Figure 1.2. Anatomy of the human lung. Adapted from Wheater's Functional Histology (Young, 2014).

Briefly, the upper tract includes the large airways including the nasal cavities, the larynx (voice-box) and trachea (windpipe). The upper respiratory tract merges with the lower tract just beyond the major branches of the trachea (bronchi). The lower tract consists of the distal conducting airways which include the branches of the bronchi (bronchioles), broncho-alveolar duct junctions and alveoli. In some texts, the term “upper airway” includes the paranasal sinuses, Eustachian tube and middle ear simply because they contain air and are located anatomically above the larynx and trachea.

## 1.5 Micro-anatomy of the lung

The epithelium of the respiratory tract in the lung changes from proximal to distal i.e., from the upper airway trachea and bronchi to the peripheral alveoli. This transition is similar in human and rodent. Despite the variations in the height of cells lining the airway, the epithelium of the respiratory tract remains a simple epithelium all the way from the tallest cells of the upper trachea to the flattest, thinnest cells of the peripheral alveoli. Figure 1.3 illustrates some airway cells.



**Figure 1.3. Diagram showing variation in height of cells composing the simple epithelium of the respiratory tract (Source: Kotton, 2008). The dark blue cell is a type 2 alveolocyte and it is adjacent to the very large, flat, pale blue type I alveolocytes. The red cells are Clara cells which also secrete SP-A; green cells are basal cells; grey cells are neuro-endocrine cells; tall pale blue cells are typical ciliated cells. Some Clara cells at the bronchiolo-alveolar junction are thought to have regenerative potential (variant-Clara cells, yellow). These have been found to give rise to standard tall ciliated cells and secretory Clara cells.**

Amongst the cells lining the airways, the tallest ciliated cells are termed *pseudostratified*. These appear stratified because their nuclei are at different levels and, on histological cross-sections, they appear stratified.

Within the alveoli, the majority of cells (type I alveolocytes) are flat cells which exchange the gases O<sub>2</sub> and CO<sub>2</sub>. The cuboidal cells which make surfactant protein are a minority (type II alveolocytes). Hence, within alveoli, Type II alveolocytes are surrounded by Type I alveolocytes (see Figure 1.4). Type II alveolocytes are well established as precursors to type I alveolocytes from studies on lung injury (McElroy, 2004).

These two types of alveolocytes can be distinguished even on H&E staining partly because alveoli are polygonal spaces lined mainly by flat type I cells. The type II alveolocytes are cuboidal cells which tend to be found in the corners of the polygonal alveoli, "*aggregated...where the walls of several adjacent alveoli meet*" (Marin, 1991). Outside of this polygonal space, type II cells would be more difficult to distinguish from type one cells by H&E staining alone.

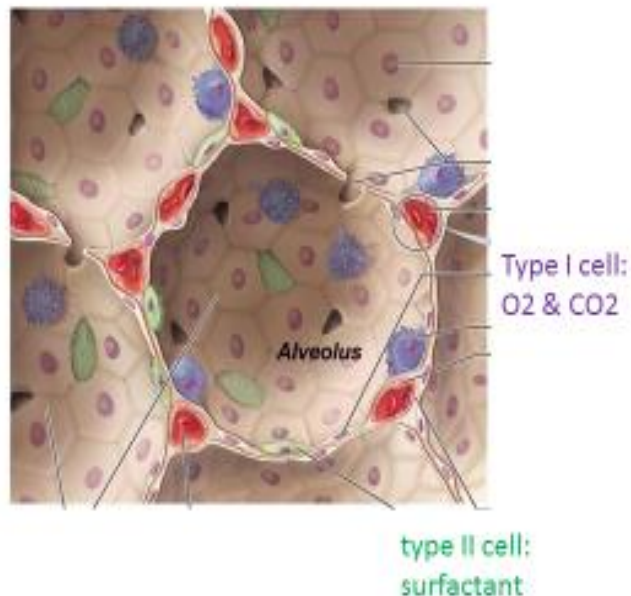


**Figure 1.4.** Section of lung alveoli showing type I alveolocyte (pale cells, purple nuclei) and type II alveolocytes (green cytoplasm). Note macrophages (blue cells with ruffled cell membranes). Adapted from [www.antranik.org](http://www.antranik.org), Articles and Tutorials, Science Index, Human Anatomy series, The Respiratory System © 2010.

## 1.6 The lung and middle ear: similarities

The lung and the middle ear share similarities especially at the cellular and histological level. The windpipe (trachea) carries air from the nose to the lungs. In the same way the Eustachian tube feeds air from the nose to the middle ear. If one examines the chambers of the middle ear, one finds that the entire system is lined by different types of simple epithelium similar to the variety of cells from trachea to the peripheral lung sacs (alveoli). Similarly the Eustachian tube can be likened to a terminal bronchiole and the middle ear cavity resembles a large alveolus. The epithelium of the Eustachian tube is largely similar to the spectrum of taller and ciliated cells seen in the upper airway; the epithelium of the middle ear is largely similar to the lower airway (flatter and less ciliated).

The middle ear also needs to maintain gas exchange for its air spaces. Hence, it is also important to determine whether there are cells analogous to the gas exchanging lung cells (type I alveolocytes) in the middle ear. This would complement the identification of SP-A producing cells (type II alveolocytes). Table 1.1 summarises the cell types found in the lung of mouse (*Mus musculus*) and human (*Homo sapiens*). This indicates that mouse can be used for comparative study of upper and lower airway cells.

**Table 1.1. Comparison of mouse lung and human lung (Kotton, 2008).**

	Human	Mouse
Trachea	Pseudostratified ciliated; non-ciliated secretory cells (Clara), basal cells, and submucosal glandular epithelium	Pseudostratified ciliated; non-ciliated secretory cells (Clara)
Distal conducting airways	Ciliated and secretory Clara cells.	Ciliated and secretory Clara cells.
Broncho-alveolar duct junction	Bronchiolo-alveolar Clara cells (progenitor stem cells; Chang, 2008)	Broncho-alveolar stem cells confirmed in mouse (Reynolds, 2000)
Alveoli	Alveolocytes type I, II	Alveolocytes type I, II

Although the gross structure of mouse lung is very similar to human, the relative size of peripheral, distal airway lumens is larger. This larger airway calibre is proposed to decrease the airway resistance that would otherwise occur in mice due to their rapid respiration rates of 250-350 breaths per minute. As a consequence, mice lack terminal respiratory bronchioles and the larger airways open directly into clusters of alveolar sacs.

The human middle ear has been divided histologically and functionally into an anterior-inferior compartment and a posterior-superior compartment (Figure 1.5). The epithelium of the antero-inferior compartment which leads to the Eustachian tube has been found to possess ciliated and secretory epithelium whereas the postero-superior has thin, flat epithelium considered important for gas exchange (Ars, 1997). This is generally true although some earlier work on rodent middle ear reveal some tracts of ciliated respiratory epithelium in the superior compartment (Albiin, 1986). This has been confirmed in a more recent study where ciliated cells have been noted in the dorsal i.e., postero-superior, compartment (Luo, 2017).

In rodents, flat cells have no cilia and ciliated cells are cuboidal, columnar or pseudo-stratified. In human middle ear, even flat cells can possess cilia and non-ciliated cells possess microvilli, no matter what their height (Lim, 1974). Most of these features can be seen on H&E sections in both human and rodent tissues, although microvilli are best appreciated with electron-microscopy which confirms the similarity of middle ear epithelium to respiratory epithelium. Data from Bremond 1972 shows mainly two types of epithelium: ciliated, low cuboidal and squamous i.e., non-ciliated with microvilli. It emphasised the poorly differentiated, flat epithelium of the mastoid but also referred to its capacity for differentiation under inflammatory conditions to increase the number of secretory cells as well as its capacity to undergo metaplasia to squamous epithelium. Data from Lim 1974 applying electron microscopy to guinea pig middle ear showed similar findings. This study gives an idea of the dimensions of the non-ciliated squamous cell which are 20-25  $\mu\text{m}$  diameter. In the human lung

these have been reported as up to 50  $\mu\text{m}$  although this may reflect type I cells captured in the expansion phase of breathing.

The human lung and middle ear are also subject to similar types of viral and bacterial infection and inflammation. In humans, bacteria such as *Streptococcus pneumoniae* and non-typable *Haemophilus influenzae* can infect both ear and lung. Vaccination against *S. pneumoniae* which has up to 21 serotypes has some correlation in reduced incidence of otitis media due to the same organism (Taylor, 2012).

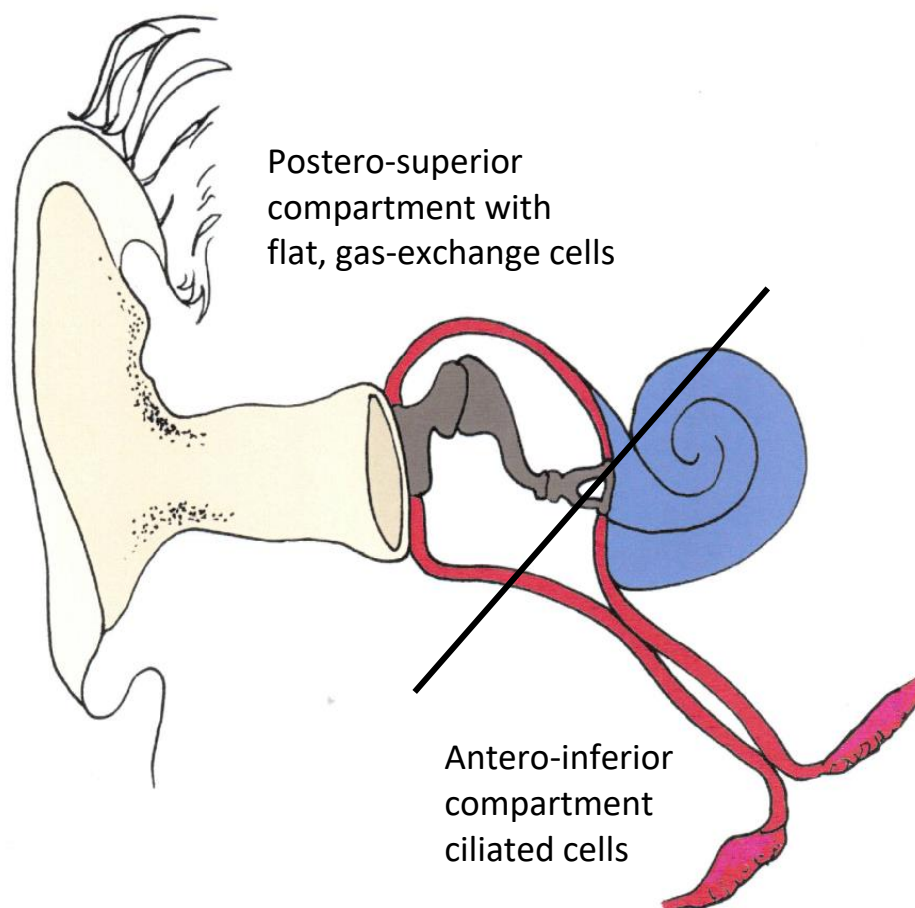


**Figure 1.5. Schematic of middle ear with oblique line dividing two functional compartments of the middle ear into postero-superior gas exchange and antero-inferior ciliated and mucus-secreting cells.**

The difference between the antero-superior and postero-inferior compartments is not just in their cell types. More recent data from transgenic mice indicates that these compartments are also a reflection of their embryological and genetic origin (Tucker 2013). In the embryo, the middle ear develops as a cavity filled with mesenchymal cells before it becomes lined with epithelium. Originally, the cavity was thought to be lined by epithelium entirely derived from the endoderm of the pharyngeal pouch. This study has confirmed that only the epithelium of the antero-inferior compartment is embryologically derived from the endoderm of a pharyngeal pouch. The postero-superior compartment which includes the roof (attic) of the middle ear is derived from neural crest epithelium and extends to surround the epithelium over the footplate of the stapes. The main conclusion from the study is that the mesenchyme which initially fills the middle ear cavity does not contribute to the definitive layer of lining epithelium. Histologically, the two compartments possess the same variety of cell types although in different proportion and distribution. They differ significantly in their complement of ciliated epithelium.

## **1.7 Surfactant proteins: history, biochemical structure, functions and genetics**

Surfactants are amphiphilic fluids i.e., they mix in polar and non-polar environments and operate at interfaces. They form monolayers at air-water interfaces e.g., lungs and oil-water interfaces (emulsions) and can form aggregates at the solid-water interface e.g., articular joint surfaces. Pulmonary surfactant proteins are a small but important proportion of surfactant fluid. Pulmonary surfactant is like a biological detergent and lubricant. Its ability to keep surfaces clean includes its ability to bind to microbes. The lubricant function is best seen when lung expands and contracts without collapsing but it is also seen in sliding joint surfaces. Human lung surfactant and its constituent proteins were discovered during the 20<sup>th</sup> century (Creuwels, 1997). Apart from SP-A, SP-B, SP-C and SP-D, two more have been identified recently in human lung called SP-G and SP-H (Vieira, 2017). In the following subsections, the biochemical structure,

physiological and immunological functions and comparative genetics will be reviewed.

### **1.7.1 Surfactant protein biochemistry**

Surfactant proteins are apoproteins of the collectin family. The two hydrophilic proteins - SP-A and SP-D - belong to the collectin family of calcium-dependent carbohydrate binding proteins, which also includes mannose-binding lectin (MBL) and conglutinin (Floros et al., 1998; Crouch et al., 2001). Collectins are related to collagens, the structural connective tissue proteins of the extracellular matrix. A collagenous or collagen-like domain is found in surfactant proteins A and D (see Figure 1.6). Lectins are saccharide-binding glycoproteins. These are characterised by N-terminal collagen-like domains and C-terminal carbohydrate recognition domains (CRD) which allow them to bind to various types of macromolecules, including carbohydrates, phospholipids and proteins (Shepherd, 2002), hence their role in binding to microbial walls and membranes. The term apoprotein refers to the functional form of the surfactant protein wherein the protein is a small component of a large lipid and/or carbohydrate component. This is explained in more detail in section 1.6.2 and summarised in review papers (Crouch, 2001; Sano, 2005).

SP-A and SP-D are hydrophilic proteins whereas SP-B and SP-C are hydrophobic. SP-B and SP-C are bound to phospholipids within lamellar bodies of type II alveolocytes and are secreted in the bound form. Surfactant proteins A and D are secreted separately but have non-polar components which allow them to mix with the secreted phospholipid film of surfactant. About 5% of the weight of isolated surfactant is attributable to SP-A (van Rozendaal, 2001). SP-A and SP-D also have a hydrophilic head which is polar (anionic or cationic) and is capable of binding with the charged LPS component of bacterial cell walls. SP-A recognises the lipid component of lipopolysaccharide (dipalmitoylphosphatidylcholine, DPPC) whereas SP-D binds to the core oligosaccharides and recognises the minor component of surfactant A (phosphatidylinositol; Head, 2003). We have chosen Surfactant protein A as it is the most abundant of the four main surfactant

proteins (Hawgood, 1990). For a review of the structure and function of pulmonary surfactant proteins, see Perez-Gil, 2008. The general structure of these two hydrophilic proteins is shown in Figure 1.6. The tertiary structure is seen in the 3 polypeptides joining as a trimer by non-covalent bonds and van der Waal forces. The quaternary arises from non-polar bonding of N-terminal ends.

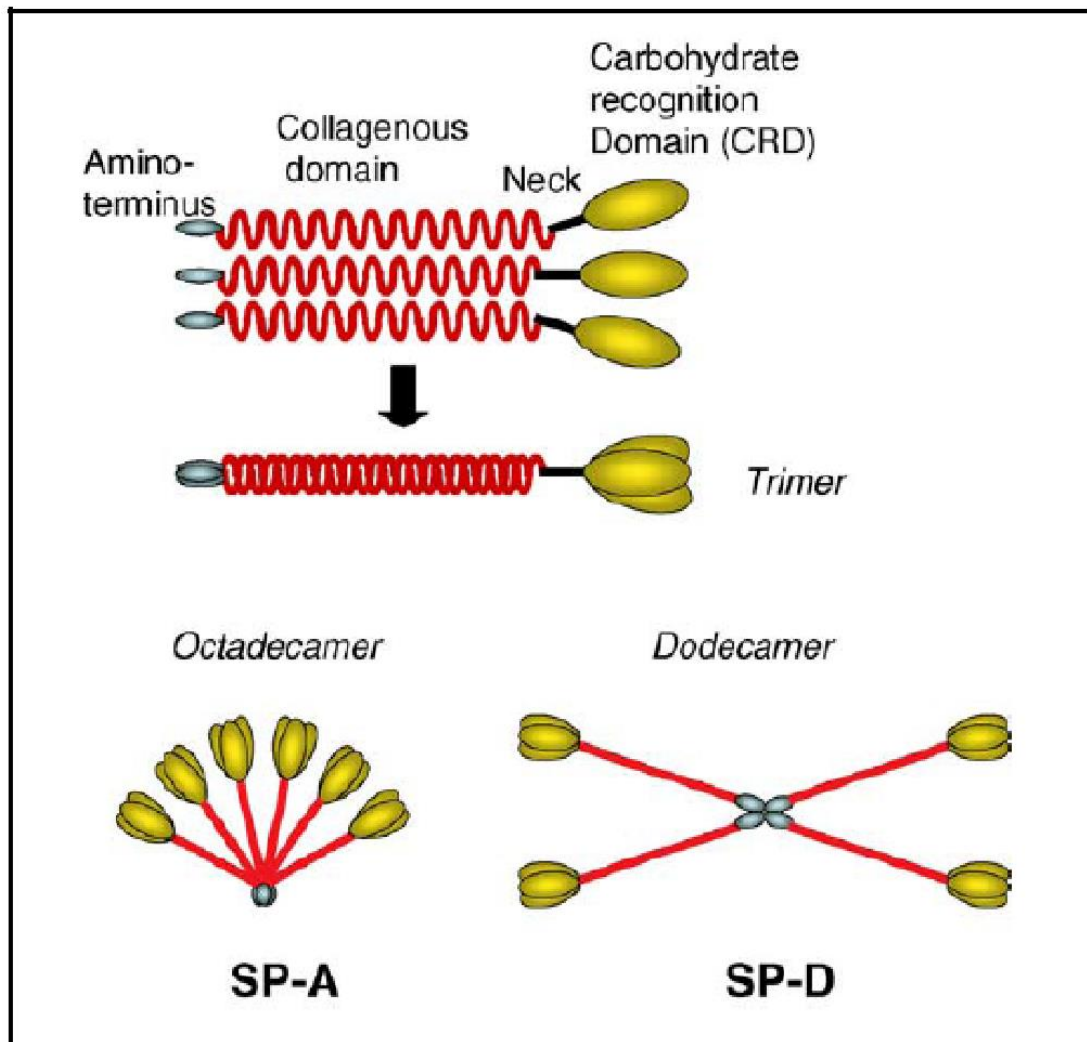


**Figure 1.6. Quaternary structure of SP-A and SP-D. Both are hydrophilic proteins with an N-terminal collagen-like domain and carbohydrate recognition domain (Sano and Kuroki, 2005).**

The C-type (Ca-binding) lectins have a CRD which recognises pathogens in the presence of calcium. This is important in the design of antibodies to complement this segment of the protein. In the case of the mouse SP-A, the antibody combines with a terminal 15 amino acid sequence of the carbohydrate recognition domain (see Table 1.2 below).

**Table 1.2. Summary of amino acid sequence of SP-A peptide showing sequence carbohydrate recognition domain which complements the antibody (data from Abcam ab115791).**

N-terminal	Collagenous domain	Neck	CRD
7 amino acids (AA)	73 AA	34 AA	123 AA
Hydrophobic	gly x-y repeats (gly-proline-hydroxyproline)	Rigid $\alpha$ -helical folds	Hydrophilic Ca <sup>++</sup> binding sites
AA sequence of peptide target (immunogen) SP-A			WNDKGCLQYRLAICEF
AA length of peptide target (immunogen) SP-A			233-248
References	1. <a href="https://www.abcam.com/surfactant-protein-apsap-antibody-ab115791.html">https://www.abcam.com/surfactant-protein-apsap-antibody-ab115791.html</a> 2. Sano and Kuroki, 2005		

In the lung, surfactant proteins are not confined to the type II alveolocyte. They are also found proximal to the alveoli within the larger airways of human lung in Clara - or club - cells (Reynolds, 2010). Surfactant proteins have been identified in many other body tissues in both humans (Bourbon, 2001; Hills, 1983) and mammals (Akiyama, 2001). Pulmonary surfactant has been identified in various tissues and organs including the pleura, peritoneum and joints (Akiyama, 2002).

The molecular structure of SP-A consists of a trimer replicated six times as 18 primary proteins united to make an octodecamer. The total molecular weight of the octodecamer SP-A is 630 kDa although its peptide subunit is 35 kDa and its trimer is 105 kDa (Vieira, 2017). These molecular weights are relevant to the finding of dimers of 66 kDa in electrophoresis bands which represent partially reduced molecules – otherwise they would yield a 70 kDa band.

Antibodies to the various surfactant proteins have long been available for signalling in immunohistochemistry. They are designed to match amino acid sequences of the carbohydrate binding segment. This is further described in Chapters 2 and 3.

### **1.7.2 Surfactant proteins: functional roles**

Surfactant proteins have two broad roles: the mechanical role of allowing epithelial surfaces to slide upon each other and various immunomodulatory functions. The sliding function on surface epithelium involves binding and aggregation of phospholipids and is seen in:

1. Alveolar expansion and contraction without collapse i.e., reduction of surface tension at the air-liquid interface of the lung in the alveoli.
2. Articular joint surfaces sliding together.
3. Pleura, peritoneum and pericardium surfaces sliding as well as similar functions in other organ systems.

The immunomodulatory functions include:

1. Non-immune recognition of bacteria, virus and fungal organisms (LeVine, 2000).
2. Binding to the flagella of opportunistic bacteria such as *Pseudomonas* species (Ketko, 2013).

Surfactant protein is active when it is bound to a lipid and/or carbohydrate component. For example, it is active when it is bound to the carbohydrate of the cell wall of a bacteria or when it is bound to phospholipids in the fluid film lining the alveoli of the lung. In these situations it is called an apoprotein to distinguish it from its pure protein form in isolation as a tetramer or separated into its fundamental peptide of 35 kDa size.

### **1.7.3 Surfactant proteins: history and genetics**

Alterations in the structure and function of SP-A and SP-D have been implicated in inflammatory lung disorders, both acute and chronic, such as pulmonary interstitial fibrosis. Only one genetic disease, cystic fibrosis – an autosomal recessive disease - is clearly associated with impaired SP-A and SP-D protein function (Lin, 2018).

The molecular weight of SP-A is generally described as a range 29-35 kDa because of its complex quaternary structure. Its principal isoform is 30 kDa (King, 1989). It is an octodecamer made up of 6 trimers (McCormack, 1998). This results in, for example, an electrophoresis study of rat lung showing bands of 26, 32 and 38 kDa as well as dimer forms of 66 kDa (Bourbon, 2001). SP-A and SP-D are present in mouse and have been analysed in gene-knockout models bearing in mind that human SP-A exists in 2 forms (SP-A1 and SP-A2 which have different coding to mice which is a single SP-A form (Crouch, 2000). SP-A deficiency (SP-A -/-) seems to have more subtle effects such as reduced uptake of microbes by alveolar macrophages whereas SP-D deficiency (SP-D-/-) seems to result in abnormal lung structure and function such as increased alveolar proteinosis and emphysematous change (Sano, 2005; McGuire, 2002; Lin 2018). Also, deficient uptake of bacteria by alveolar macrophages has been observed in both SP-A and SP-D deficient mice (LeVine, 2000).

## **1.8 Surfactant protein within the middle ear**

One of the first references to surfactant within the middle ear describes “lamellar substances similar to phospholipids in the secreta of the tube and middle ear mucosa of the guinea pig” (Lim, 1974). Lim referred to an “auditory surface active agent”. In this electron microscopic study of the middle ear, lamellar granules similar to those found in lung cells were identified. Using a flocculation method for phospholipids, protein and mucopolysaccharides (the three constituents of surfactant), a reaction was noted in both the Eustachian tube and middle ear mucosa.

Surfactant protein has been found in the in the Eustachian tube (which is a part of the middle ear) rather than in the main bony middle ear cavity. Prior to SP-A being identified in mucosa, it was assayed as free protein from middle ear fluid of patients (Grace, 1987). More specific identification of SP-A protein has been achieved by mRNA expression in the middle ear and paranasal sinuses of rabbits (Dutton, 1999). This study did not attempt to localise SP-A topographically within the middle ear nor was it seeking to distinguish type I and type II cells. SP-A has

been identified within the Eustachian tube mucosa of pigs (Panaanen, 2001). Even an extensive review paper referring to surfactant in the middle ear localised it only to cells in the epithelium of the Eustachian tube rather than to the middle ear without stipulating what type of cell produced it (McGuire, 2002). Mouse middle ear epithelium has been studied in vivo using cell culture models and electron microscopy to study cell morphology and immunofluorescence to identify several proteins including surfactant D, the other hydrophilic protein related to SP-A (Mulay, 2016).

Pulmonary surfactant has been identified in various tissues and organs including the pleura, peritoneum and joints (Akiyama, 2002). Commenting upon the presence of surfactant within gut epithelium, Hills postulated that there might exist the equivalent of a type II alveolocyte in the gut i.e., outside the lung (Hills, 1983). The suggestion that the middle ear might also have such cells is a reasonable proposition.

The various surfactant proteins have been identified in the middle ear and Eustachian tube by immunohistochemistry (IHC) as well as by electron microscopy (McGuire, 2002). The best known are SP-A, SP-B, SP-C and SP-D all of which are to be found in lung. The current understanding of their physiological and immunological roles as well as their interactions with each other are well summarised in Nunn's textbook of respiratory physiology (Nunn, 2017). We have chosen Surfactant protein A (SP-A) for this study as it is the most abundant of the four types.

### **1.9 Surfactant protein A antibody: a tool to identify the type II alveolocyte**

Antibodies specific to the 15 AA sequence of the carbohydrate recognition domain of SP-A can be applied to middle ear epithelium to test whether SP-A is produced by middle ear epithelium by a cell analogous to a type II alveolocyte. Studies on lung injury have revealed that type II alveolocytes can divide into a type I cell and another type II cell thereby acting as precursors to both cell types

(Xiao, 2012). In the middle ear such a cell would replenish type I analogues important for gas exchange.

In the lung, all surfactant proteins (SP-A, SP-B, SP-C, SP-D) are either in stored, intracellular form or secreted, extracellular form when examined at the alveolar level (Ochs, 2002). SP-A can also be derived from cultured lung cells from mice (Gobran, 2003). The type II cell and the Clara cell both make SP-A and both are non-ciliated cells. They differ in their anatomical location and hence their role within their own local cell populations. It is interesting that both cell types (type II and Clara) which make SP-A are have a progenitor potential. Even though IHC methods can accurately label SP-A in lung alveolocytes, one must not mistake this signal for SP-A scavenged within alveolar macrophages which help to recycle SP-A.

### **1.10 Cytokeratins: tools to distinguish type I and type II alveolocytes**

Cytokeratins (CK) are keratin-containing intermediate filaments belonging to a family of structural proteins within cell bodies (cytoplasm) which help to give shape and structural stability to the cell. Several CKs have been identified in the middle ear in both human and other mammals. Although antibodies to SP-A can label a type II cell unequivocally in lung, it does not mean that cells which are not positive for SP-A must be type I cells. Fortunately, lung research has succeeded in distinguishing the type I cell and the type II cell by revealing a distinct pattern of CK protein expression.

The panel of cytokeratin protein markers proposed for this study (CK7, CK8, CK18, CK19) were originally applied to rat lung (Kasper, 1993). This panel of CKs was used to differentiate alveolar cells as type I and type II alveolocytes. All four CKs were identified within the alveoli, CK7 and CK19 only in type I alveolocytes and CK8 and CK18 only within type II alveolocytes. The majority of antibodies directed against CK8, CK18 and CK19, CK7 reacted against the upper airway epithelium as well. CK7 was also positive in the bronchial cells of the upper airway but was absent from the terminal bronchioles.

### 1.11 Data from research using cytokeratins in human middle ear

Several CKs have been identified in human middle ear epithelium including CK4, CK5, CK7, CK14, CK18 and CK19 (Broekaert, 1988; Table 1.3, Figure 2.1). A later study confirmed more specific localisation of CK7, CK8, CK14, CK18 and CK19 in epithelium on the medial side of the tympanic membrane and in the middle ear (Broekaert, 1993).

**Table 1.3. Cytokeratins expressed in human outer ear canal, tympanic membrane (lateral and medial surfaces) and middle ear cavity (data from Broekaert, 1988).**

	Cartilaginous canal	Bony canal	Lateral tympanic membrane	Medial tympanic membrane	Middle ear mucosa
CK 4	-	-	-	+ <sup>a</sup>	+
CK 5	+	+	+	-	-
CK 7	-	-	-	+	+
CK 8	-	-	-	+	+
CK 10	+	+	+	-	-
CK 13	-	-	-	+ <sup>a</sup>	-
CK 14	+	+	+	+	+
CK 16	-	+	+	-	-
CK 18	-	-	-	+	+
CK 19	-	+	+	+	+

a: focally expressed (in stratified epithelium) from Broekaert 1988.

The topographical location of various cytokeratins within the human middle ear is summarised in Figure 1.7 below. In the human embryo and infant, there is consistent expression of various cytokeratins within the epithelium of the middle ear (Liang, 2003). CK19 is expressed in simple epithelium and in pseudo-stratified columnar epithelium from gestational week 6 to 8 months post-partum. CK18 is

expressed in both simple and pseudo-stratified cells from gestational week 26 to 8 months post-partum.

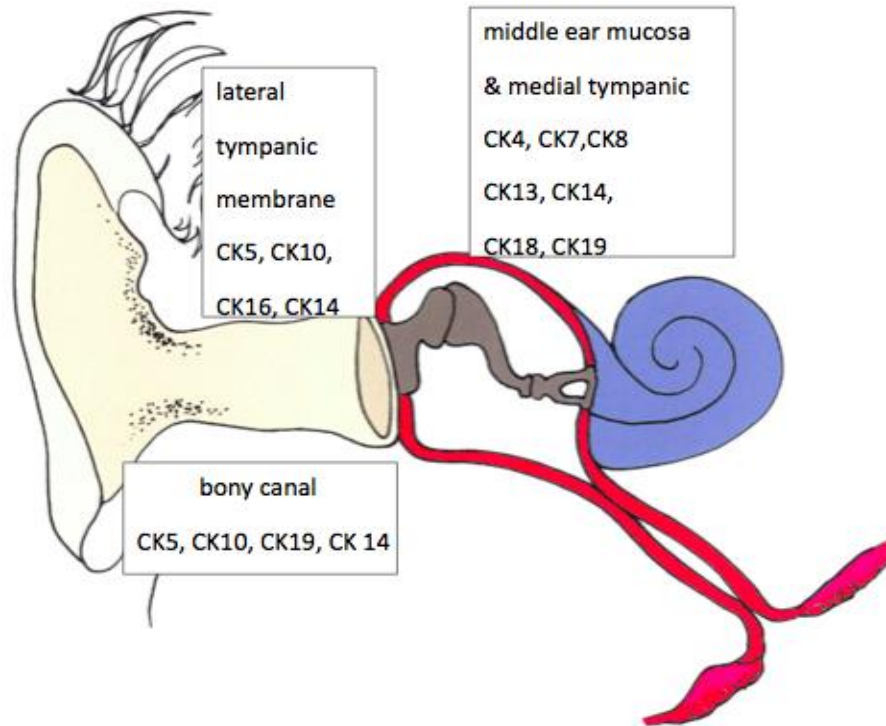


**Figure 1.7. Diagram of outer and middle ear showing distribution of cytokeratins (based on Broekaert, 1988).**

CK14 is present on lateral tympanic membrane as well as meatal epidermis. The lateral tympanic membrane has a modified squamous epithelium which does not stratify fully until it reaches the lateral bony canal because it is migrating laterally and does not have the opportunity to stratify until it reaches the cartilaginous canal. Hence it makes sense that CK14 is expressed in this part of the outer ear as it is expressed in suprabasal cells i.e., in stratified epithelium.

In the adult, CK8, CK18 and CK 19 are homogeneously expressed whereas CK7 and CK4 are heterogeneously expressed. CK14 is present in all basal cells. All of this indicates that CKs can give reliable signal in the middle ear where the epithelium is simple in type.

### 1.12 Data from research using cytokeratins in rat middle ear

In a developmental study of rat Eustachian tube, several cytokeratins have been used including CK7, CK8, CK18 and CK19 as markers of simple epithelium (Mulder, 1998). It was noted that all four CKs were present also in the middle ear and that there are ciliated tracts within the rat middle ear. The target of the study was the tall and ciliated epithelium of the Eustachian tube rather than an attempt to identify cells analogous to the type I or type II lung cells in the middle ear. The study does highlight the usefulness of these CKs as markers of simple epithelium. It also shows that this specific set of four CK markers originally used in rat lung were labelled positive in rat middle ear.

### 1.13 Data from research using cytokeratins in mouse middle ear

Cytokeratins have been used in mouse middle ear but these did not aim to identify potential analogues of type I and type II alveolocytes. One study used CK5 which is a marker for non-ciliated cells including goblet cells and the basal epithelium of ciliated regions (Luo, 2017). By definition basal cells are not ciliated. To distinguish basal cells from goblet cells, this study also used CK14 which labels basal cells but does not label goblet cells.

On this basis, it is reasonable to propose that CKs 18, 8, 19 and 7 should help to distinguish type I and type II alveolocyte analogues in the middle ear although CKs alone will not be enough to establish such a distinction. The pattern of cytokeratin expression for the two cell types is summarised below in Table 1.4.

**Table 1.4. Cytokeratin Profile in Type 1 and Type II cells.**

	<b>CK8, CK18</b>	<b>CK7, CK19</b>
Type II	+	-
Type I	-	+

### 1.14 Strategy for using SP-A and cytokeratins together in the middle ear

In the alveoli, markers for type I cells such as CK7 and CK19 are evident in simple flat epithelial cells situated side-by-side forming the walls which outline the alveolus. In fact, the lack of continuity of CK 19 signal is usually due to the presence of intervening type II cells (Kasper, 1995). In the absence of the alveolar space within the middle ear, an extra marker is required to distinguish type I and type II alveolocytes in the middle ear. As type II alveolocytes express SP-A, it is expected that SP-A will be expressed in cells expressing CK8 and CK18 (analogous to type II alveolocytes). Cells expressing CK7 and CK19 would not express SP-A and therefore correspond to type I alveolocytes. This pattern shown in Table 1.5 below. Cytokeratin studies have been done in both middle ear and lung but no studies have been attempted to correlate the location of surfactant protein and CKs in middle ear or lung. This type of co-location is necessary because the middle ear lacks the orientation provided by the small alveolar units of lung which also help to identify type II cells.

**Table 1.5. Cytokeratin and SP-A Profile in Type I and Type II cells.**

	CK8, CK18	CK7, CK19	SP-A
Type II	+	-	+
Type I	-	+	-

### 1.15 Surfactant and type II alveolocytes

In all mammals, the type II alveolocyte of the lung secretes all four types of surfactant protein (SP-A, SP-B, SP-C, SP-D). The most abundant is SP-A of which humans have two forms, SP-A1 and SP-A2. Because it is a secreted protein, immunohistochemistry (IHC) can locate it outside cells at low power magnification and, using high magnification with oil immersion, one can confirm its intracellular location. Previous work on lung sections using SP-A antibodies has shown signal simultaneously within type II cells and within the intra-alveolar space in lung sections (Helms, 2008) implying that the target sequence of amino acids is the same inside the cell and outside in the secreted form. SP-A does

undergo post-translational modification by glycosylation as well as removal of its signal peptide which both occur prior to secretion (Johansson, 1997). If glycosylation involved the 15 AA sequence of the CRD, it would involve only the single hydroxylysine within this short sequence.

Apart from the type II cells of the alveoli, there are other non-ciliated cells of the upper airway which produce surfactant proteins. These include the Clara cell, a club-shaped cell. In the lung, three cells – type I and type II alveolocytes and Clara cells - can be distinguished within the lung by H&E staining because of their characteristic shapes which are seen in the lung alveoli and bronchioles. They may be cuboidal or columnar and are found in increasing frequency from the distal trachea to the respiratory bronchioles. This is useful as a positive control marker in lung when examining alveoli for positive signal by IHC. It enables one to confirm a continuous signal in sheets of cells in the upper airways at low power magnification before proceeding to the more challenging examination of alveoli at higher magnification. Surfactant protein A (SP-A) is situated in apical micro-villi of these non-ciliated cells.

The term “simple” refers to single layer epithelium and includes mucociliary epithelium which are tall ciliated cells which can give a pseudostratified appearance. These ciliated cells are easy to distinguish from non-ciliated cells by H&E staining. To distinguish potential type I and type II cells in the middle ear by H&E is even more difficult because in the middle ear there is not the background of alveolar polygons found in lung. Even in lung, IHC can label free alveolar macrophages laden with SP-A which can be mistaken for type II alveolocytes even though macrophages are generally larger. This is important because free macrophages are present in the middle ear and may contain engulfed SP-A.

Beyond the main cavity of the middle ear there also exist non-ciliated columnar cells in the Eustachian tube including its opening in the nasopharynx. Our study may identify such cells and determine whether or not they are positive for surfactant protein and perhaps analogous to Clara (club) cells.

## **1.16 Beyond lung and middle ear: Surfactant protein A in body tissues**

Although originally described as an important functional component of lungs, surfactant proteins are found in several body tissues. They are important in places where epithelial surfaces need to slide upon each other e.g., lung pleura, abdominal peritoneum, articular cartilage joint surfaces (Akiyama, 2002; Vieira, 2017). Surfactant protein is also found in bone marrow where it is thought to originate in mesenchymal stem cells (Huang, 2015; Kotton, 2008; Popov, 2008).

## **1.17 Aim and objectives of the thesis**

The aim of this thesis was to investigate the protein localisation of SP-A in the rodent middle ear and compare to that in the rodent lung. The objectives of the thesis were:

1. To demonstrate that there are cells within the epithelium of the middle ear which makes SP-A, making these cells the equivalent of a type II alveolocyte. This involves using IHC methods with immunofluorescent antibodies that are specific to SP-A.
2. To demonstrate that there are cells within the middle ear with IHC features similar to type I alveolocytes. Type I alveolocytes are SP-A negative but would need to be distinguished further by using IHC methods with immunofluorescent antibodies to cytokeratins. SP-A positive cells would label positive for CK8 and CK18 whereas SP-A negative cells should label positive for CK7 and CK19.

## 2 Chapter 2

### Materials and Methods

---

#### 2.1 Materials

Unless otherwise stated, all processes were carried out within the C.2.03 Molecular Genetics Laboratory at the University of Waikato, Hamilton, New Zealand. All solutions were made up using autoclaved 15-18 megOhm-cm double distilled deionised water (mQH<sub>2</sub>O) using a Barnstead double distilled/deionisation system unless otherwise stated. All chemicals and solvents were obtained from Sigma-Aldrich® Co unless otherwise stated. All experiments were carried out aseptically on bench tops cleaned with 70% ethanol (ETOH). Various steps involving toxic solvents were carried out in a laminar flow cabinet. All glassware was washed in the dishwasher and then autoclaved before use. All solutions and buffer recipes can be found in Appendix One. A considerable number of experimental conditions were tested and the final approach is summarised below.

#### 2.2 Animal ethics

All tissue sections were of fresh deceased rodent species, either *Mus musculus* (mouse) or *Rattus rattus* (rat) that were kindly donated from Agresearch Ruakura, Hamilton, New Zealand (NZ) and the Animal Facility at the University of Waikato, NZ using approved safety operating procedures. Mice included strains BALBc and C57/B6 whereas the rat strain was Sprague-Dawley (SD). Under the NZ Animal Welfare Act 1999, ethics approval was given by University of Waikato Animal Ethics Committee (protocol number 932, 2014) for a preliminary project to develop a mouse model of middle ear infection (see Discussion Chapter 5). No animal ethics approval was required for the main study since no live animals were used for the purposes of this study.

## 2.3 Histology

For the purpose of providing histological tissue whether temporal bone or lung, both rodent models used in this study offer a range of advantages and disadvantages over each other. After some trial and error, tissues were derived from both species and the differences between rodent are summarised in Table 2.1.

**Table 2.1. Summary of the advantages and disadvantages using two different rodent models for histological purposes.**

<b>Advantages</b>	<b>Mouse</b>	<b>Rat</b>
Temporal bone	Easier to fit a cross-section of both middle ears onto one microscope slide.	Easier to identify and dissect middle ear mucosa from temporal bone bulla than mouse.
	Can fit two temporal bones onto one microscope slide (Fig 2.1).	Dissected tissue suitable for whole mount IHC.
Lung	Can fit one entire lung onto a microscope slide (Fig 2.2).	Can expand lung with fixative solutions and maintain expansion (Fig.2.3).
<b>Disadvantages</b>	<b>Mouse</b>	<b>Rat</b>
Lung	Lung can rupture more easily during attempts to expand with fixative.	

For the purposes of this study, Haematoxylin and eosin (H&E) staining was selected as it allows appreciation of the histological structure of the middle ear in three planes, of which the coronal plane is the most useful for showing the continuity between Eustachian tube and middle ear cavity. The axial plane provides a better cross-section for the cochlea. These two plus the sagittal plane provide the three planes necessary for the three semicircular canals of balance which can serve as landmarks for orientation.



**Figure 2.1. Microscope slide showing two H&E stained sections derived from one paraffin-embedded block containing a decalcified mouse head. The processed paraffin block is shown underneath the slide.**

Immediately after removal from the euthanised animal, both lung and temporal bones were immersed in fresh 4% paraformaldehyde (PFA) for at least 2 hours in order that the middle ear epithelium is fixed and less cellular autolysis occurs. Longer than 2 hours can promote cross-linking of disulphide bonds and alter antigenicity. In order to facilitate permeation of fixative fluid into the middle ear chamber, the bony wall of the bulla was perforated with a 25G needle and syringe filled with PFA.

Because mouse middle ear was to be used in this study, mouse lung was used to study lung airway epithelium and ultimately test antibodies against this epithelium in order to compare this with middle ear epithelium.



Figure 2.2. Mouse thorax and ribs viewed from behind with lungs showing in front.



Figure 2.3. Inflation of a rat lung *in vitro* using a 5ml syringe and 18G blunt needle.

### **2.3.1 Fixation, decalcification and embedding of rodent temporal bones**

Lung tissue does not require decalcification. However, decalcification of temporal bone requires immersion in a chelating agent (EDTA) which removes calcium assisted by heating. Although use of the microwave is the fastest heating method, it was avoided as it can cause damage to antigens. Thus, a slower modified method for dental decalcification (Cho, 2010) was used. Mouse heads were placed into 10% PFA for 2 hours. Next, the specimens were transferred to 10% EDTA solution for 48 hours and then transferred into fresh 10% EDTA for a further 48 hours. Pressure on the temporal bone calvarium with a metal probe revealed softening effect as early as 24 hours. Subsequently temporal bones were dehydrated through an alcohol series of increasing concentration followed by NeoClear (Stoddart, cat 8052-41-3) a xylene substitute. Following fixation, the tissue was dehydrated, cleared and then infiltrated with paraffin as outlined in Table 2.2. Finally, the tissue was embedded into a labelled cassette using the Thermofisher Paraffin Embedding Station and then stored in a sealed plastic bag at room temperature (RT).

### **2.3.2 Sectioning**

Sectioning of the mouse middle ear was carried out on a microtome (Leica 2025) using a disposable blade (ThermoScientific, MX35 Ultra) to generate 5 $\mu$ M sections. The slides containing the 5 $\mu$ M sections were stored in a slide box at 4°C.

**Table 2.2. Dehydration, clearing and infiltration of tissue.**

Chemical	Time (min)	Temperature (°C)	Location
1x PBS	60	4	Cold room
0.85% NaCl	60	4	Cold room
50% ETOH: 0.425% NaCl	30	RT	Fume hood
70% ETOH (X2)	30	RT	Fume hood
85% ETOH	60	RT	Fume hood
95% ETOH	60	RT	Fume hood
100% ETOH (X2)	60	RT	Fume hood
Neoclear (X3)	30	RT	Fume hood
1:1 Neoclear/ paraffin	45	60	Histology room Incubator
Paraffin (X3)	20	60	Histology room Incubator

### 2.3.3 Haematoxylin and eosin (H&E) staining

Haematoxylin (H) is a basic dye that dyes basophilic structures purple-blue in the cytoplasm or nucleus such as nucleic acids, ribosomes, chromatin-rich cell nucleus, and cytoplasmic regions rich in RNA (Merchant & Nadol, 2010). In comparison, Eosin (E) is acid counter-staining dye that stains basic materials red-pink. Eosin staining will allow the non-nuclear tissue components to be clearly differentiated from each other, e.g., muscle from collagen.

The microscope slides and the microtome sections were brought to RT and transferred to a slide rack (5-well plastic container, 12-well plastic, or 24-well metal). The slides were incubated 2X in Neoclear – a xylene analogue - for 10 min at RT to remove the paraffin; then, dehydrated at RT with two washes in 100% Ethanol for 5 min, followed by 95% Ethanol for 2 min, 70% Ethanol for 2 min, and 35% Ethanol for 1 min. The slides were washed in double distilled (dd) H<sub>2</sub>O for 5 min at RT and then incubated in H stain for 5 min, followed by rinsing with ddH<sub>2</sub>O to wash excess dye away. Then, the tissue was rinsed in Scott's tap water

substitute for 2 min. After that, the slides were counter-stained in E stain for 5 min and washed three times for 1 min intervals with ddH<sub>2</sub>O to remove excess dye. The slides were then transferred to the fume hood for dehydration by successively immersing in 70% Ethanol for 1 min, 90% Ethanol for 30 sec, 100% Ethanol for 30 sec and finally, Xylene for 30 sec. Then, the slides were mounted with xylene-based mounting media, carefully covered with a cover slip, and sealed using transparent nail polish. Next, the slides were air-dried at RT, labelled and photographed using a Leica DMRE fluorescence microscope with Photometrics Coolsnap CCD FX camera and transferred into a slide box for long-term storage at RT.

Type I and type II alveolocytes can be distinguished in expanded lung by H&E staining. This is because the expansion of the alveoli flattens the type I cells so that they contrast with the more cuboidal type II cells which are located in the corners of polyhedral alveoli. As the middle ear lacks such polyhedral spaces, this distinction is more difficult and demands immunohistochemical methods. Furthermore, alveoli have capillaries which have their own individual endothelial cells which, being flat with flat nuclei, can be difficult to distinguish from type I alveolocytes.

We found that the recommended time of 5 min for haematoxylin immersion was adequate to colour the nuclei blue. However, the recommended time of 10 min for eosin resulted in a very intense, dominant red. Hence, we reduced the time of eosin immersion to 5 min which gave a strong pink. H&E staining allows one to distinguish the three general cell types found in middle ear mucosa (squamous, cuboidal and columnar) as well as identifying cilia which may or may not be present. H&E staining is not adequate for distinguishing type I and type II alveolocytes in lung even though they can be seen labelled as such in histology texts. Usually the type I cell is a flat, squamous cell with a corresponding long nucleus. The type II cell is cuboidal with a round nucleus.

## 2.4 Immunohistochemistry

Immunohistochemistry (IHC) involved the detection of antigen expression through the use of fluorescent antibodies using tissue sections on gelatine-coated microscope slides. Initially, we tested the antibodies on rat lung because it is easier to inflate than mouse lung. This makes the alveolar spaces larger and the surrounding epithelium more distinct. Antibodies target different cell types with differing cell shapes based on expression of their specific epitope of the protein of interest.

Apart from expressing signals in individual cells of lung tissue, IHC can reveal patterns in epithelia lining the various compartments of the lower airway. For example, the antibodies which label type II cells - CK18, CK8 and surfactant protein A (SP-A) - will label the Clara cells of terminal bronchioles in continuity while providing a more sporadic signal in alveoli. Conversely, the antibodies which label type I cells (CK7, CK19) produce a continual signal in alveoli where type II cells are side by side. In fact, points of discontinuity in alveoli have been attributed to the presence of type II cells (Kasper, 1995). These comments are derived from observations in rat lung and it is our hope to replicate this in mouse lung before applying the same approach to mouse middle ear.

Before applying these antibodies to mouse tissues, an isotype control staining was applied to rat lung using a pre-immune rabbit IgG antibody (Rb 086199, Life Technologies) at 0.5 µg/mL to check for cross reactivity. Thereafter, the main control used was replacement of the primary antibody with 5% goat serum to demonstrate that both that the protocol is working and the ratio of signalling to noise was appropriate.

Antibodies were generally polyclonal or monoclonal. SP-A antibody is anti-rabbit polyclonal. The CKs were monoclonal (derived from rabbit except for one CK7 which was derived from mouse). Details of the antibodies are set out in Table 2.3 below with dilutions according to manufacturer's recommendations.

**Table 2.3. List of antibodies used. WB = western blot, IHC = immunohistochemistry, ab = Abcam, GTX = GeneTex.**

Antibody Name	Antibody	Host	Clonality	Conc	Method	Catalog n#	Expected size (kDa)
Cytokeratin 7 (CK7) **	Primary	Mouse	Monoclonal	1:500	WB IHC	ab9021	51
Cytokeratin 7 (CK7)*	Primary	Rabbit	Monoclonal	1:1000	WB IHC	ab181598	51
Cytokeratin 8 (CK8)	Primary	Rabbit	Monoclonal	1:10,000 1:1000	WB IHC	ab32579	55
Cytokeratin 18 (CK18)	Primary	Rabbit	Monoclonal	1:2000 1:800	WB IHC	ab181597	47
Cytokeratin 19 (CK19)	Primary	Rabbit	Monoclonal	1:10,000 1:200	WB IHC	ab52625	44
Surfactant A (SP-A)	Primary	Rabbit	Polyclonal	1:500 1:200	WB IHC	ab115791	29-35
$\beta$ -actin	Primary	Rabbit	Polyclonal	1:5000	WB	GTX 110564	42
GAPDH	Primary	Mouse	monoclonal	1:500	WB	GTX 627408	36
Anti-rabbit FITC	Secondary	Goat	Polyclonal	1:1000	IHC	ab6785	NA
Anti-rabbit HRP	Secondary	Goat	Polyclonal	1:2000	WB	ab97051	NA

\*\*this CK7 antibody reacts with human target tissue, not mouse.

\* this CK 7 reacts with mouse target tissue.

For antigen retrieval, heating is essential to remove sticky protein(s) that cover the antigenic target. We found that microwave methods, although very fast at 3-8 minutes, tended to cause tissues to lift off glass slides during the boiling phase. Another method involved placing glass slides into a programmable thermal controller unit (PTC-100, MJ Research Inc., Biolab Scientific Ltd.) using Gene Frame cassettes (AB Gene AB-0577) but this was just as aggressive to the tissues as the microwave. We eventually found that prolonged gentle heating at 60°C for 12 hours overnight in a water bath within an oven improved the quality of tissue.

Images were taken using the Leica DMRE incident fluorescence microscope with mercury bulb coupled to a Photometrics Coolsnap CCD FX camera. The images were merged and reconstituted using Image-J software.

## 2.5 Western blotting

A western blot was carried out to ensure that the antibodies used in the IHC experiments recognised their specific epitope according to the molecular weight of the intended target. To determine if epithelium contains surfactant protein by western blotting, it is necessary to use mouse lung as a positive control. The tissue load provided from a single mouse middle ear is significantly less and several pairs of middle ears need to be pooled to provide enough protein concentration. To carry out a western blot, protein lysates were prepared from euthanised mouse tissues, the resulting protein was measured and estimated using the Bradford Assay and the quality examined using PAGE and Coomassie blue staining. The SP-A and cytokeratins CK8, CK18, and CK9 antibodies were compared to reference controls of  $\beta$ -actin or GAPDH enzyme.

In general, commercial pre-cast gels were used in the interest of time. The percentage of acrylamide gels varied in the commercial pre-cast gels due to availability but they were suitable to observe the expected protein band. For pre-cast gels, the ratio of Acrylamide to Bis-acrylamide was 37.5:1. Some hand-cast gels were prepared using a method previously used in our lab (Forrester-Gauntlett, B.K.E., 2013).

For the purposes of protein extraction and analysis, four lung pairs (Samples 1-4) were removed but two (Samples 3 and 4) were too big and thus, were split into two tubes (i.e. Samples 3 and 3A; 4 and 4A).

In preparing middle ear tissue derived from temporal bones, prevention of cellular autolysis is important. For this purpose temporal bones containing middle ear and cochleae were dissected and immediately placed into protease and phosphatase inhibitor solution (RIPA buffer with Phos STOP tablets) to reduce autolysis of cells (see Appendix 1). Some temporal bones were then immersed in trypsin. Then, the protein was loaded and run on a PAGE gel, transferred to a membrane (either PVDF or nitrocellulose), blocked, incubated with appropriate antibodies (Table 2.3), washed, and then developed.

### **2.5.1 Preliminary Bradford assay of lung tissue**

To estimate the protein concentration of samples of mouse lung tissues, the Bio-Rad Protein Assay Dye Concentrate (Bio-Rad, NZ) was diluted one part of dye to four parts of MQ water and filtered through a Whatman® #1 filter to remove particulates. The filtered diluted dye (100µL) was added to the required number of wells of a Jet BIOFIL® non-surface treated, flat-bottomed 96-well plate. Standards of bovine serum albumin (BSA) were diluted from 10mg/mL stock BSA (Sigma-Aldrich, NZ) with 1x PBS giving a total of 10 different protein standard concentrations ranging from 0-10 mg/mL. A 1µL volume of each of these standards was then added to 10 different wells containing 100µL of the diluted Bio-Rad dye and mixed well by pipetting up and down. The protein samples of unknown concentration (i.e. four lung samples) were added to separate wells also containing 100µL of dye. Triplicate wells were loaded for all standards and unknown samples (Figure 2.5). Samples were incubated at RT for 5 min and then the absorbance measured at 595nm using the Thermo 56 Fisher Scientific Multiskan™ GO Microplate Spectrophotometer. The software produced a standard curve from the absorbance readings plotted against standard BSA protein concentrations, an R value, and estimation of the protein concentration in the unknown lung samples. The Bradford standard can be found in Appendix 3.

Protein lysates from four lungs from four individual mice (C57/B6, Agresearch Ruakura) as well as a separate control of spleen were used. These provided a preliminary visual estimate of protein concentration.

### **2.5.2 Coomassie blue staining of electrophoresed protein lysates on PAGE gel**

Protein samples for gel electrophoresis analysis were prepared by using a final protein mass of up to 40µg diluted in 1X PBS and containing 1X Laemmli dye in a boil-proof 2mL microcentrifuge tubes (VWR, NZ). Laemmli buffer contains 2-mercaptoethanol which reduces the intra and inter-molecular disulphide bonds; SDS detergent which denatures the proteins and subunits and gives each an overall negative charge so that each will separate based on size; bromophenol

blue serving as a dye front that runs ahead of the proteins so the sample is seen during loading and glycerol which increases the density of the sample so that it forms a layer in the sample well. The prepared samples were then placed into a thermomixer at 95°C for 5 min to aid in denaturing the proteins to enable them to be run on SDS- PAGE gels. Then, 10µL of each sample was loaded onto a 12% PAGE gel (Genscript Express Plus cat. no. M01215) with MOPS buffer as the running buffer (Genscript cat. no. M00138). At times an alternative concentration e.g., 8-16% or 4-20% was used depending on availability of 12% gel.

The six lung samples (Lung 1, 2, 3, 3A, 4, 4A) were then duplicated so that a total of 15 wells were used including 5µL of PAGE Master Protein Standard Plus (Genscript cat. no. MM1397-500) ladder. Electrophoresis was conducted at 135-140V and 35-40mA. Following this, the gel was used directly for Coomassie blue staining or western blot.

In addition to lung, it was necessary to identify protein in the middle ear as well other tissues including brain, heart, liver, kidney and spleen to further validate the specificity of the antibodies being investigated. Four pairs of mouse middle ears were acquired (C57/B6, 4 month old males, Agresearch Ruakura). Each pair was transferred to a 3mL vial and sonicated with glass beads by centrifugation at 300g. The supernatant was collected and transferred to a new tube and stored at -80°C.

Samples for electrophoresis were prepared as stated above and were loaded onto an 8-16% gel of 12 wells (Genscript, # MG 816W12). Using a MOPS buffer, the gel was then run at 130 V with 35-40 mA. The gel was then transferred to a PVDF nitrocellulose membrane using the Genscript eBlot protein transfer system (cat. No. L3010). This involves activating the white membrane in 100% Methanol for about 10 sec. The membrane is then immersed into eBlot equilibrium buffer (Genscript cat.no M01078). The protein transfer was carried out for 7-8 min. A Coomassie blue stain was applied to confirm that protein transfer had occurred. Then, the membrane was placed in 5% blocking buffer at 4°C overnight.

### 2.5.3 Western blotting analysis

Protein samples were loaded in serially increasing concentrations onto a 12% PAGE gel using 1, 5, 10, 15, 20 $\mu$ L loads. A further dilution series was carried out using protein extracts from lung 1 and lung 4. Using volumes of 2, 10, 20, 30 and 40 $\mu$ L, an 8 $\mu$ L sample from tube 1b and tube 4b was included in each series. Initially concentrations of SP-A 1:1000 were used with little signal and then this was increased to 1:500.

For western blot analysis, a 5 $\mu$ L volume of WB-MASTER protein standard (Genscript cat. no.M00521) was loaded onto the gel to serve as a positive control for developing reaction and molecular weight determination. Following gel electrophoresis, the gel was rinsed with distilled water before being transferred to the eBlot<sup>®</sup> protein transfer system, which was set up according to manufacturer's instructions (Genscript, USA). The eBlot<sup>®</sup> machine was then run for 7 min, to transfer across all protein to the PVDF membrane (Amersham Hybond-P membrane 0.45 $\mu$ m, RPN2020F) that had been previously activated in methanol for 20 sec and equilibrated for 5 min in transfer buffer. An alternative membrane used was a nitrocellulose type (Genscript WestClear<sup>™</sup> Nitrocellulose LO 0224A60).

Once the protein was transferred to the membrane (evident by the two bands in the PAGE ladder or Ponceau staining, Appendix 1), the membrane was carefully transferred to a container and washed three times at RT with TBS-T for 15 min per wash, then once for 15 min with TBS before being blocked with 5% blocking buffer containing skim milk. The membrane was incubated for 1 hour to prevent the nonspecific binding of the antibodies before being washed three times with TBS-T for 15 min per wash, then once for 15 min. The primary antibody (Table 2.3) was then applied to the membrane in a sealed plastic envelope and incubated on a rotating wheel for 2 hours at RT then overnight at 4<sup>°</sup>C. The membrane was then washed 3 times in TBST (5, 10, 15 min) before application of secondary conjugated goat anti-rabbit IgG polyclonal antibody for 1 hr at RT (Table 2.3). Finally, chemiluminescent developer was applied using either ThermoScientific<sup>™</sup> Supersignal<sup>™</sup> Western Substrate (cat. No. 34577) or Western

Bright before being photographed and analysed on the iBright analyser (FL1000, Invitrogen). Alternatively we used the Aplegen analyser.

## 3 Chapter 3

### Bioinformatics

---

A number of gene aliases have been described for SP-A. These include *SPA*, *PSAP*, *PSPA*, *SP-A*, *SPA1*, *PSP-A*, *SFTP1*, *SP-A1*, *COLEC4* and *SFTPA1B* (<https://www.ncbi.nlm.nih.gov/gene/729238>).

The official gene symbol recognised by the human nomenclature committee is *SFTPA* and two alternative isoforms exist: A1 and A2. To date, six alternative transcripts have been described for *SFTPA1* in human but only one transcript in mouse, pig and rabbit. Interestingly, three alternative transcripts have been identified for rat.

Table 3.1 shows that surfactant A1 varies considerably at the molecular level between the mammalian species in its chromosomal location and number of mRNA transcripts although the resultant proteins are similar in size in human, mouse, pig, rabbit and rat (24-26 kDa). Figure 3.1 shows the genomic structure of the six *SFTPA1* transcripts on human chromosome 10q22.3. With alternative splicing, the first and last two exons are the same between the depicted transcripts. A high homology was observed with the coding exons when compared against 30 mammals including mouse, particularly transcript 1.

**Table 3.1. Comparison of the mammalian surfactant A1 at the molecular Level. Source: gene cards and NCBI. GenBank accession numbers are provided for the mRNA and protein sequences.**

Organism	Gene Symbol	Locus	mRNA Length (nt, Accession n#)	Protein Size (AA, Accession n#)	Predicted Molecular Weight (kDa)
Human	<i>SFTPA1</i>	10q22.3			
	transcript 1		2230, NM_005411.4	248, NP_005402.3	24.17
	transcript 2		2216, NM_001093770.3	263, NP_001087239.2	24.17
	transcript 3		2186, NM_001164644.2	248, NP_001158116.1	24.17
	transcript 4		2159, NM_001164647.1	248, NP_001158119.1	24.17
	transcript 5		2072, NM_001164645.2	214, NP_001158117.1	19.61
	transcript 6	2080, NM_001164646.2	199, NP_001158118.1	19.61	
Mouse	<i>Sftpa1</i>	14	2775, NM_023134.5	248, NP_075623.2	24.1
Pig	<i>SFTPA1</i>	14	1895, NM_001348959.1	248, NP_001335888.1	24.3
Rabbit	<i>SFTPA1</i>	Un defined	2978, NM_001082229.1	247, NP_001075698.1	24.6
Rat	<i>Sftpa1</i>	16p14			
	transcript 1		1635, NM_001270645.1	258, NP_001257574	24.53
	transcript 2		1632, NM_017329.2	257, NP_059025.2	24.53
	transcript 3	1,846 NM_001270647.1	248, NP_001257576	24.19	

**Table 3.2. Official name of the protein isoforms generated by alternative mRNA splicing of *SFTPA1*. The six *SFTPA1* mRNA transcripts results in four different isoforms of the surfactant A1 protein.**

Genbank Accession n#	Official Protein Name
NP_005402.3	Pulmonary surfactant-associated protein A1 isoform 1 precursor
NP_001087239.2	Pulmonary surfactant-associated protein A1 isoform 2 precursor
NP_001158116.1	Pulmonary surfactant-associated protein A1 isoform 1 precursor
NP_001158119.1	Pulmonary surfactant-associated protein A1 isoform 1 precursor
NP_001158117.1	Pulmonary surfactant-associated protein A1 isoform 3 precursor
NP_001158118.1	Pulmonary surfactant-associated protein A1 isoform 4 precursor

## UCSC Genome Browser on Human Dec. 2013 (GRCh38/hg38) Assembly

move <<< << < > >> >>> zoom in 1.5x 3x 10x base zoom out 1.5x 3x 10x 100x

chr10:79,609,809-79,616,584 6,776 bp.

enter position, gene symbol, HGVS or search terms

go

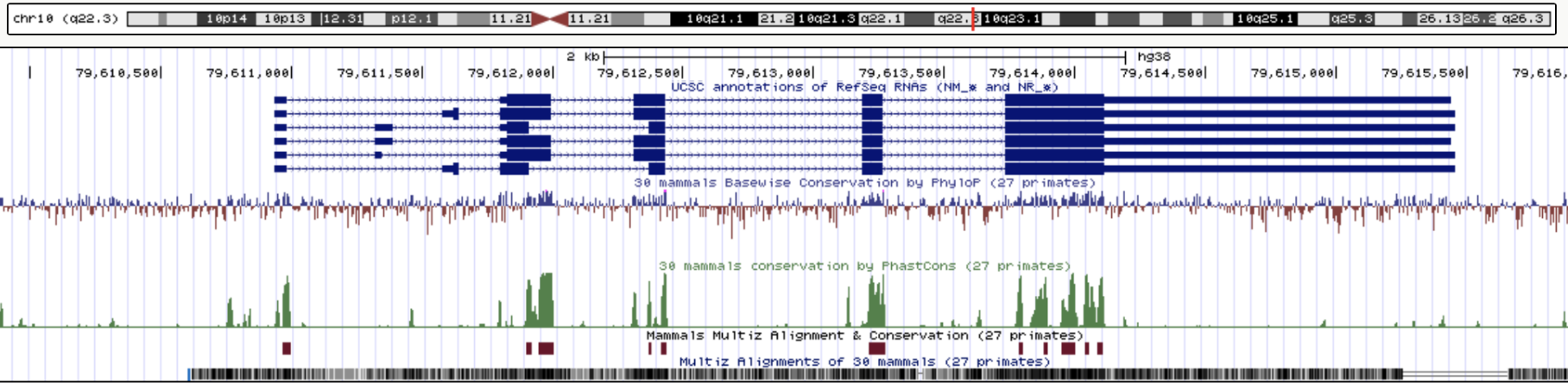


Figure 3.1. Comparative genomics of human alternative transcripts of *STPPA1*. Shown are the six reported human *STPPA1* transcripts in the sense direction on chromosome 10 (Table 3.1). The number and size of exons (blue rectangle) differs between the mRNA transcripts. The green peaks show high homology with the coding exons when compared against 30 mammals including mouse. In addition, high nucleotide identity between mouse and human *STPPA1* (bottom bar - black vertical lines) (UCSC Genome Browser, 2019).

Next, the six *SFTPA1* transcripts were translated into amino acid sequences which were then aligned using the online tool, Clustal Omega (<https://www.ebi.ac.uk>). Figure 3.2 shows the highest level of amino acid identity is at the C-terminal end of the protein with most variability being observed at the N-terminal (positions 1-15 and 31-56). Also, three mRNA transcripts (NP\_005402.3, NP\_001158119.1 and NP\_001158116.1) are predicted to translate into the same protein, isoform 1, with a molecular weight of 24.17 kDa (Table 3.1).

NP_005402.3	-----MWLCPALNLIILMAASGAVCEVKDVCVSGSPGIPGTPGSHGLPGRD	45
NP_001158116.1	-----MWLCPALNLIILMAASGAVCEVKDVCVSGSPGIPGTPGSHGLPGRD	45
NP_001087239.2	MRPCQVPGAATGPRAMWLCPLALNLIILMAASGAVCEVKDVCVSGSPGIPGTPGSHGLPGRD	60
NP_001158119.1	-----MWLCPALNLIILMAASGAVCEVKDVCVSGSPGIPGTPGSHGLPGRD	45
NP_001158117.1	MRPCQVPGAATGPRAMWLCPLALNLIILMAASGAVCEVKDVCVSGTPG-----	46
NP_001158118.1	-----MWLCPALNLIILMAASGAVCEVKDVCVSGTPG-----	31
	*****:*	
NP_005402.3	GRDGLKGDGPPGPMGPPGEMPCPPGNDGLPGAPGIPGECGEKGEGERGPPGLPAHLDE	105
NP_001158116.1	GRDGLKGDGPPGPMGPPGEMPCPPGNDGLPGAPGIPGECGEKGEGERGPPGLPAHLDE	105
NP_001087239.2	GRDGLKGDGPPGPMGPPGEMPCPPGNDGLPGAPGIPGECGEKGEGERGPPGLPAHLDE	120
NP_001158119.1	GRDGLKGDGPPGPMGPPGEMPCPPGNDGLPGAPGIPGECGEKGEGERGPPGLPAHLDE	105
NP_001158117.1	-----IPGECGEKGEGERGPPGLPAHLDE	71
NP_001158118.1	-----IPGECGEKGEGERGPPGLPAHLDE	56
	*****	
NP_005402.3	ELQATLHDFRHQILQTRGALS LQGSIMTVGEKVFSSNGQSITFDAIQEACARAGGRIAVP	165
NP_001158116.1	ELQATLHDFRHQILQTRGALS LQGSIMTVGEKVFSSNGQSITFDAIQEACARAGGRIAVP	165
NP_001087239.2	ELQATLHDFRHQILQTRGALS LQGSIMTVGEKVFSSNGQSITFDAIQEACARAGGRIAVP	180
NP_001158119.1	ELQATLHDFRHQILQTRGALS LQGSIMTVGEKVFSSNGQSITFDAIQEACARAGGRIAVP	165
NP_001158117.1	ELQATLHDFRHQILQTRGALS LQGSIMTVGEKVFSSNGQSITFDAIQEACARAGGRIAVP	131
NP_001158118.1	ELQATLHDFRHQILQTRGALS LQGSIMTVGEKVFSSNGQSITFDAIQEACARAGGRIAVP	116
	*****	
NP_005402.3	RNPEENEAIASFVKKNTYAYVGLTEGSPGDFRYS DGTVPVNYTNWYRGEPAGRGKEQCV	225
NP_001158116.1	RNPEENEAIASFVKKNTYAYVGLTEGSPGDFRYS DGTVPVNYTNWYRGEPAGRGKEQCV	225
NP_001087239.2	RNPEENEAIASFVKKNTYAYVGLTEGSPGDFRYS DGTVPVNYTNWYRGEPAGRGKEQCV	240
NP_001158119.1	RNPEENEAIASFVKKNTYAYVGLTEGSPGDFRYS DGTVPVNYTNWYRGEPAGRGKEQCV	225
NP_001158117.1	RNPEENEAIASFVKKNTYAYVGLTEGSPGDFRYS DGTVPVNYTNWYRGEPAGRGKEQCV	191
NP_001158118.1	RNPEENEAIASFVKKNTYAYVGLTEGSPGDFRYS DGTVPVNYTNWYRGEPAGRGKEQCV	176
	*****	
NP_005402.3	EMYTDGQWDRNCLYSRLTICEF	248
NP_001158116.1	EMYTDGQWDRNCLYSRLTICEF	248
NP_001087239.2	EMYTDGQWDRNCLYSRLTICEF	263
NP_001158119.1	EMYTDGQWDRNCLYSRLTICEF	248
NP_001158117.1	EMYTDGQWDRNCLYSRLTICEF	214
NP_001158118.1	EMYTDGQWDRNCLYSRLTICEF	199
	*****	

**Figure 3.2. CLUSTAL alignment of the six human SFTPA1 protein isoform sequences.** Listed on the left are the Protein GenBank Accession numbers (Table 3.1). \* = amino acid identity; : = conservative substitutions; . = semiconservative substitutions.

When the mouse SP-A protein is aligned against the human isoforms 1-4, it has the highest homology against SFTPA1 isoform 1 (Figure 3.3).

NP_075623.2	-----MSLGSLAFTLFLTVVAGIKCNGTEVCAGSPGIPGTPGNHGLPGRD	45
NP_005402.3	-----MWLCPLALNLIILMAASGAVCEVKDVCVGSPIPGTPGSHGLPGRD	45
NP_001158116.1	-----MWLCPLALNLIILMAASGAVCEVKDVCVGSPIPGTPGSHGLPGRD	45
NP_001087239.2	MRPCQVPGAATGPRAMWLCPLALNLIILMAASGAVCEVKDVCVGSPIPGTPGSHGLPGRD	60
NP_001158119.1	-----MWLCPLALNLIILMAASGAVCEVKDVCVGSPIPGTPGSHGLPGRD	45
NP_001158117.1	MRPCQVPGAATGPRAMWLCPLALNLIILMAASGAVCEVKDVCVGTGP-----	46
NP_001158118.1	-----MWLCPLALNLIILMAASGAVCEVKDVCVGTGP-----	31
	* * *:.*:* ..:* *: .:***:**	
NP_075623.2	GRDGIKGDPPGPMGPPGMPGLPGRDGLPGAPGAPGEHGDKEPGERGLPGFPAYLDE	105
NP_005402.3	GRDGLKGDPPGPMGPPGEMPCPPGNDGLPGAPGIPGECGEKGEGERGPPGLPAHLDE	105
NP_001158116.1	GRDGLKGDPPGPMGPPGEMPCPPGNDGLPGAPGIPGECGEKGEGERGPPGLPAHLDE	105
NP_001087239.2	GRDGLKGDPPGPMGPPGEMPCPPGNDGLPGAPGIPGECGEKGEGERGPPGLPAHLDE	120
NP_001158119.1	GRDGLKGDPPGPMGPPGEMPCPPGNDGLPGAPGIPGECGEKGEGERGPPGLPAHLDE	105
NP_001158117.1	-----IPGECGEKGEGERGPPGLPAHLDE	71
NP_001158118.1	-----IPGECGEKGEGERGPPGLPAHLDE	56
	*** *:***** **:**	
NP_075623.2	ELQATALYEIKHQILQTMGVLSLQGSMLSVGDKVFS TNGQSVNFD TIREMCTRAGGHIAAP	165
NP_005402.3	ELQATLHDFRHQILQTRGALS LQGSIMTVGEKVFSSNGQSITFD AIQEACARAGGRIAVP	165
NP_001158116.1	ELQATLHDFRHQILQTRGALS LQGSIMTVGEKVFSSNGQSITFD AIQEACARAGGRIAVP	165
NP_001087239.2	ELQATLHDFRHQILQTRGALS LQGSIMTVGEKVFSSNGQSITFD AIQEACARAGGRIAVP	180
NP_001158119.1	ELQATLHDFRHQILQTRGALS LQGSIMTVGEKVFSSNGQSITFD AIQEACARAGGRIAVP	165
NP_001158117.1	ELQATLHDFRHQILQTRGALS LQGSIMTVGEKVFSSNGQSITFD AIQEACARAGGRIAVP	131
NP_001158118.1	ELQATLHDFRHQILQTRGALS LQGSIMTVGEKVFSSNGQSITFD AIQEACARAGGRIAVP	116
	***:.*:.*:***** *.*****:.*:***:****:****:.*:** *:*:***:**	
NP_075623.2	RNPEENEAIASITKKYNTYAYVGLTEGSPGDFRYS DGTVPVNYTNWYRGEPAGRGKEQCV	225
NP_005402.3	RNPEENEAIASFVKKYNTYAYVGLTEGSPGDFRYS DGTVPVNYTNWYRGEPAGRGKEQCV	225
NP_001158116.1	RNPEENEAIASFVKKYNTYAYVGLTEGSPGDFRYS DGTVPVNYTNWYRGEPAGRGKEQCV	225
NP_001087239.2	RNPEENEAIASFVKKYNTYAYVGLTEGSPGDFRYS DGTVPVNYTNWYRGEPAGRGKEQCV	240
NP_001158119.1	RNPEENEAIASFVKKYNTYAYVGLTEGSPGDFRYS DGTVPVNYTNWYRGEPAGRGKEQCV	225
NP_001158117.1	RNPEENEAIASFVKKYNTYAYVGLTEGSPGDFRYS DGTVPVNYTNWYRGEPAGRGKEQCV	191
NP_001158118.1	RNPEENEAIASFVKKYNTYAYVGLTEGSPGDFRYS DGTVPVNYTNWYRGEPAGRGKEQCV	176
	*****:.*:.*:***: ** :***** * *: ***** ** *****:**	
NP_075623.2	EMYTDGKWNDRNCLYSRLTICEF	248
NP_005402.3	EMYTDGQWDRNCLYSRLTICEF	248
NP_001158116.1	EMYTDGQWDRNCLYSRLTICEF	248
NP_001087239.2	EMYTDGQWDRNCLYSRLTICEF	263
NP_001158119.1	EMYTDGQWDRNCLYSRLTICEF	248
NP_001158117.1	EMYTDGQWDRNCLYSRLTICEF	214
NP_001158118.1	EMYTDGQWDRNCLYSRLTICEF	199
	*****:***:.* ** ** :***** * *: ***** ** *****:**	

**Figure 3.3. CLUSTAL alignment of the six human SFTP1 protein isoform sequences and mouse Sfta1. Listed on the left are the Protein GenBank Accession numbers. \* = amino acid identity; : = conservative substitutions; . = semiconservative substitutions. NP\_075623.2 = mouse. Human Isoform 1 = NP\_005402.3, NP\_001158116.1 and NP\_001158119.1.**

Figure 3.4 shows the CLUSTAL alignment of Human SFTP1 Protein Isoform 1 (generated from mRNA transcripts 1, 3 and 4) against mouse Sfta1.

NP_075623.2	MSLGLAFTLFLTVVAGIKCNGTEVCAGSPGIPGTPGNHGLPGRDGRDGIKGDGPPPGPM	60
NP_005402.3	MWLCPLALNLIILMAASGAVCEVKDVCVGSPIPGTPGSHGLPGRDGRDGLKGDGPPPGPM	60
NP_001158116.1	MWLCPLALNLIILMAASGAVCEVKDVCVGSPIPGTPGSHGLPGRDGRDGLKGDGPPPGPM	60
NP_001158119.1	MWLCPLALNLIILMAASGAVCEVKDVCVGSPIPGTPGSHGLPGRDGRDGLKGDGPPPGPM * * **:.*: * ..:* *: .: **.*****.*****:*****	60
NP_075623.2	GPPGMPGLPGRDGLPGAPGAPGEHGDKEGEPGERGLPGFPAYLDEELQATALYEIKHQILQ	120
NP_005402.3	GPPGMPCPPGNDGLPGAPGIPGECGEKGEGERGPPGLPAHLDEELQATLHDFRHQILQ	120
NP_001158116.1	GPPGMPCPPGNDGLPGAPGIPGECGEKGEGERGPPGLPAHLDEELQATLHDFRHQILQ	120
NP_001158119.1	GPPGMPCPPGNDGLPGAPGIPGECGEKGEGERGPPGLPAHLDEELQATLHDFRHQILQ **** * * **.***** * * *:***** ** **:*****:***:****	120
NP_075623.2	TMGVLSLQGSMLSVGDKVFTNGQSVNFDTIEMCTRAGGHIAAPRNPEENEAIASITKK	180
NP_005402.3	TRGALSLSQGSIMTVGEKVFSSNGQSITFDAIQEACARAGGRIAVPRNPEENEAIASFVKK	180
NP_001158116.1	TRGALSLSQGSIMTVGEKVFSSNGQSITFDAIQEACARAGGRIAVPRNPEENEAIASFVKK	180
NP_001158119.1	TRGALSLSQGSIMTVGEKVFSSNGQSITFDAIQEACARAGGRIAVPRNPEENEAIASFVKK * *.*****:***:*****:****:.* **:***:*.*****:*****:.*	180
NP_075623.2	YNTYAYVGLTEGSPGDFRYSDGTPVNYTNWYRGEPAAGRGKEQCVEMYPDQWDRNCLY	240
NP_005402.3	YNTYAYVGLTEGSPGDFRYSDGTPVNYTNWYRGEPAAGRGKEQCVEMYPDQWDRNCLY	240
NP_001158116.1	YNTYAYVGLTEGSPGDFRYSDGTPVNYTNWYRGEPAAGRGKEQCVEMYPDQWDRNCLY	240
NP_001158119.1	YNTYAYVGLTEGSPGDFRYSDGTPVNYTNWYRGEPAAGRGKEQCVEMYPDQWDRNCLY **** *: *: * :****: * **: ***** * * *****:*****:***:.*	240
NP_075623.2	YRLAICEF	248
NP_005402.3	SRLTICEF	248
NP_001158116.1	SRLTICEF	248
NP_001158119.1	SRLTICEF **:*	248

**Figure 3.4. CLUSTAL alignment of human SFTPA1 protein isoform 1 (generated from mRNA transcript 1) and mouse Sfta1. Listed on the left are the Protein Genbank Accession numbers. \* = amino acid identity; : = conservative substitutions; . = semiconservative substitutions; blue line = ab115791 peptide sequence: WNDKGCLQYRLAICEF. Mouse = NP\_075623.2; Human Isoform 1 = NP\_005402.3, NP\_001158116.1 and NP\_001158119.1.**

Then, the Human SFTPA1 Protein Isoform (generated from mRNA transcript 6, Query: NP\_005402.3) and Mouse Sfta1 (Subject: NP\_075623.2) were aligned using BLASTp, This alignment provided an E-value of 2e-119 with 71.37% identity and 80% similarity at the amino acid level (Figure 3.5).

Score	Expect	Method	Identities	Positives	Gaps
328 bits(841)	2e-119	Compositional matrix adjust.	177/248(71%)	199/248(80%)	0/248(0%)
Query	1	MWLCPLALNLILMAASGAVCEVKDVCVGGSPGIPGTPGSHGLPGRDGRDGLKGDPPGPM			60
Sbjct	1	M L LA L L +G C +VC GSPGIPGTPG+HGLPGRDGRDG+KGDPPGPM			60
Query	61	GPPGEMPCPPGNDGLPGAPGIPGECGKGEKGERGPPGLPAHLDEELQATLHDFRHQILQ			120
Sbjct	61	GPPG MP PG DGLPGAPG PGE G+KGEKGERG PG PA+LDEELQ L++ +HQILQ			120
Query	121	TRGALSLQGSIMTVGKVFSSNGQSITFDALQEQACARAGGRIAVPRNPEENEAIASFVKK			180
Sbjct	121	T G LSLQGS+++VG+KVFS+NGQS+ FD I+E C RAGG IA PRNPEENEAIAS KK			180
Query	181	YNTYAYVGLTEGPPSPGDFRYSDGTPVNYTNWYRGEPAGRGKEQCVEMYTDGQWDRNCLY			240
Sbjct	181	YNTY Y+G+ EG +PGDF Y DG VNYTNWY GEP GRGKE+CVEMYTDG+WND+ CL			240
Query	241	SRLTICEF 248			
		RL ICEF			
Sbjct	241	YRLAICEF 248			

**Figure 3.5. Summary of BLASTp alignment of human SFTPA1 protein isoform (generated from mRNA transcript 6, Query) and mouse Sfta1 (Subject = Sbjct).**

The *SFTPA1* gene is conserved in human, chimpanzee, Rhesus monkey, dog, cow, rat and chicken (NCBI Gene online database, 2019). The online human protein atlas databased reports a high protein expression score for SFTPA1 in the lung but no detection in the remaining 60 tissues (e.g. kidney, colon) or cells (e.g. T-cells) examined (Human Protein Atlas, 2019; Uhlén 2015).

Surfactant proteins have also been identified in many body tissues in both humans (Bourbon, 2001; Hills, 1983) and mammals (Akiyama, 2001). In humans, the peptide for SP-A is in a trimer arrangement (Table 1.2). The trimer requires two SP-A1 gene products and one SP-A2 gene product (Vieira, 2017) whereas the mouse only has one gene product.

CLUSTAL Alignment of the *Sftpa1* mouse protein against the three rat isoforms shows high conservation at the amino acid level with rat isoform 3 with the highest homology. The antibody used for the purposes of this research was a commercial antibody, Anti-Surfactant Protein A antibody (ab115791) and targets a sequence at the C-terminal (AA 233-248) of mouse surfactant protein A AA 233-248 (C terminal). It is noted that this peptide does not have 100% identity with the three rat isoform proteins and differs by two amino acids. Thus, the antibody is suitable for detecting mouse and rat surfactant A protein.

```

NP_075623.2      -----MSLGSLAFTLFLTVVAGIKCNGTEVCAGSPGIPGTPGNHGLPGRDGRDGI      50
NP_059025.2      MW-KPLGIVAMSLCSLAFTLFLTVVAGIKCNVTDVCAGSPGIPGAPGNHGLPGRDGRDGV      59
NP_001257574.1  MWQKPLGIVAMSLCSLAFTLFLTVVAGIKCNVTDVCAGSPGIPGAPGNHGLPGRDGRDGV      60
NP_001257576.1  -----MSLCSLAFTLFLTVVAGIKCNVTDVCAGSPGIPGAPGNHGLPGRDGRDGV      50
                  *** ***** *;*****:*****:
                  *****:*****:*****:*****:

NP_075623.2      KGDPGPPGPMGPPGGMPGLPGRDGLPGAPGAPGERGDKGEPGERGLPGFPAYLDEELQTA      110
NP_059025.2      KGDPGPPGPMGPPGGMPGLPGRDGLPGAPGAPGERGDKGEPGERGLPGFPAYLDEELQTE      119
NP_001257574.1  KGDPGPPGPMGPPGGMPGLPGRDGLPGAPGAPGERGDKGEPGERGLPGFPAYLDEELQTE      120
NP_001257576.1  KGDPGPPGPMGPPGGMPGLPGRDGLPGAPGAPGERGDKGEPGERGLPGFPAYLDEELQTE      110
                  *****:*****:*****:*****:

NP_075623.2      LYEIKHQILQTMGVLSLQGSMLSVGDKVVFSTNGQSVNFDTIREMCTRAGGHIAAPRNPEE      170
NP_059025.2      LYEIKHQILQTMGVLSLQGSMLSVGDKVVFSTNGQSVNFDTIKEMCTRAGGNIIVPRTPEE      179
NP_001257574.1  LYEIKHQILQTMGVLSLQGSMLSVGDKVVFSTNGQSVNFDTIKEMCTRAGGNIIVPRTPEE      180
NP_001257576.1  LYEIKHQILQTMGVLSLQGSMLSVGDKVVFSTNGQSVNFDTIKEMCTRAGGNIIVPRTPEE      170
                  *****:*****:*****:*****:

NP_075623.2      NEAIASITKKYNTYPYLVGIEGQTPGDFHYLDGASVNYTNWYPGEPRGRGKEKCVEMYTD      230
NP_059025.2      NEAIASIAKKYNNYVYLGMIEDQTPGDFHYLDGASVNYTNWYPGEPRGQGKEKCVEMYTD      239
NP_001257574.1  NEAIASIAKKYNNYVYLGMIEDQTPGDFHYLDGASVNYTNWYPGEPRGQGKEKCVEMYTD      240
NP_001257576.1  NEAIASIAKKYNNYVYLGMIEDQTPGDFHYLDGASVNYTNWYPGEPRGQGKEKCVEMYTD      230
                  *****:*****:*****:*****:

NP_075623.2      GKWNDKGCLQYRLAICEF      248
NP_059025.2      GTWNDRGCLQYRLAVCEF      257
NP_001257574.1  GTWNDRGCLQYRLAVCEF      258
NP_001257576.1  GTWNDRGCLQYRLAVCEF      248
                  * . ***:*****:***

```

**Figure 3.6. CLUSTAL alignment of the mouse and rat Sftpa1 protein sequences. Listed on the left are the Protein GenBank Accession numbers (Table 3.1). \* = amino acid identity; : = conservative substitutions; . = semiconservative substitutions; blue line = ab115791 peptide sequence: WNDKGCLQYRLAICEF. Mouse = NP\_075623.2; Rat Isoform 1 = NP\_001257574, Rat Isoform 2 = NP\_059025.2 and Rat isoform 3 = NP\_001257576.**

Next, it was considered if Anti-Surfactant Protein A antibody (ab115791) could cross react with other mouse Surfactant proteins (B-D). Figure 3.7 shows the CLUSTAL alignment of the four surfactant mouse proteins, with surfactant D having the highest homology to SP-A. Next, we directly compared the SP-A peptide sequence against the SP-A and SP-D amino acid sequences. The CLUSTAL alignment depicted in Figure 3.8 shows that there is not 100% identify of the peptide against SP-D. Further analysis using SmartBLAST of the SP-A peptide sequence, demonstrated amino identity of 69% and similarity of 75% (Figure 3.9) (NCBI SMARTBLAST online database, 2019).

NP_075623.2	-----	0
AAA92021.1	-----	0
AAB34846.2	MAKSHLLQWLLLLPTLCCPGAITSASSLECAQGPQFQCQSLHAVQCRAHGCLQEVWG	60
AAA40010.1	-----	0
NP_075623.2	-----	0
AAA92021.1	-----MLPFLSMLV-----L-LVQ	13
AAB34846.2	HAGANDLCQECEDIVHLLTKMTKEDAFQEAIRKFLEQECDILPLKL-LVPRCRQVLDVY-	118
AAA40010.1	-----MDMSKVEVLMESPDPDYSAGPRSQFRIPCCPVHLKRLLIVVVVVVLLVVVV	49
NP_075623.2	-----MSL	3
AAA92021.1	PLGNLGAEMKSLSQRSVPNTCTLVMCSPTEENGLPGRDGRDREGPRGEKGDPLPGPMGL	73
AAB34846.2	--LPLVIDY-FQSQINPKAICNHVGLCPRGQAKPEQNPGMPDAV-----PNP-LL	164
AAA40010.1	IVGALLMGL-HMSQKHTEMLV-MS-----IGAPETQKRLA-----PSE-RA	88
NP_075623.2	GSLAFTLFLT-----VVAGIKCNGTEVCAGSPGIPGTPGNH---GLPGRDGRDGKGD	53
AAA92021.1	SGLQGPTGVPVPGKGENGSAGEPGPKGERGLSGPPGLPGIPGAPGKEGKQGNIGPQK	133
AAB34846.2	DKLVLPVLPGALLARPGPHT-----QDFSEQQLPIPLPFCWLCR-----TLIKR-	208
AAA40010.1	DTIA-----TFSIGSTGIVV---YDYQRLLTAYKPAAGTYCYIMK-----MAPES-	130
	. : * :	
NP_075623.2	PGPPGPMGPPGG--M-----PGLPGRDGL	75
AAA92021.1	PGPKGEAGPKGEVGPAGPMQGSTGAKGSTGPKGERGAPGVQAGPAGNAGAAGPAGPQGA	193
AAB34846.2	-----VQAV-----	212
AAA40010.1	-----IPSLEAFAR-----KLQNF-----AKPSTPTSKLGO	157
NP_075623.2	PGAPGAPGEHGDKEPG-ERG-LPGFPAYLDEELQTALYEIKHQILQ-----TMGVLS	126
AAA92021.1	PGSRGPPGLKGDGRVPG-DRG- IKGESGLPDSAALRQMEALKGKLRLEVAFVSHYQKAA	251
AAB34846.2	-----IPKGVLAVALVSQVCHVVPLVVGICQCLAERYTVLLLDA	251
AAA40010.1	-----EEGHDTGSESDSSGRDLAFLGLAVSTLCGELPLYI-----	193
	. . .	
NP_075623.2	LQGSMLS--VGDKVFTNGQSVNFDTIREMCTRAGGHIAAPRNPEENEAIASITKKYNTY	184
AAA92021.1	LFPDGRS--VGDKIFRTADSEKPFEDAQEMCKQAGGQLASPRSATENAAIQQLITAHNKA	309
AAB34846.2	LLGRVVPQLVCGLVLR-----CSTE--DAMGPALP---AVEPLIEEW---	288
AAA40010.1	-----	193
NP_075623.2	PYLVGIEGQTPGDFHYLDGASVNYTNWYPGEPRGR--GKEKCVEMYTDGKWND-----	235
AAA92021.1	AFLSMTDVGTEGKFTYPTGEPLVYSNWAPGEPNNN--GGAENCVEIFTNGQWND-----	361
AAB34846.2	PLQ-----DTEC---HFCKSVINQAWNTSEQAMPQAMHQACLRFWLDROKCEQFVEQHM	339
AAA40010.1	-----	193
NP_075623.2	-----KGCLQYRLAICEF-----	248
AAA92021.1	-----KACGEQRLVICEF-----	374
AAB34846.2	PQLLALVPRSQDAHITCQALGVCEAPASPLQCFQTPHL	377
AAA40010.1	-----	193

**Figure 3.7. CLUSTAL alignment of the mouse surfactant protein sequences. Listed on the left are the Protein GenBank Accession numbers. \* = identities; : = conservative substitutions; . = semiconservative substitutions; blue line = ab115791 peptide sequence: WNDKGCLQYRLAICEF. NP\_075623.2 = pulmonary surfactant-associated protein A precursor; AAB34846.2 = surfactant protein B; AAA40010.1 = pulmonary surfactant protein SP-C; AAA92021.1 = surfactant protein D.**

SpD	MLPFLSMLVLLVQPLGNLGAEMKSLSQRSVPNTCTLVMCSPTENGLPGRDGRDREGPRG	60
Peptide	-----	0
SpA	-----	0
SpD	EKGDPGLPGPMGLSGLQGPTGPVGPKEGENSAGEPGPKGERGLSGPPGLPGIPGPAGKEG	120
Peptide	-----	0
SpA	-----MSLGS�AFTLFLT-----VVAGIKCNGTEVCAGSPGIPGTPGNH---G	40
SpD	PSGKQGNIGPQGKPGPKGEAGPKGEVAGPMQGSTGAKGSTGPKGERGAPGVQGAPGNAG	180
Peptide	-----	0
SpA	LPGRDGRDGIKGDPPGPMGPPGG--M-----	66
SpD	AAGPAGPAGPQGAPGSRGPPGLKGRGVPGDRGIKGESGLPDSAAALRQOMEALKGKLQRL	240
Peptide	-----	0
SpA	----PGLPGRDGLPGAPGAPGEHGDKEPGERGLPGFPAYLDEELQTALYEIKHQILQ--	120
SpD	EVAFSHYQKAALFPDGRSVGDKIFRTADSEKPFEDAQEMCKQAGQLASPRSATENAAIQ	300
Peptide	-----	0
SpA	----TMGVLSLQGSMLSVMGDKVFSTNGQSVNFDTIEMCTRAGGHIAAPRNPEENEAIA	175
SpD	QLITAHNKAFLSMTDVGTEGKFTYPTGEPLVYSNWAPGEPNNNGGAENCVEIFTNGQWN	360
Peptide	-----WN	2
SpA	SITKKYNTYPYLVGIEGQTPGDFHYLDGASVNYTNWYPGEPRGR-GKEKCVEMYTDGKWN	234
		**
SpD	DKACGEQRLVICEF	374
Peptide	DKGCLQYRLAICEF	16
SpA	DKGCLQYRLAICEF	248
	**.* : **.****	

**Figure 3.8. CLUSTAL alignment of the ab115791 peptide sequence against mouse surfactant A and B protein sequences. Listed on the left are the Protein GenBank Accession numbers. \*= amino acid identity; := amino acid similarity; SP-A = NP\_075623.2 = pulmonary surfactant-associated protein A precursor; SP-D = AAA92021.1 = surfactant protein D.**

pulmonary surfactant-associated protein D precursor [Mus musculus]

Sequence ID: [NP\\_033186.1](#) Length: 374 Number of Matches: 1

Range 1: 359 to 374 [GenPept](#)

▼ Next Match ▲ Previous Match

Score	Expect	Method	Identities	Positives	Gaps	Frame
32.0 bits(71)	0.027()	Composition-based stats.	11/16(69%)	12/16(75%)	0/16(0%)	
Query	1	WNDKGCLQYRLAICEF	16			
		WNDK C + RL ICEF				
Sbjct	359	WNDKACGEQRLVICEF	374			

Figure 3.9. SmartBLAST of the ab115791 peptide sequence.

## 4 Chapter 4

### Results

---

#### 4.1 Histology, IHC and western blotting

This section sees a progression from basic histology to IHC to western blotting. Basic histology by H&E staining was used initially to clarify structural and morphological aspects of the various simple epithelia of rat and mouse lung before moving onto rodent middle ear. Immunohistochemistry enabled identification of SP-A protein and CKs within cells and tissues pointing towards a more functional characterisation of the epithelia. Western blotting enabled validation of the antibodies applied to various tissues.

##### 4.1.1 Histology of rat lung

Lungs from Sprague-Dawley rats were easily expanded using fresh 5% PFA solution. They were then dehydrated through the range of alcohols until paraffinised. Initial staining with H&E was sub-optimal in that there is less contrast between the weak blue for haematoxylin and stronger red for eosin but adequate to outline alveolar spaces, epithelial cells, capillaries and larger vessels as shown in below in Fig 4.1.

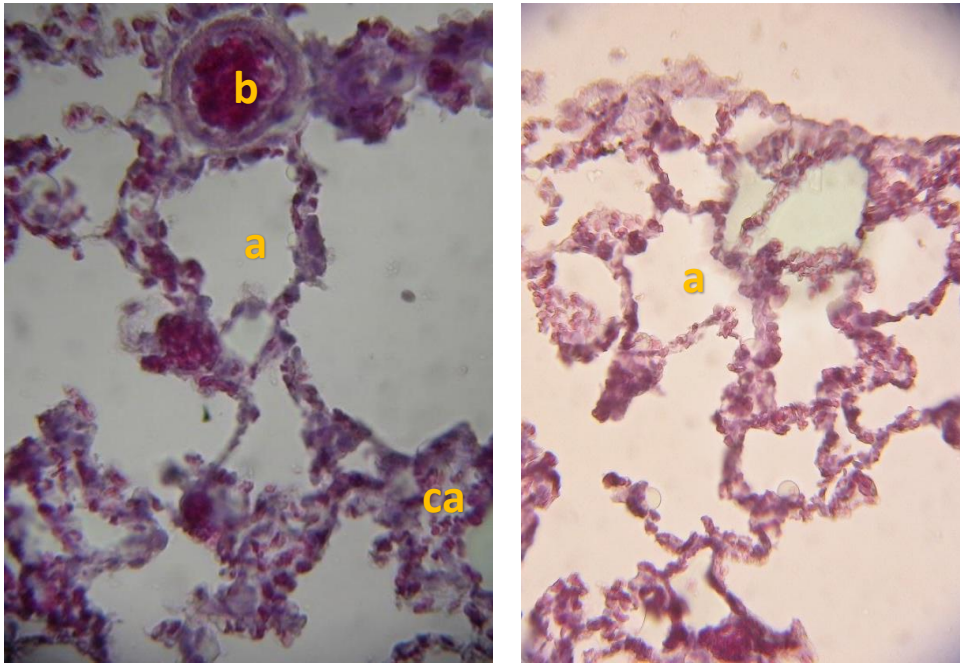


**Figure 4.1.** Initial results for H&E of rat lung. Shown are expanded alveoli (a), adjacent blood vessels (b) and engorged capillaries (ca).

#### **4.1.2 Histology of mouse lung**

Mouse lung is more delicate and far easier to rupture when expanded with liquid fixatives. Nevertheless, the experience gained from rat lung helped to refine methods for mouse specimens. H&E staining shows the general morphological differences between cells of simple epithelium such as cell height and whether or not these are ciliated.

The transition from terminal bronchioles directly to alveolar ducts is easily seen in low power magnification (Fig 4.2A). The terminal airways are lined by secretory Clara cells (Fig 4.2B). At highest power X100 one can confirm that these lack cilia (Fig. 4.2C). They are columnar but not pseudo-stratified. It is a particular characteristic of mice that terminal bronchioles are lined entirely by Clara cells (Fig. 4.2D; Irwin, 2003). Clara cells are interesting also because they are capable of secreting surfactant protein.

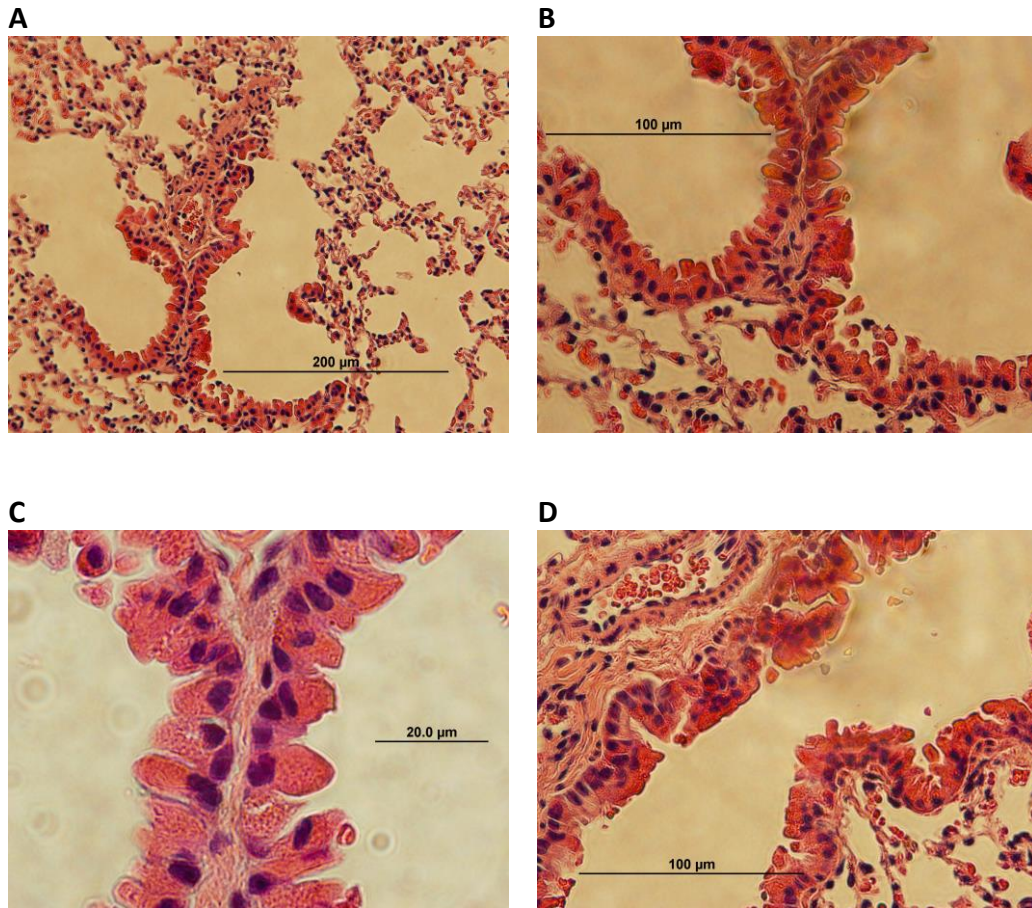


**Figure 4.2.** H&E stained sections showing distribution of Clara cells with their strong pink cytoplasm and their histological features. Fig 4.2A shows alveolar ducts leading to alveoli. Fig 4.1 A is X20, Fig 4.2 B, and Fig 4.2D are X40 and Fig 4.2C is X100 magnification.

Using H&E staining with higher power X100 magnification, various cell types can be distinguished within the expanded alveoli which assume an almost polygonal shape (Fig. 4.3). The presence of cells with rounded nuclei at the “corners” of alveoli is interpreted as type II alveolocytes. Flat cells with flat nuclei lining the side walls of the alveoli are interpreted as type I cells although some of these could also represent the endothelial cells of adjacent capillaries which abound in alveoli. Pulmonary macrophages are present in the luminal surface of alveoli. These engulf cellular debris, microbes and used proteins including surfactant.

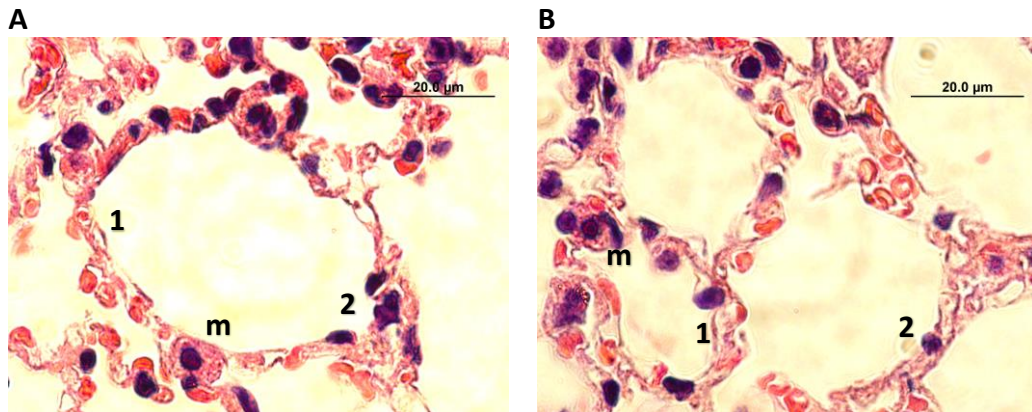


**Figure 4.3.** Oil immersion image X100 showing alveoli containing very thin, flat type I cells (1), cuboidal type II cells (2) and large foamy macrophages (m). Capillaries are evident by their enucleate red blood cells.

#### **4.1.3 Histology of mouse middle ear epithelium**

The middle ear begins in the nasopharynx, the common cavity at the back of the nose from which a right and left Eustachian tube ascend to their respective middle ear cavities (see Figures 4.4 A and 4.4B below). The lower ends of the Eustachian tubes are supported by muscles related to the palate, pharynx and larynx. The upper ends of the Eustachian tubes in mice are supported by cartilage whereas the human Eustachian tube has a cartilaginous lower end and a bony upper end. Also visible in the nasopharynx is free mucus and cellular debris some of which comes from the nose and paranasal sinuses and some of which comes from the middle ear cavity. This is because the epithelium of the Eustachian tube is lined by ciliated pseudostratified epithelium which beats mucus and debris down towards the common airway (nasopharynx) in the same way as the epithelium of the trachea beats mucus up to the common larynx and pharynx. Several paraffin sections were taken from both BALBc and C57/B6 mice from which a series of H&E slides were made corresponding to the various segments of the middle ear seen in the coronal (vertical) plane.

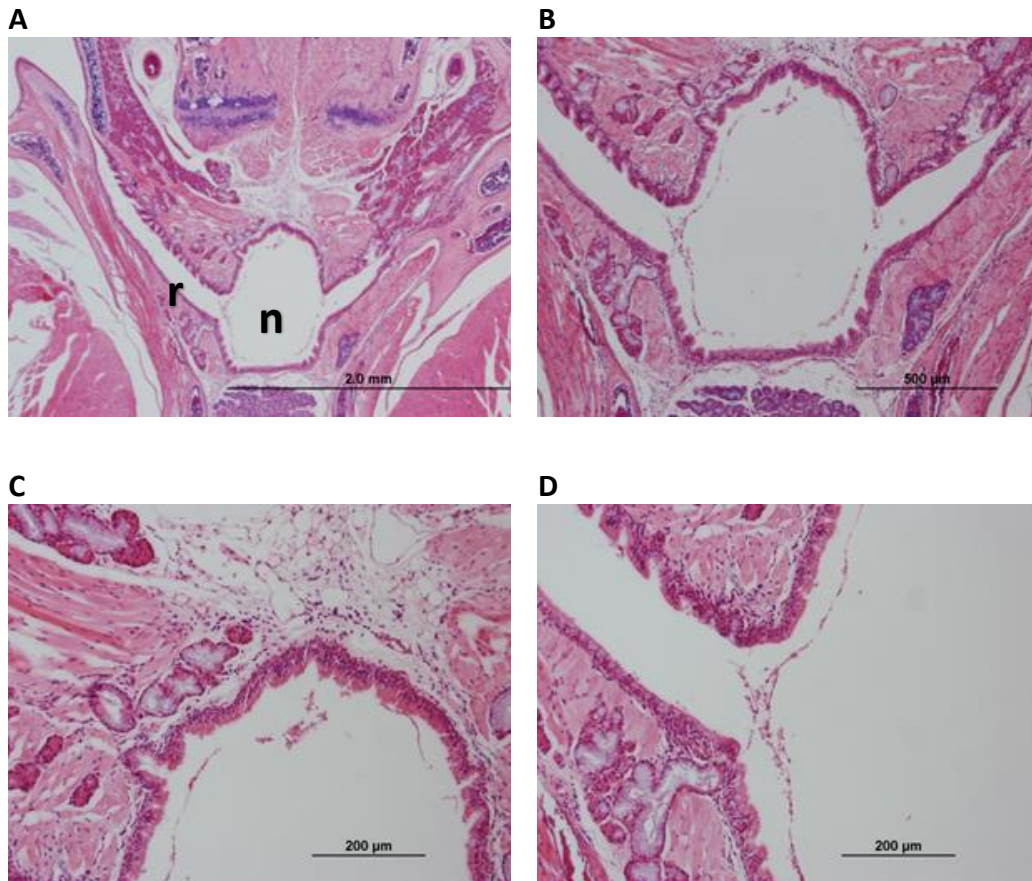


**Figure 4.4. Coronal cross-sections of nasopharynx and Eustachian tubes in BALBc mice using H&E staining. A. Panoramic view of nasopharynx (n) and a complete Eustachian tube orifice on the right side (r). The right tube extends into the middle ear cavity (tympaanum) via a narrowing (cartilaginous isthmus). Both Eustachian tubes show adjacent mucous glands. Magnification X2.5. B. Closer view showing pharyngeal openings of Eustachian tube with mucus and some cellular debris in the nasopharynx. Magnification X5. C. View of the roof of the nasopharynx showing epithelium which is pseudostratified, simple, columnar. Supporting connective tissue contains lymphoid tissue and mucous gland elements. D. Opening of pharyngeal end of right Eustachian tube with some mucus and cellular debris.**

The Eustachian tube is mostly cartilaginous at its upper end. The lower end near the medial or proximal opening is lined by ciliated columnar cells, often pseudostratified. More laterally, the tube has a narrow isthmus which is lined by flat cells which are usually simple but can appear stratified on oblique sections. The lateral or tympanic opening of the Eustachian tube into the middle ear is lined by ciliated epithelium and goblet cells.

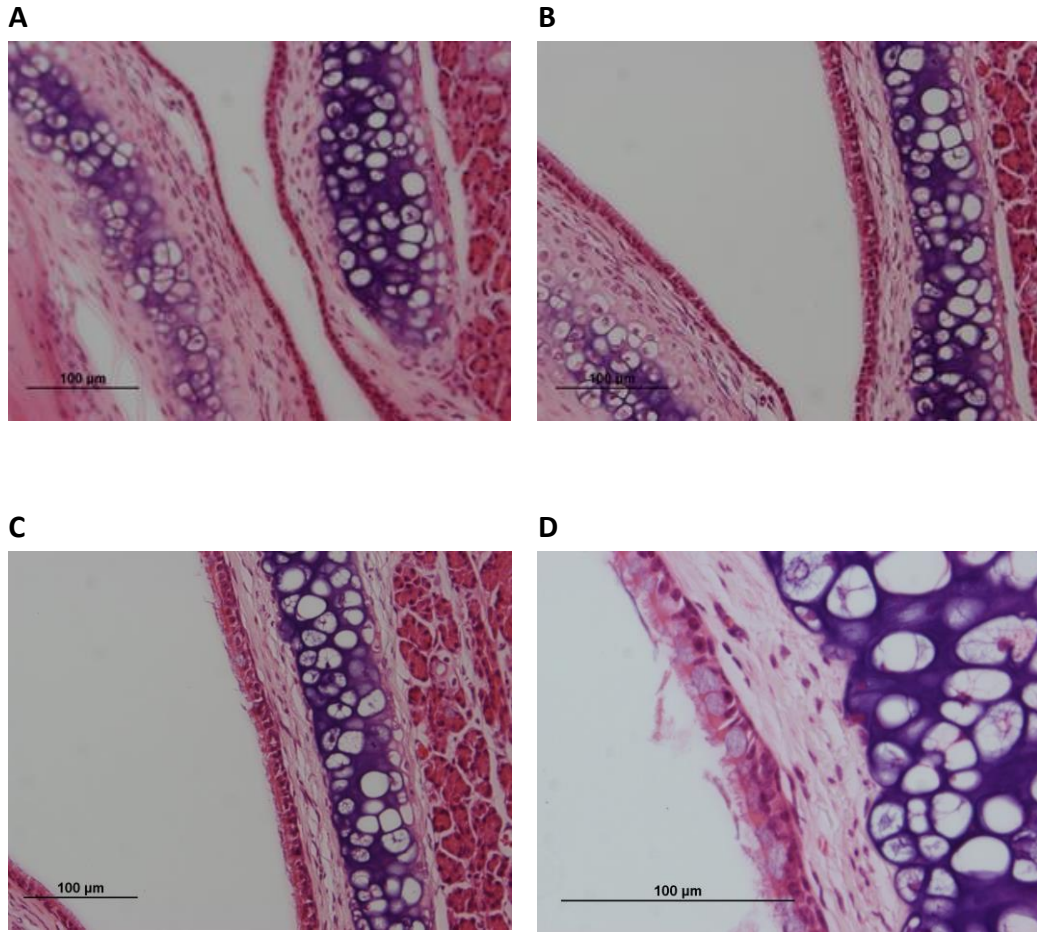


**Figure 4.5. Coronal cross-sections of BALB/c mice upper Eustachian tube adjacent to middle ear using H&E staining. Image A and B are X10 magnification; image C is X20, D is X40. A. Junction of right Eustachian tube with middle ear cavity (cartilaginous isthmus) showing simple epithelium with slight stratification sometimes referred to as transitional epithelium. B. Middle ear (tympanic) opening of right Eustachian tube showing change from transitional stratified epithelium to simple ciliated, low cuboidal epithelium. C. Lateral right Eustachian tube lumen showing mainly pseudostratified, low columnar, ciliated epithelium. D. Tympanic opening of Eustachian tube: Cartilaginous isthmus of lateral right Eustachian tube lumen showing mainly low cuboidal ciliated epithelium with Goblet cells.**

The next series of images (Figure 4.6 to Figure 4.9) begins at the roof of the middle ear cavity just beyond the tympanic opening of the Eustachian tube and moves further laterally to reach the upper tympanic membrane then down to the floor of the middle ear before returning to the Eustachian tube opening. There is a transition from ciliated cuboidal to flat squamous epithelium in the roof of the middle ear which is seen below (Figure 4.6).

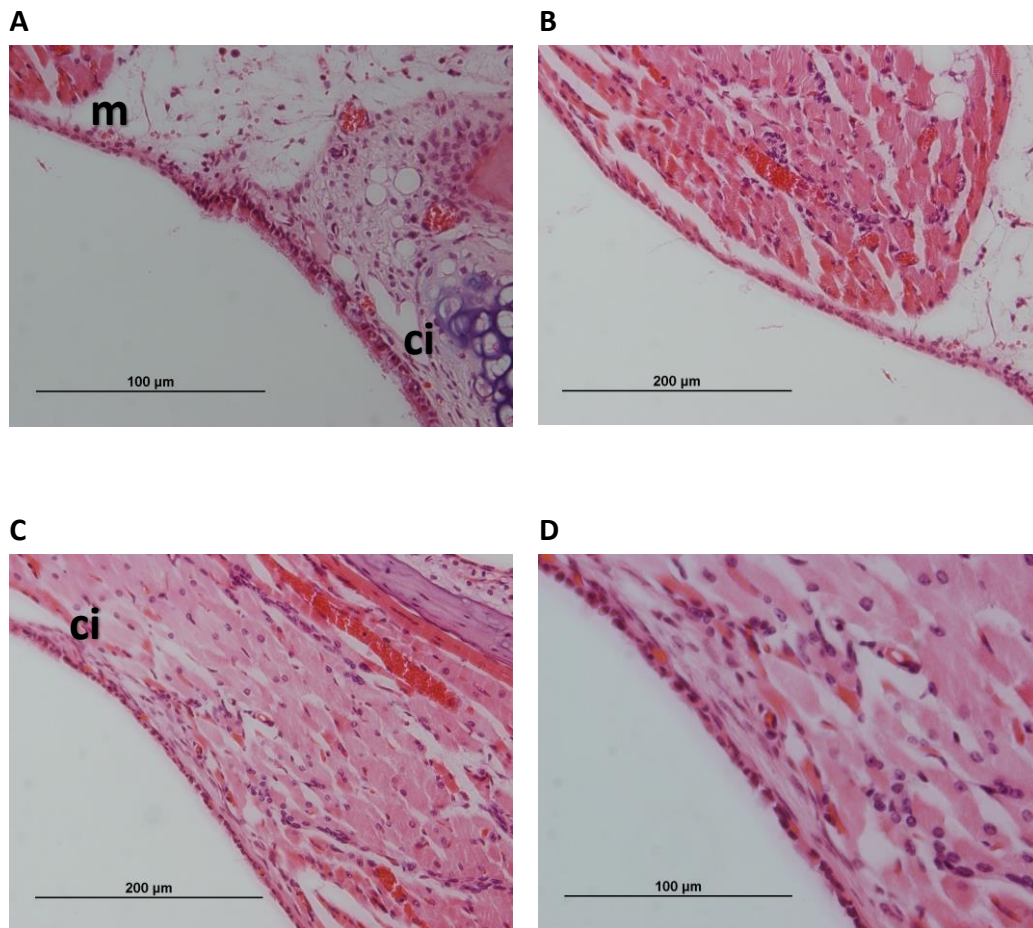
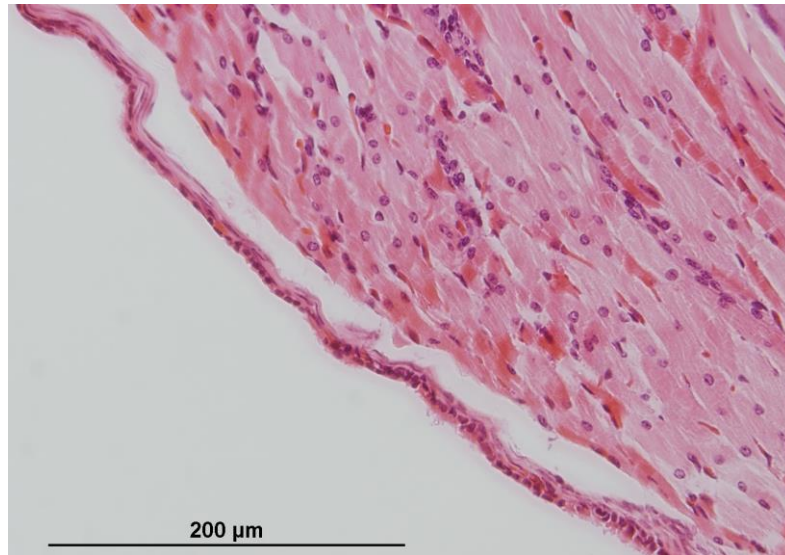


**Figure 4.6.** Coronal cross-sections of BALBc mice middle ear at the supero-medial level using H&E staining. Images A, B and C are X10 and D is X 40 magnification. A. Roof of right middle ear cavity showing the transition from cuboidal, ciliated epithelium on cartilage (ci) to flatter epithelium over the tensor tympani muscle (m). B. Roof of right middle ear cavity showing flatter epithelium overlying tensor tympani muscle. C. Roof of right middle ear cavity showing flatter epithelium overlying tensor tympani muscle undergoing transition to ciliated cuboidal epithelium (ci). D. Closer view of roof of right middle ear cavity showing flatter epithelium overlying tensor tympani muscle undergoing transition with cuboidal epithelium some of which is ciliated.

In the literature, the roof of the middle ear is considered mainly a region of flat epithelium suited to gas exchange but there are regions of ciliated epithelium suited to clearing any mucus or cellular debris.

**A**



**B**

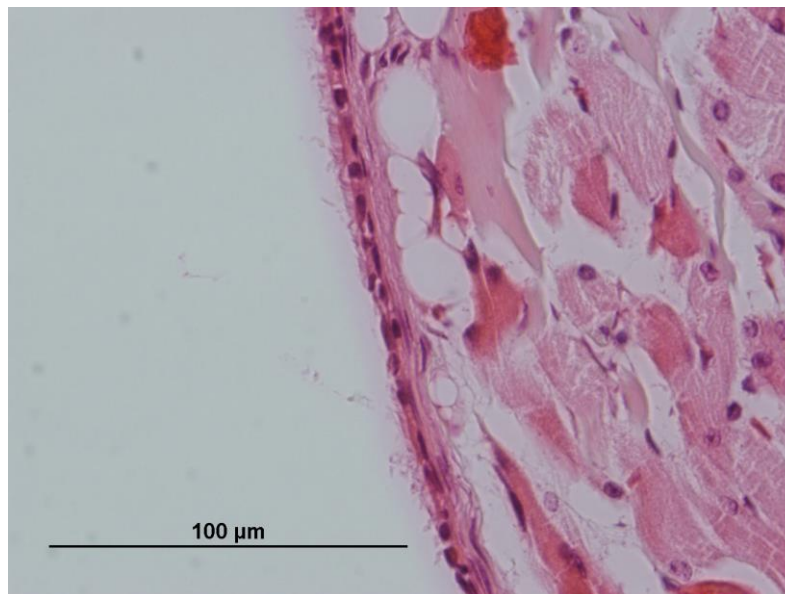


**Figure 4.7. Coronal cross-sections of BALBc mice middle ear using H&E staining. A. Roof of right middle ear cavity showing flatter epithelium with areas of cuboidal, ciliated epithelium. B. Closer view of roof of right middle ear cavity showing mostly cuboidal ciliated epithelium.**

The middle ear space has irregular boundaries due to the presence of adjacent structures including the hearing bones (ossicles), facial nerve as well as the stapedia artery which passes through the arch of the stapes bone. This artery is common to all mature rodents and is also present in the developing human foetus although it obliterates during later embryonic growth. There are also bone marrow spaces above the middle ear.

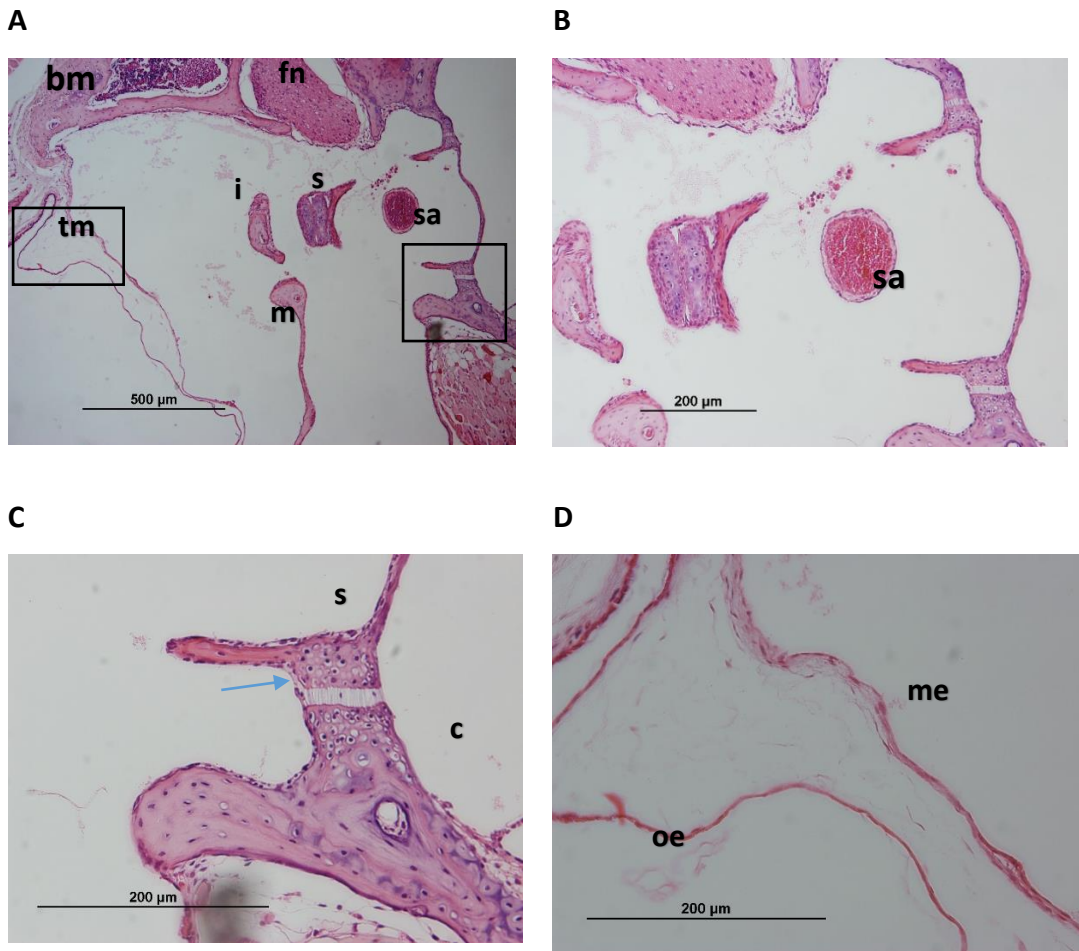


**Figure 4.8. Coronal cross-sections of BALBc mouse middle ear. A. Panoramic view of middle ear ossicles: malleus (m); incus (i); stapes(s); also seen is stapedial artery (sa); facial nerve (fn); bone marrow (bm) and tympanic membrane in two layers (tm). B. Closer view of stapes bone with its incomplete arch and stapedial artery (sa). C. Junction of stapes footplate (s) and oval window of cochlea (c) with intervening stapedial ligament (arrow). Note very thin flattened epithelium lining bony structures. D. Closer view of roof of right tympanic membrane showing a bilayered structure of modified outer squamous epithelium (oe) separated from flat middle ear epithelium (me).**

The flat epithelium is fairly continuous from the roof of the middle ear, over the medial surface of the tympanic membrane and onto the floor of the middle ear. The epithelium of the floor of the medial middle ear becomes ciliated in the antero-inferior part of the middle ear as it approaches the Eustachian tube opening. The following series of images are taken from the floor of the middle ear (Figure 4.9). The images begin with the lower eardrum (Fig 4.9A) and move medially to reach the mouth of the Eustachian tube (Fig 4.9D).

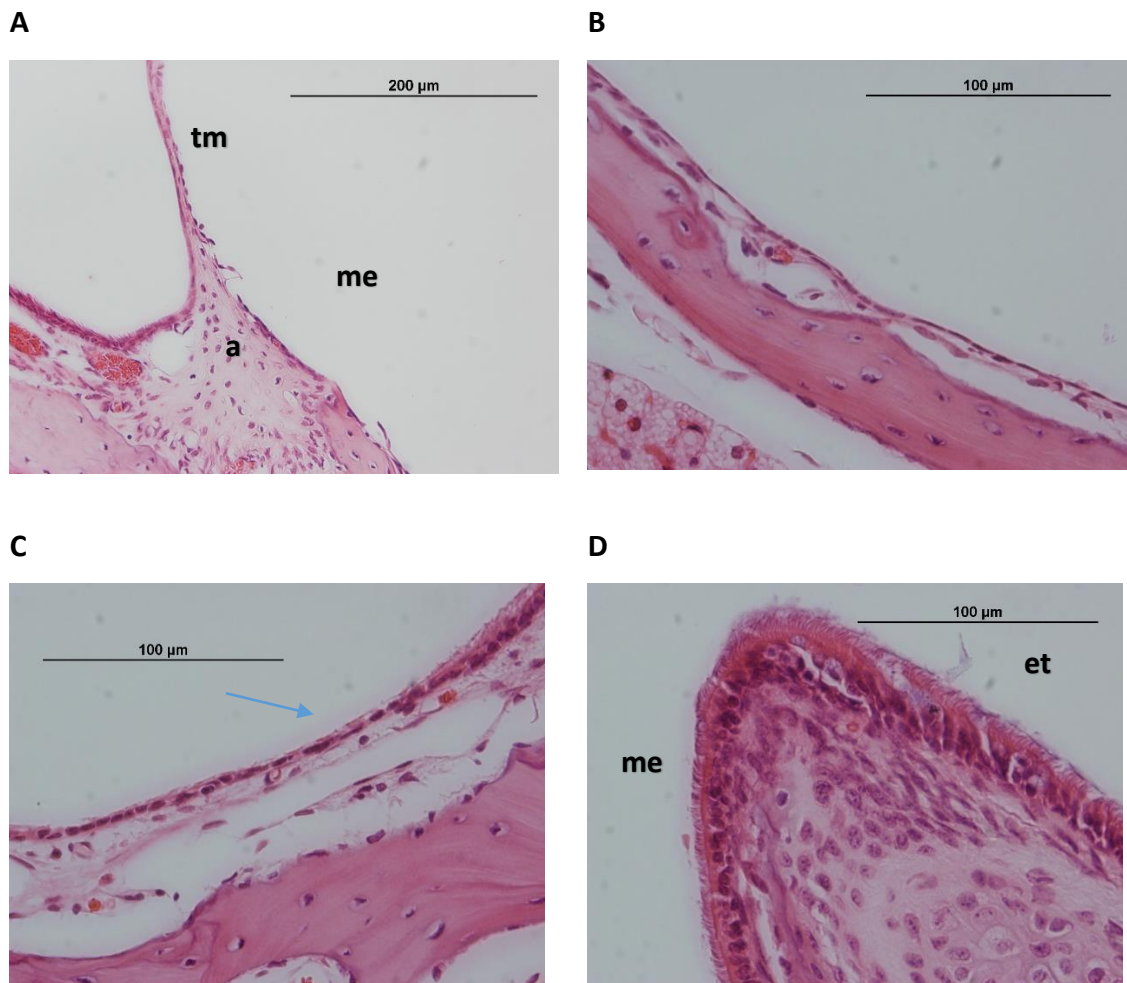


**Figure 4.9.** Coronal cross-sections of BALBc mice floor of middle ear using H&E staining. **A.** View of inferior tympanic membrane (tm) attached to connective tissue annulus (a) adjacent to the floor of the middle ear (me); the bilayered structure of the tm is still evident by the two layers of nuclei. **B.** Closer view of thin flattened epithelium lining bony floor of middle ear still within the postero-superior zone of the middle ear. **C.** Transition (arrow) from thin flattened epithelium lining bony floor of middle ear to the ciliated cuboidal epithelium. **D.** Closer view of ciliated epithelium of the middle ear (me) as it ascends to reach the mouth of the tympanic end of the Eustachian tube (et) which is supported by a cartilaginous framework.

#### 4.1.4 An unexpected finding in mouse middle ear: communications with bone marrow

Surrounding the mouse middle ear cavity are bone marrow nests situated within the bony wall. A number of mouse middle ears were sectioned in the axial plane including some C57/B6 mice which had been used in the initial inflammation experiments. In two of these animals it was noted that there were short passages in the bony walls of the middle ear passing from the bone marrow nests to reach the connective tissue stroma underlying the middle ear epithelium. We examined two BALBc mice by axial sectioning and found similar perforations. The communications are not an artefact of sectioning because they are lined by cells and the bony margins are generally smooth. The first image below (Figure 4.10) shows a low power panoramic view of the middle ear without any communications.

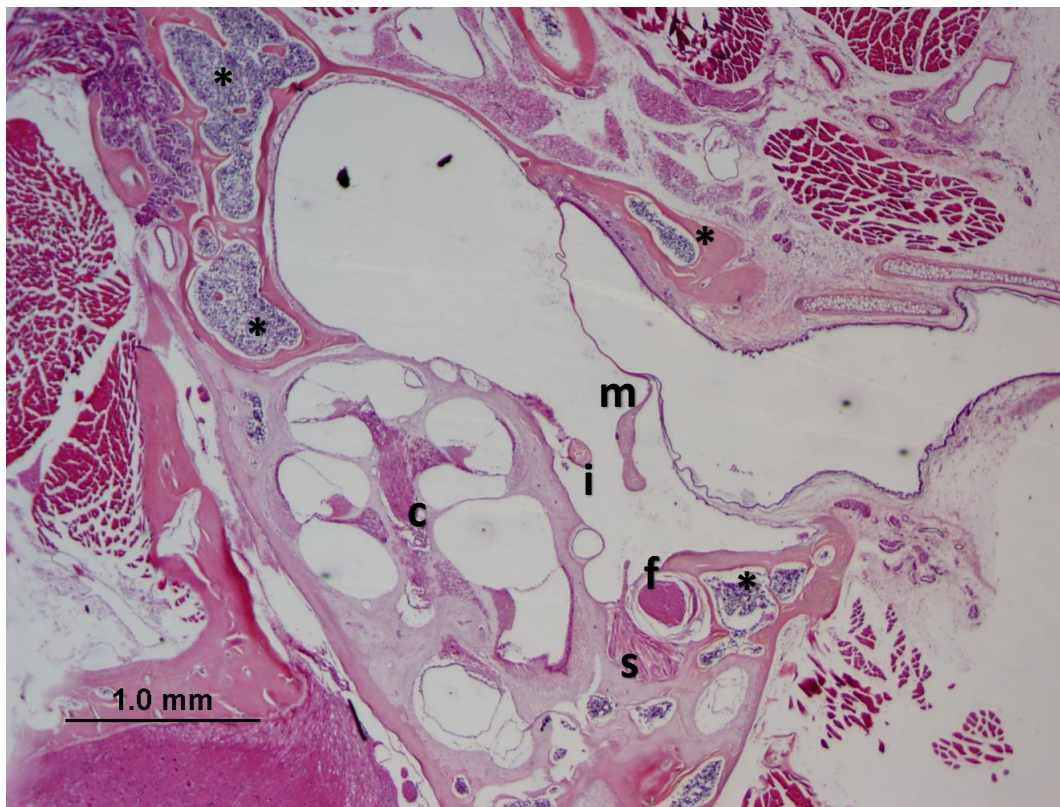
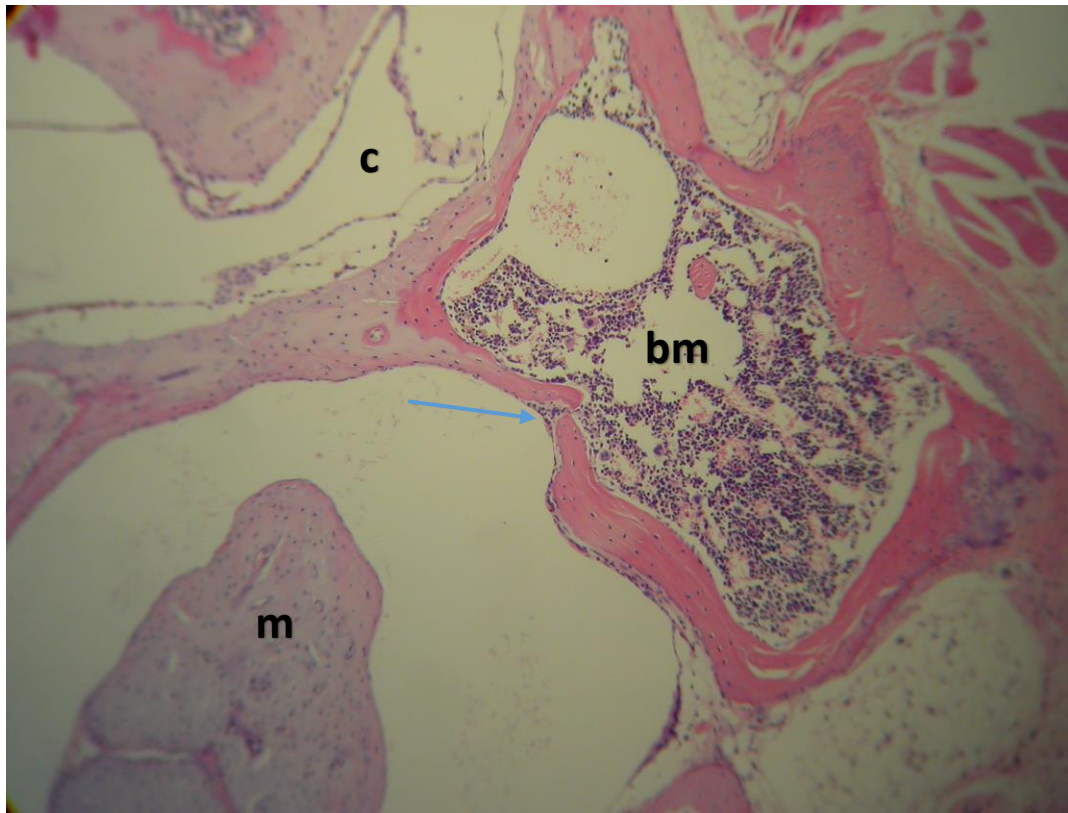


Figure 4.10. Axial cross-section of C57/B6 (17.2.17) mouse middle ear magnification X2.5. Note malleus bone (m), the incus (i), facial nerve (f), stapedius muscle (s), cochlea (c) and bone marrow nests (\*). There are no communicating passages in this image.

The next image below (Figure 4.11) shows a low power panoramic view of the middle ear with a communication passing from bone marrow to middle ear.



**Figure 4.11. Axial cross-section of BALBc mouse middle ear (magnification X2.5). Note malleus bone (m), the cochlea (c) anterior to the middle ear space and a bone marrow nest. Communicating passage shown by arrow.**

Below in Figure 4.12 is a closer view of the same communication between bone marrow space and the middle ear epithelium.

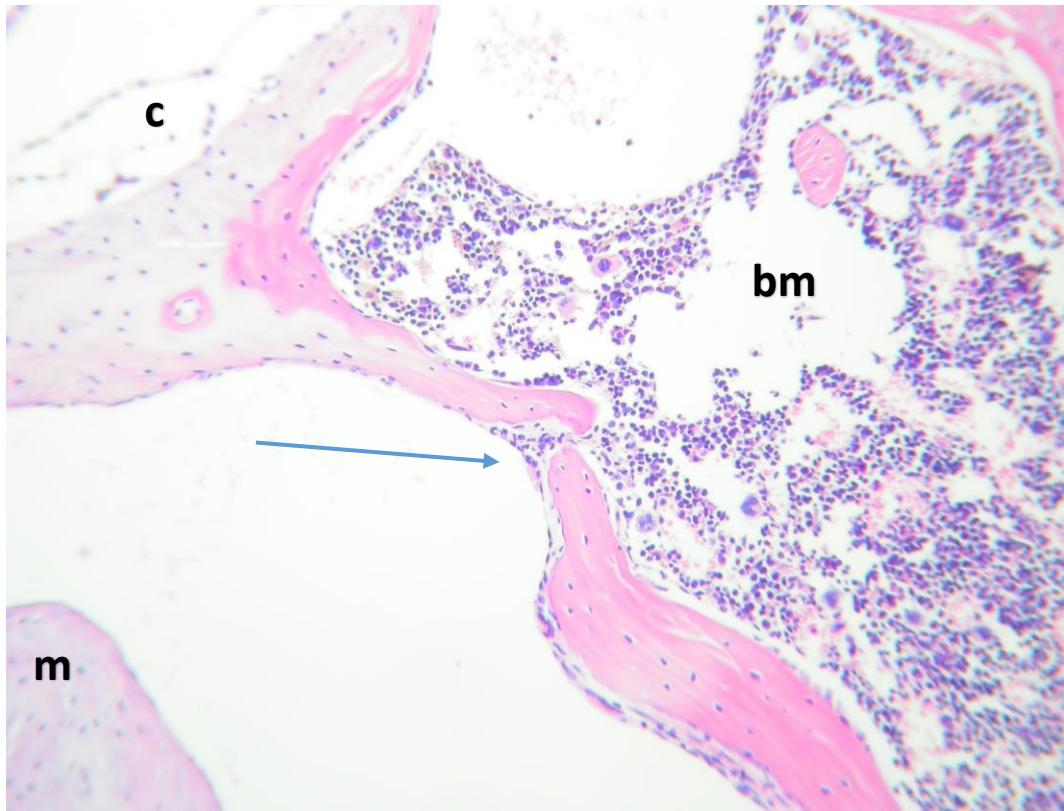


**Figure 4.12. Axial cross-section of BALBc mouse middle ear magnification X10. Note malleus bone (m), the cochlea (c) anterior to the middle ear space and a bone marrow nest (bm). Communicating passage with smooth margins shown by arrow.**

The bone marrow nests surround the middle ear space and, on axial cross-sections, can be seen within the membranous temporal bone forming the walls of the middle ear. This bone has stronger redness on than the paler otocyst-derived bone of the cochlea. The bone marrow nests can be found anterior, medial and posterior to the middle ear space.

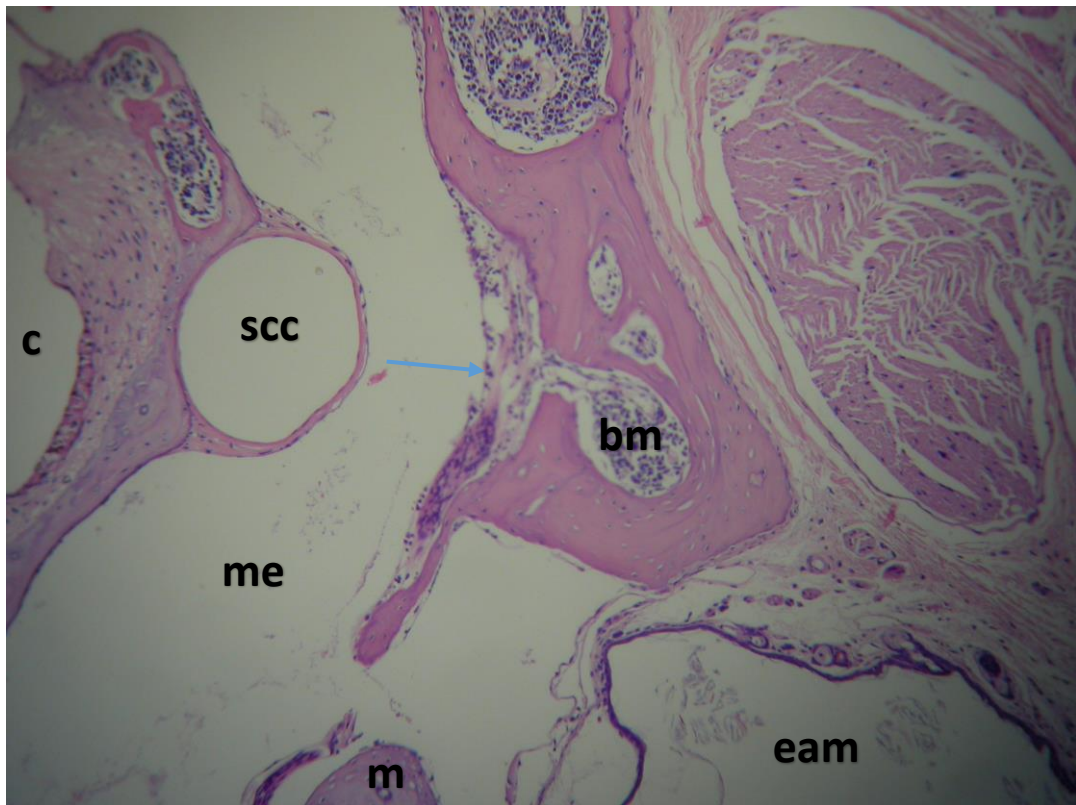
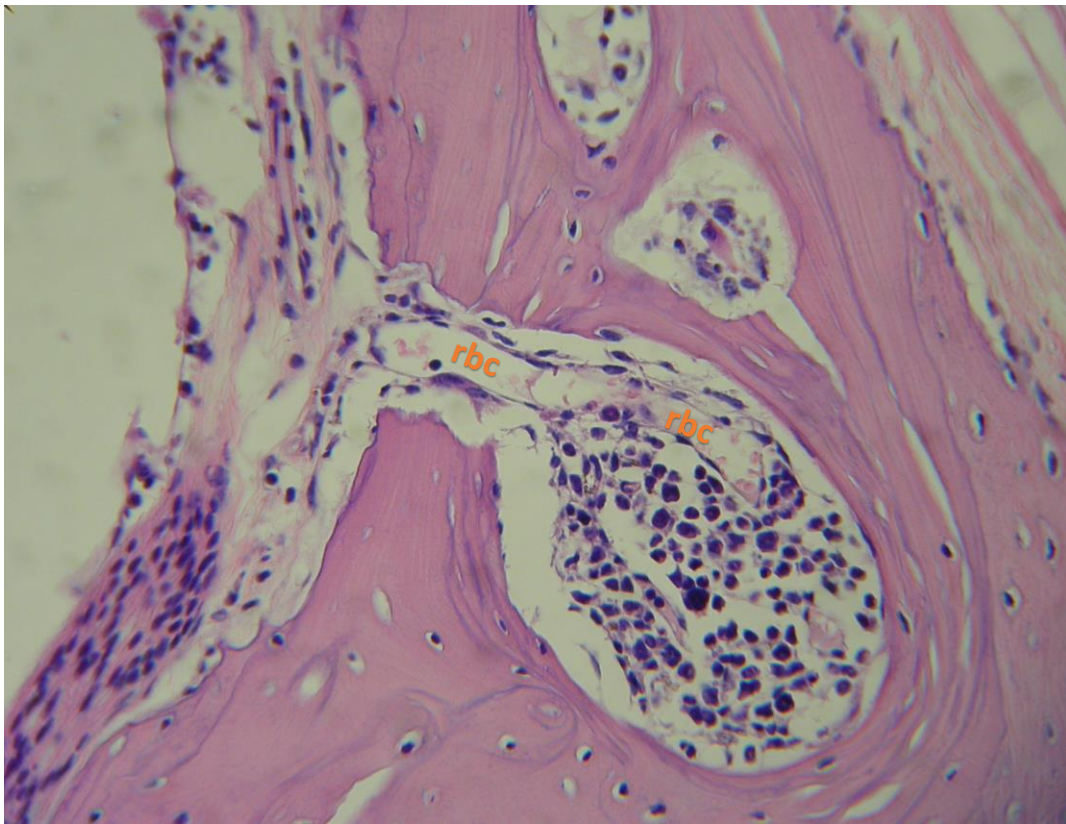


Figure 4.13. Axial cross-section of second BALB/c mouse middle ear (me) magnification X10. Note malleus bone (m) medial to external auditory meatus (eam), the cochlea (c) and an adjacent semi-circular canal (scc) opposite a bone marrow nest (bm). Communicating passage shown by arrow.

The same image at higher power the communication is reveals a capillary blood vessel within it. Red blood cells are present within the passage.



**Figure 4.14.** Axial cross-section of second BALBc mouse middle ear (me) at magnification X40. Note red blood cells (rbc) within a capillary within the bone communication. Flat endothelial cells line the capillary.

These bone communications were confirmed also in two mice of the C57/B6 strain shown below in figures 4.15 and 4.16.



**Figure 4.15. Axial cross-section of C57/B6 mouse bone communication (arrow) magnification X2.5. There are cells filling the communication between middle ear space (me) and the bone marrow nest.**

The communications may be questioned as either artefacts or genetic defects. Below in Figure 4.16 is an example of a bone communication and a separate artefact defect in bone possibly resulting from sectioning. At higher magnification, a blood vessel within the communication between the bone marrow nest and middle ear epithelium is shown (Figure 4.17).

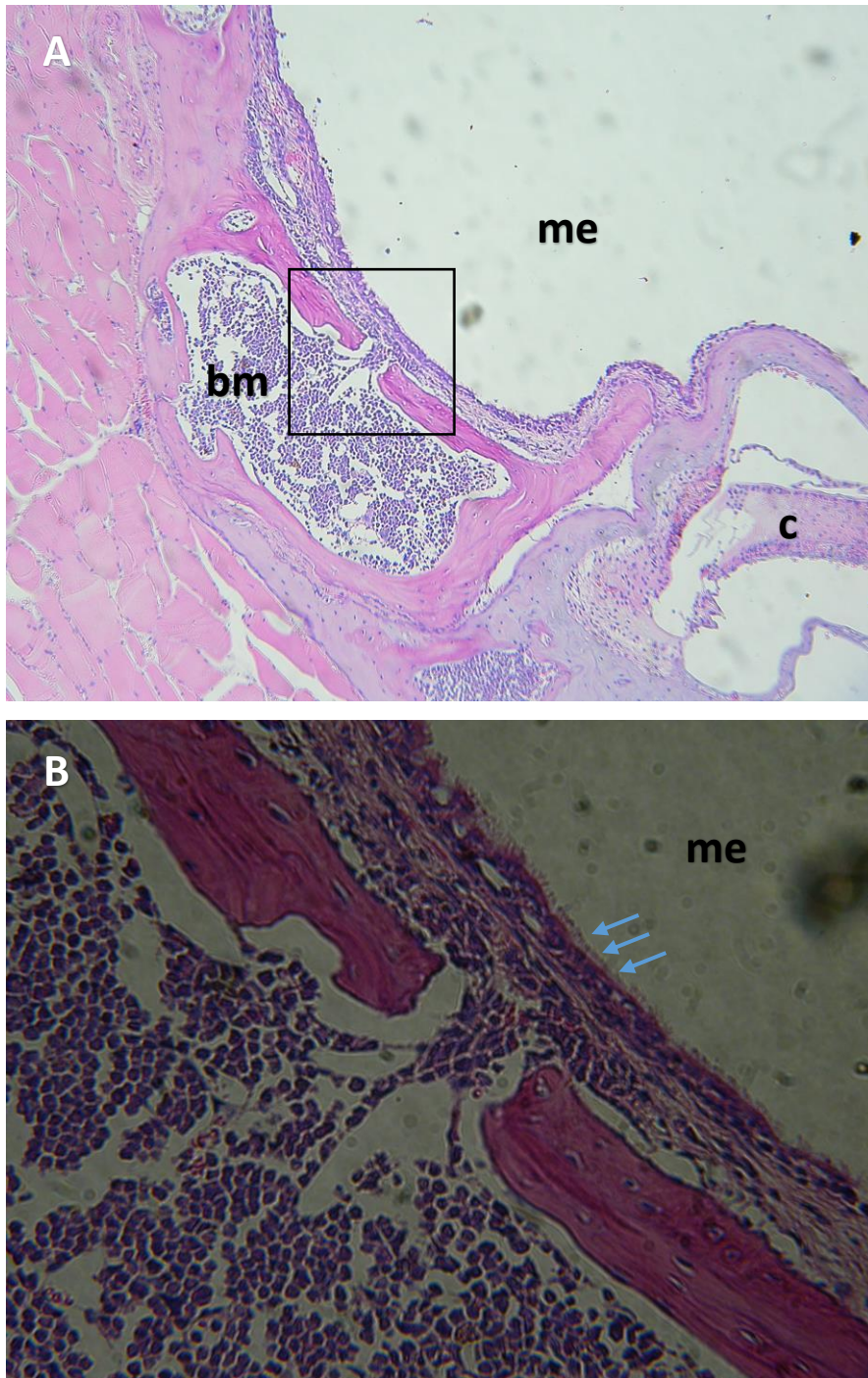


Figure 4.16. Axial cross-section of C57/B6 mouse bone communication (box). By comparison a breach in bone (thin arrow) with no intervening cells represents a sectioning artefact. There are cells filling the communication between middle ear space (me) and the bone marrow nest (bm). Note free cellular debris (cd). Magnification X2.5.



Figure 4.17. Higher magnification of Figure 4.16 showing a capillary (c) with red blood cells (rbc). There are cells filling the communication between middle ear space (me) and the bone marrow nest (bm). Magnification X40.

Closer examination reveals that the communication leads to ciliated epithelium in the middle ear (Figure 4.18).



**Figure 4.18. Axial cross-section of C57/B6 mouse bone communication.** A. There are cells filling the communication (box) between middle ear space (me) and the bone marrow (bm) nest. Note location adjacent to cochlea (c). Magnification X2.5. B. At X40 magnification, there are cells filling the communication between me and bm. Note ciliated middle ear epithelium (arrows).

On one occasion a communicating passage was found to be lined by cells (see Figure 4.20). These cells may be derived from bone marrow cells i.e., mesenchymal cells. Being near an epithelial lining they may be dendritic cells. They require further characterisation by using a selection of dendritic cell antibody markers recommended by Schraml & Sousa (2015) or alternatively a commercial mesenchymal cell marker panel available from Abcam.

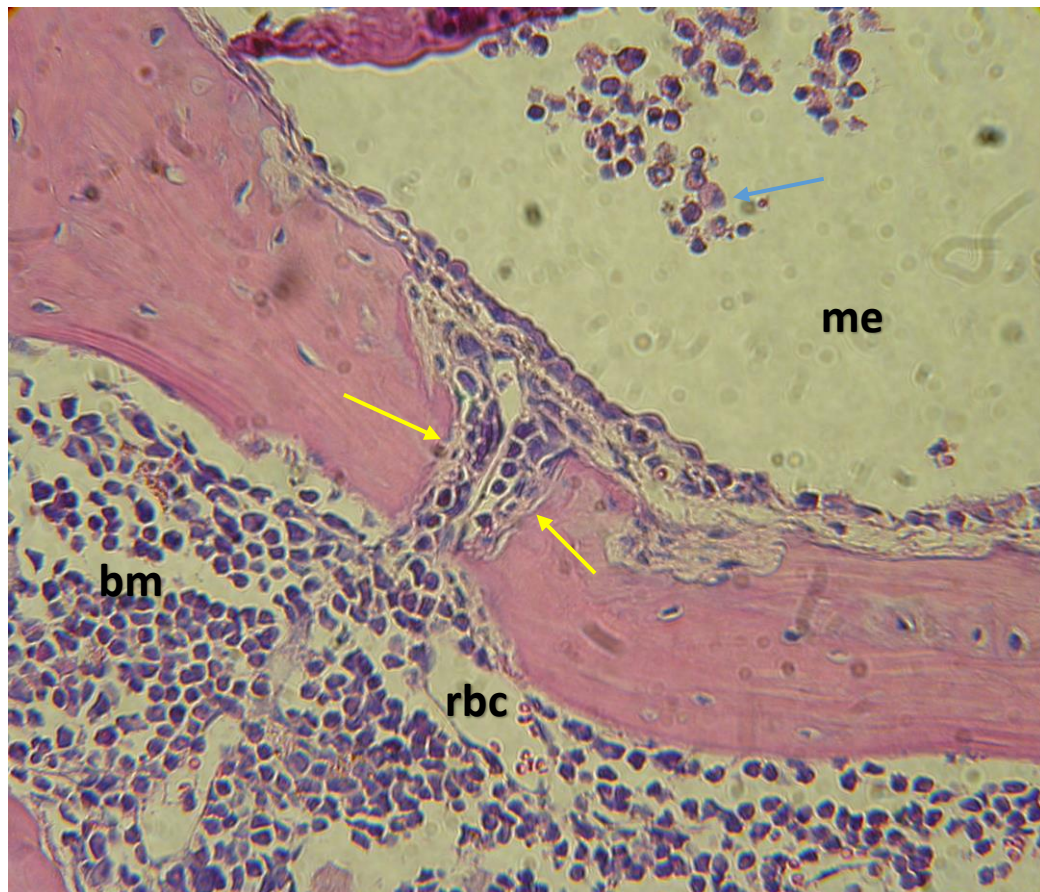


**Figure 4.19.** Axial cross-section of C57/B6 mouse communication at magnification X40. Closer view shows presence of a double layer of cells (yellow arrows) lining the wall of the communication between middle ear space and the bone marrow nest (bm). There is also a capillary present close to the communication containing red blood cells (rbc). Amongst cellular debris in the middle ear are some large cells with eccentric nuclei (blue arrow) which probably represent macrophages analogous to the “free” pulmonary macrophages seen in lung spaces.

A communication between bone marrow and middle ear epithelium is a short perforation and may be called a foramen (plural foramina). Foramina are found in bone elsewhere in the body to transmit nerves and blood vessels. This will be further discussed in Chapter 5.

## **4.2 Immunohistochemistry**

Prior to IHC testing using mouse tissue (lung and middle ear), rat lung tissue was examined first since the expression of the antibodies to be tested was originally confirmed in type I and type II alveolocytes (Kasper, 1997; Helms, 2008). Five antibodies were tested against SP-A and cytokeratins CK7, CK8, CK18 and CK19. In general, antibodies to rat SP-A are cross-reactive with mouse SP-A. In each IHC experiment four images were taken and depicted: (A) the primary antibody signal; (B) DAPI nuclear stain of tissue; (C) the merged composite image of the primary antibody and DAPI stain and (D) control images by omission of the respective primary antibody. An isotype control staining was applied to rat lung as a negative control using a pre-immune rabbit antibody (Rb 086199, Life Technologies) and confirmed negative with no signal evident above background (data not shown).

### **4.2.1 Rat lung antibody to SP-A**

At very low magnification (10X), SP-A is best seen in continuity in the walls of large airways and sporadically in the corners of alveolar walls. The continuous signal in the larger airways corresponds to SP-A present in the Clara (club) cells of bronchioles (Figure 4.20). These are columnar, secretory cells which are non-ciliated (see H&E Fig 4.2). Within alveoli, type II alveolocytes are isolated between sheets of type I cells, often in the corners of the alveolar sacs. Clara cells occur in continuous sheets in the upper or proximal airways. As a consequence, the type II cell gives an infrequent or sporadic signal in the alveolar spaces of lung tissue.

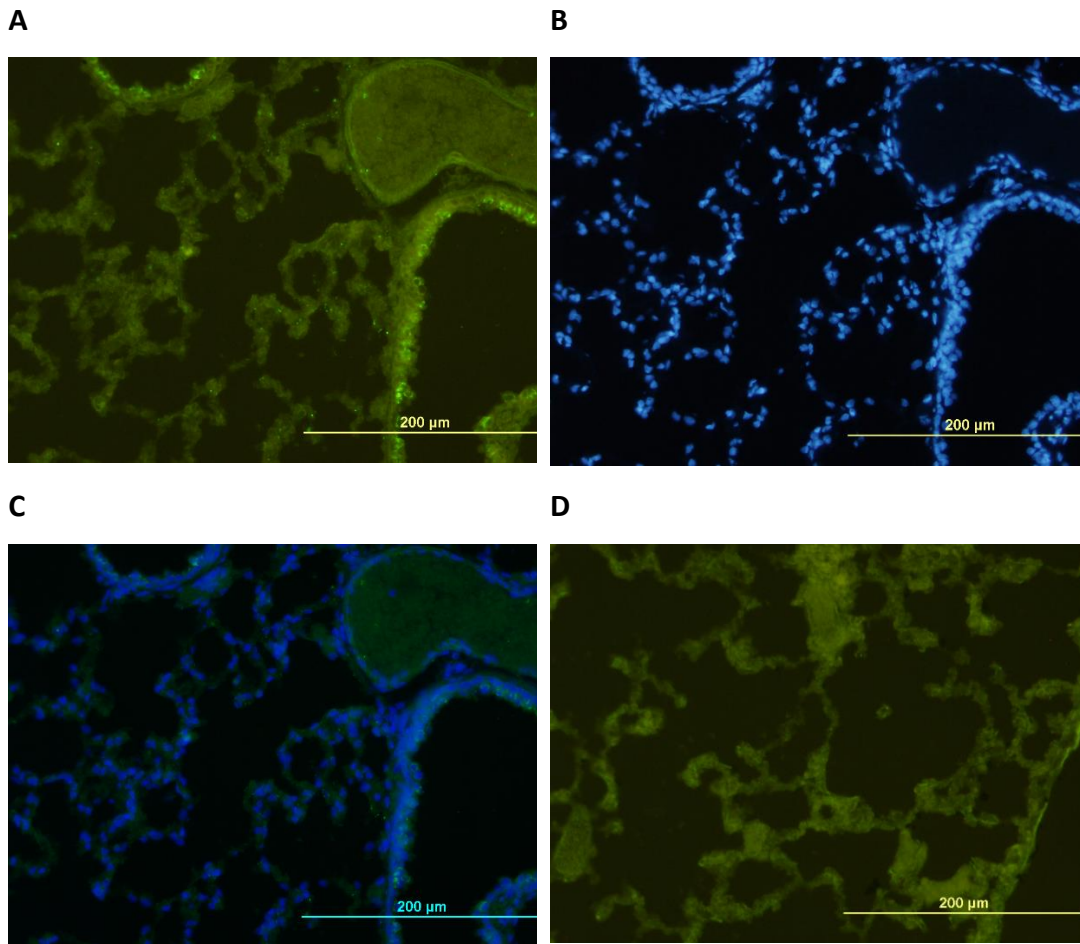


**Figure 4.20. IHC of Rat lung with SP-A 1:500 signal visible at 10X magnification. A. Shows apple-green 1:500 A SP-A signal above background. B is nuclear DAPI stain. C. Composite image shows discoloration of primary antibody signal. D. Control image from non-contiguous section of same paraffin block showing no fluorescence signal. Scale bar = 200 μM.**

In rat lung, higher power is required to appreciate the intracellular signal of SP-A. A merged image of SP-A signal and nuclear DAPI stain can reveal a perinuclear location of SP-A as in the image below (Fig 4.21C).

At times, merging images can obscure the antibody signal i.e., the blue DAPI signal can obscure green fluorescence. Below, the SP-A signal can be seen in alveolar walls in a perinuclear location (Fig. 4.21A, C). However, the merged image causes a discoloration effect possibly due to a layering effect within the programme.

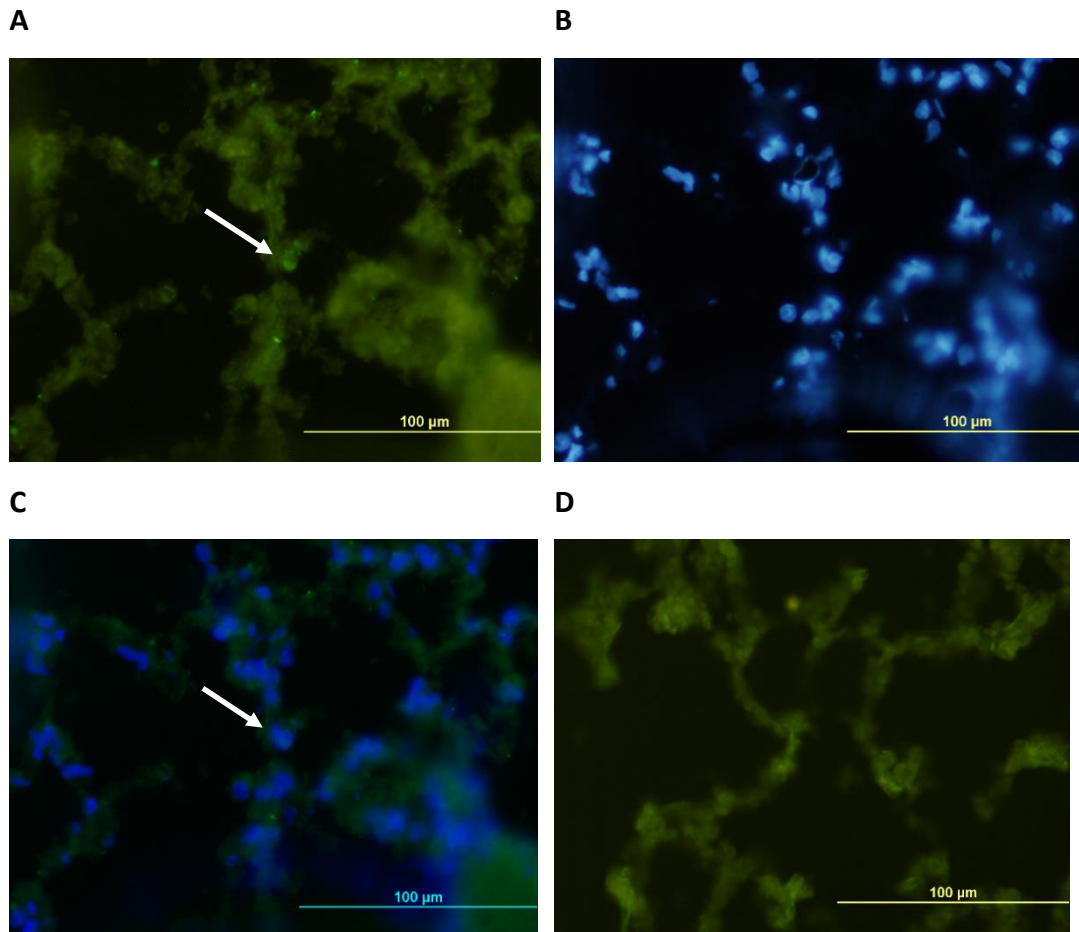


**Figure 4.21. IHC of Rat lung with SP-A 1:500. A. signal clearly visible at 20X magnification (arrow) located at corner or margin of lung alveolus. B is nuclear DAPI stain. C. Composite merged image still shows significant discoloration of primary antibody signal (arrow). D is control image from non-contiguous section of same paraffin block showing background signal only. Scale bar = 100 µM.**

#### 4.2.2 Rat lung antibody to CK18

CK18 is generally positive in cells which secrete SP-A such as type II cells and Clara cells. Thus, it gives a more sporadic signal within alveoli than CK19 because type II cells are fewer. In the image below (Figure 4.22), the lower magnification also shows the continuous signal in the large airways occurs in secretory, non-ciliated columnar cells (Clara cells or club cells).

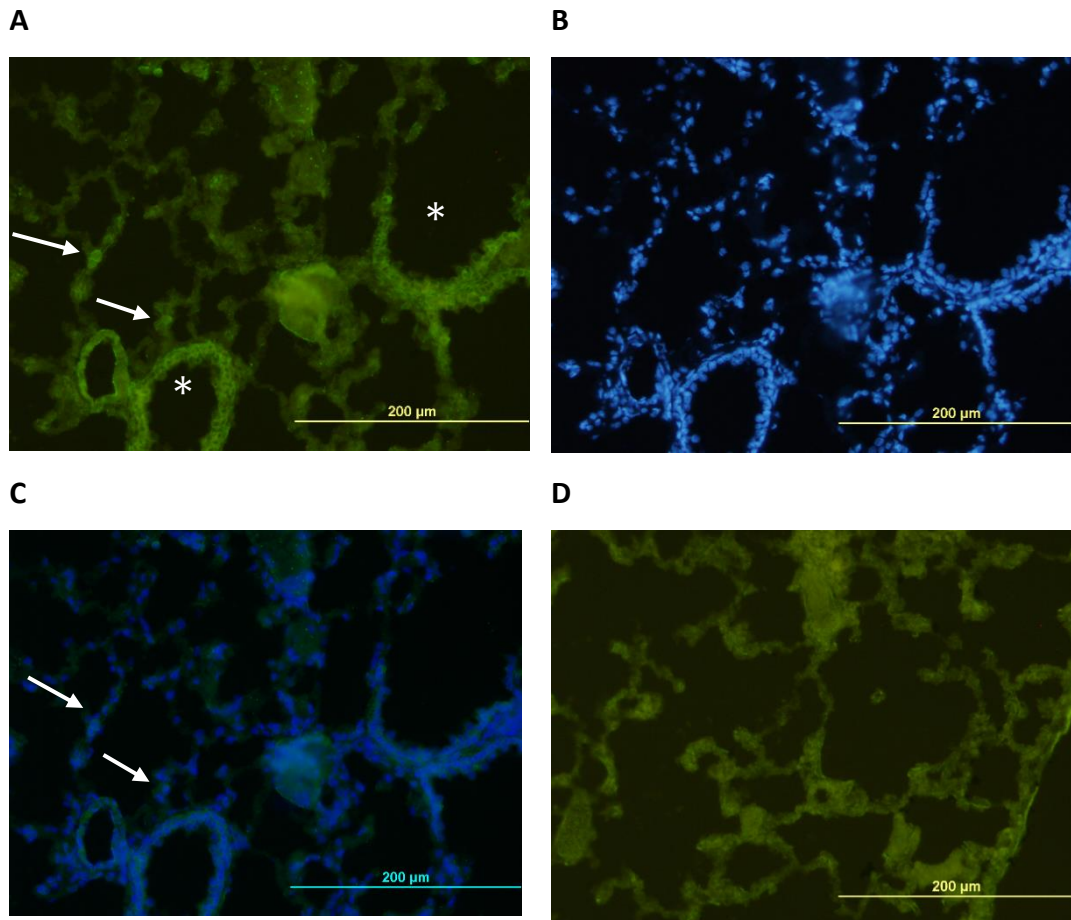


**Figure 4.22. Rat lung with CK18 antibody at 10X magnification. This shows signal in primary (A) and, to lesser extent, in the composite images (C). A. the signal is much more continuous in the larger airways (asterisk) where it corresponds to Clara cells than in the alveolar walls (arrows) where it corresponds to type II alveolocytes. B. DAPI nuclear stain. D. control from a non-contiguous slide omitting primary antibody. Scale bar = 200 μM.**

At slightly higher power (40X), the signal for CK18 is less continuous in the alveolar walls than CK19 (Fig. 4.23). In the primary image below (Fig. 4.23A), the signal is seen in the alveolar walls as a round rather than a flat signal due to the perinuclear location. This is more in keeping with signal from a type 2 alveolocyte.

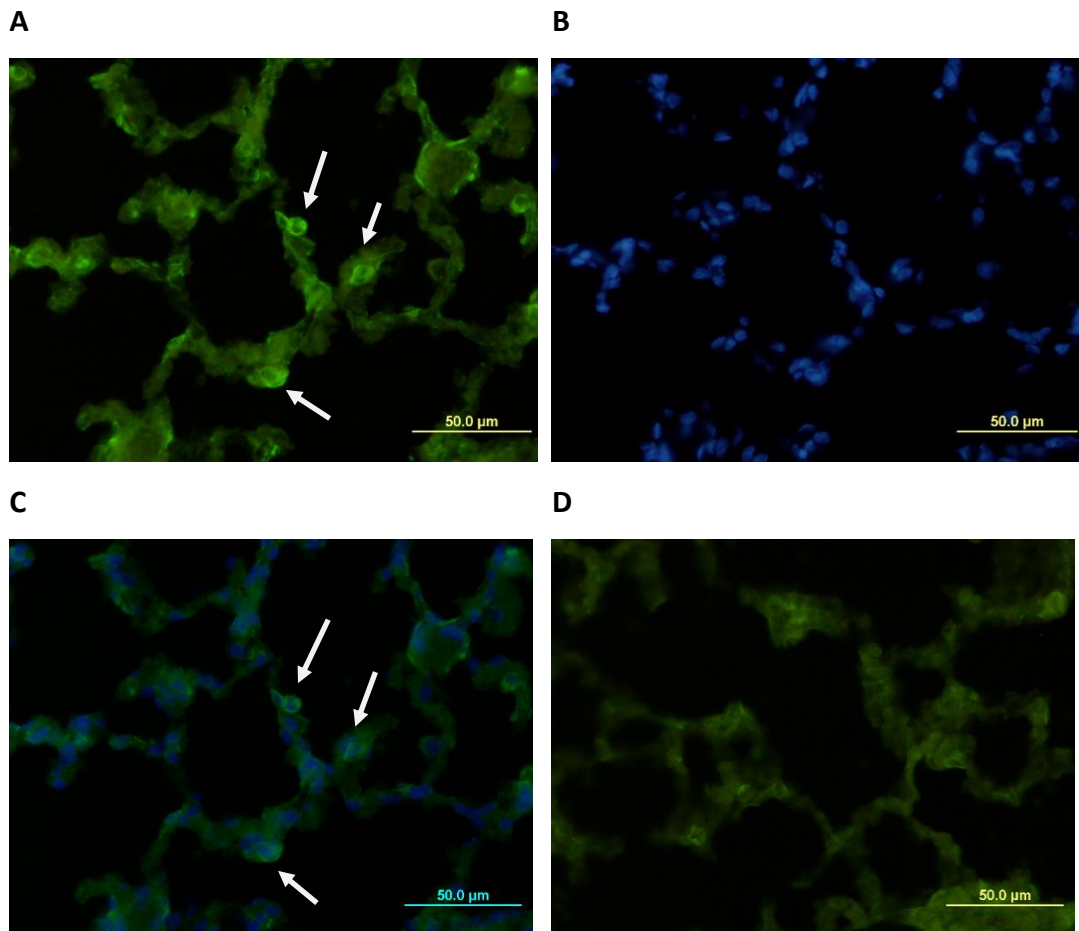


**Figure 4.23. IHC of Rat lung alveoli with CK18 antibody at X40 magnification. This shows signal in primary (A) and composite merged images (C). B. DAPI nuclear stain. D. control omitting primary antibody. Scale bar = 50 μM.**

### 4.2.3 Rat lung antibody to CK19

CK19 is a marker for the more abundant type I, gas-exchange cell. The characteristic of flat cells, side by side, forming alveolar walls can be appreciated in the following image (Figure 4.24) even at 10X magnification. The concentration of antibody for CK19 was 1:500. As type I cells are more abundant than type II, the signal for CK19 almost traces the outline of an alveolus.

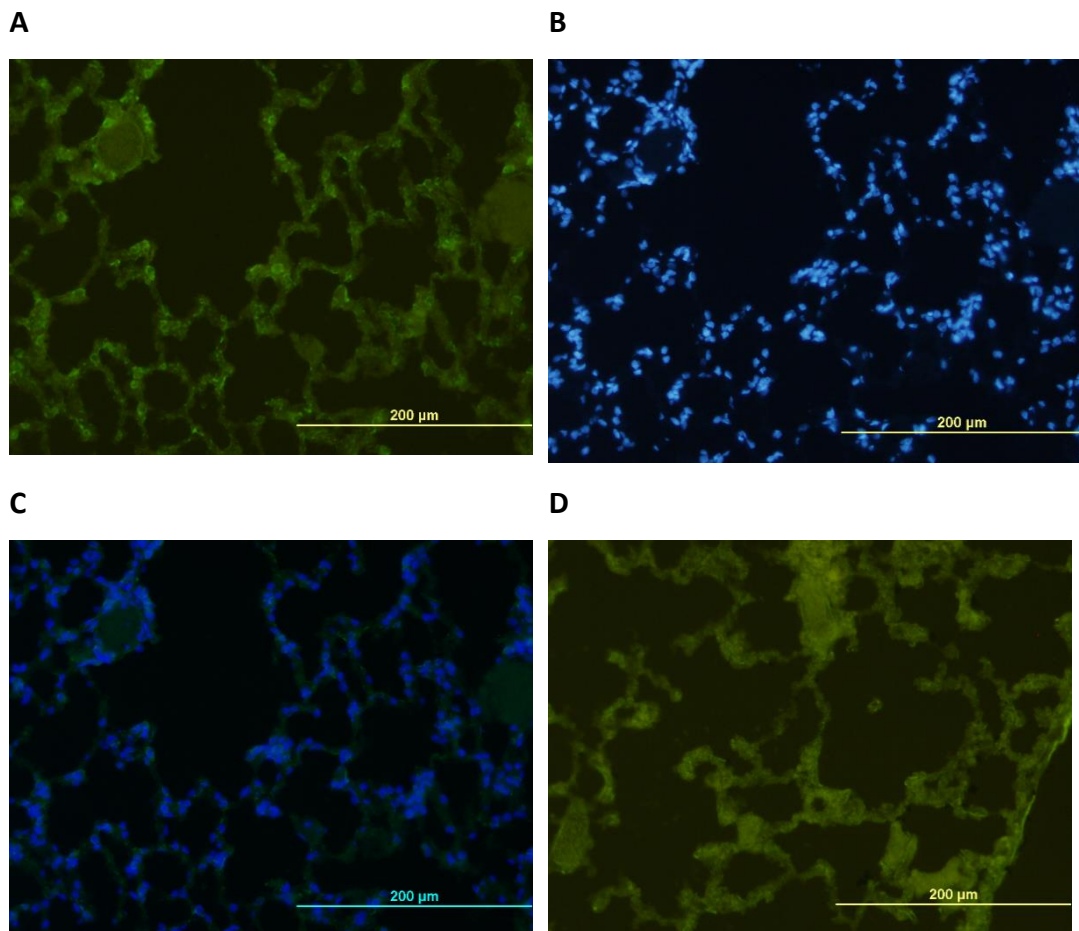


**Figure 4.24. IHC Rat lung with CK19 antibody (1:500). A. positive signal in CK19 primary with magnification 10X revealing signal in continuity along alveolar walls. C. a composite image in which the signal is less evident and requires further magnification. D. negative control from a non-contiguous section from the same paraffin block. Scale bar = 200 μM.**

At slightly higher power (20X), Figure 4.25 shows the CK19 signal expected in flat, gas-exchange cells situated side-by-side can be appreciated although this is less evident in merged images. This corresponds to the appearance of type I cells forming alveolar walls. The signal does not give the appearance of cuboidal cells (typical of type II cells).

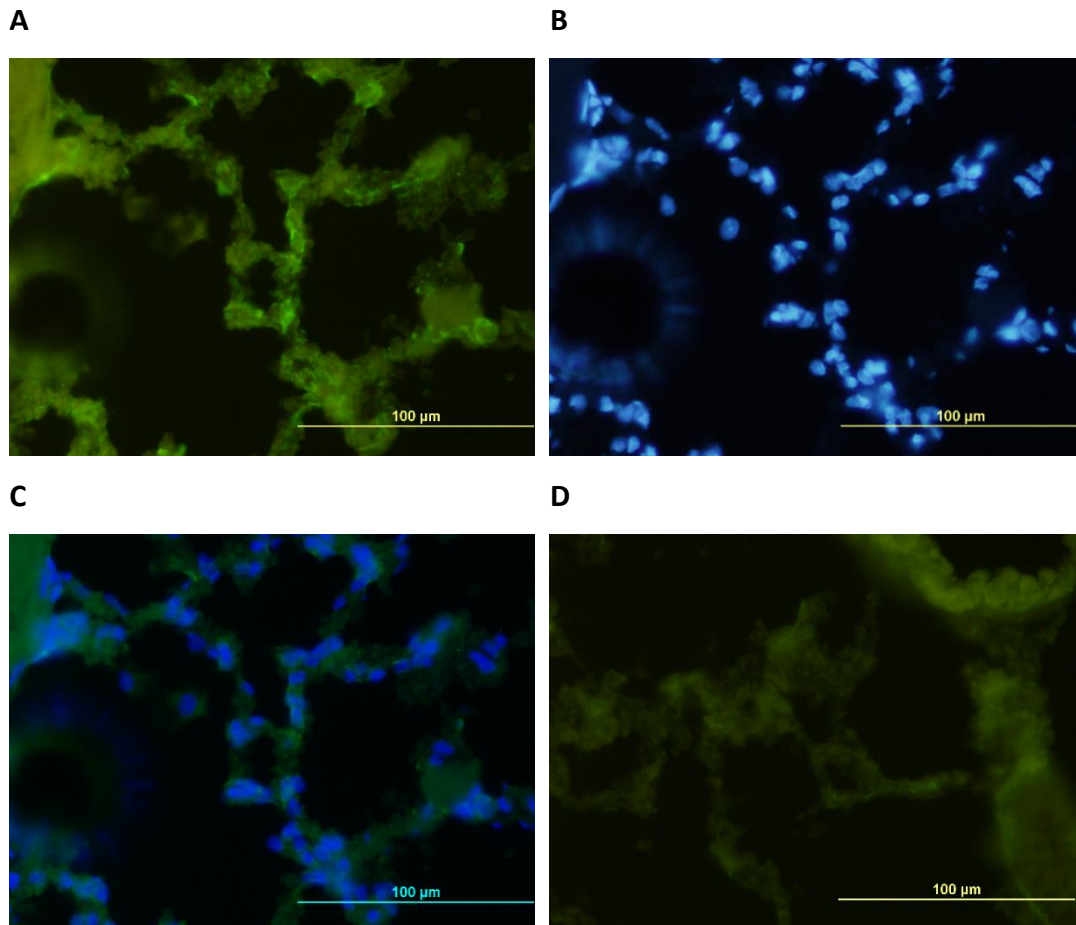


**Figure 4.25.** IHC of rat lung with CK19 antibody (1:500) showing signal in primary (A) and (C) composite images. B. DAPI nuclear stain. The associated nuclei are relatively flat compared to nuclei of type II cells. Magnification 20X. D. negative control from a non-contiguous section from the same paraffin block. Scale bar = 100 μM.

#### **4.2.4 Rat lung antibody to CK7 and CK8**

CK7 and CK8 did not produce signal and therefore no images for these are included. The antibody used for CK7 proved to be anti-human but not anti-rodent. Although the species source of the CK 8 antibody was correct (anti-rabbit, anti-goat), the quality of the antibody may not have been satisfactory.

#### **4.2.5 Rat middle ear: SP-A and cytokeratins**

After confirming positive SP-A protein and CK18 and CK19 in rat lung, an attempt was made to identify our proteins of interest in rat middle ear epithelium before proceeding to mouse middle ear. Whereas the epithelium of mouse middle ear is extremely thin and very difficult to dissect from its bony cavity, rat middle ear epithelium is thicker and easier to remove using a dissecting microscope. These strips of epithelium were also examined as wholemounts. The disadvantage of removing epithelium from its bony support is the loss of orientation with respect to the anatomical contours of the middle ear cavity. Rat skulls and temporal bones are larger than mouse and require more time for processing than mouse.

Because our temporal bone preparation and decalcification method had not been optimised for rat, the rat middle ear epithelium was examined by wholemount and also by frozen section. Control tissue was not used for frozen section thus the results for this stage are not shown but some features are described below because they bear some implication for future work.

Signal was obtained in whole-mount sections of rat middle ear for SP-A, CK18 and CK19 which included controls (data not shown). However, whole-mount does not delineate cell membrane boundaries clearly even on H&E staining. Thus, the signal from the wholemount “bird’s eye view” does not localise IHC signal to individual cells or distinguish whether it is intracellular or extracellular even when it is next to DAPI-stained nuclei.

Some frozen sections also showed positive signal for CK18 and CK19 and even showed a slight difference in distribution in that CK19 signal appeared more

continuous - as in lung alveoli - than CK18 which might reflect the lung distribution of the type I cell and the type II cell if such a pattern is present in middle ear epithelium. Surprisingly, antibody markers for both SP-A protein and pan-cytokeratin were negative. The nuclear DAPI stain was positive in all wholemount sections.

#### 4.2.6 Mouse lung

In general, the alveoli of mouse lung are less well expanded than rat (compare Figure 4.1 above to Figure 4.26 below) due to the more delicate tissue of mouse, the easier rupture of air sacs and consequent lung collapse. Below we see H&E images of mouse lung illustrating the compressed appearance (Figure 4.27A). Despite the compressed appearance, some expanded alveoli can be found which illustrate the various cell types seen in alveoli (Figure 4.27B). This results in a diffuse, uniform background signal.

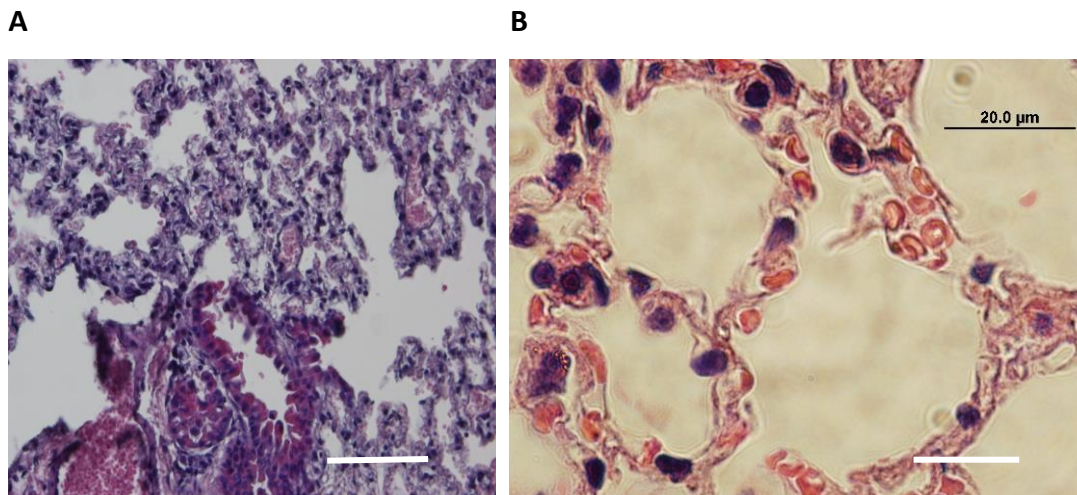


**Figure 4.26.** H&E stain of a Mouse lung A. Shown is relatively collapsed alveolar sacs. Magnification 10X; Scale bar = 200 µm. B. Adjacent H&E image at 40X shows well expanded alveoli with various cell types as seen in Figure 4.3. Scale bar = 20 µM.

#### 4.2.7 SP-A in mouse lung

At low magnification (Fig 4.27A), SP-A signal is evident within alveoli although any visible signal is likely to represent extracellular clumps of SP-A rather than intracellular signal. This lack of intracellular signal is in agreement with Schwingshackl, 2017.

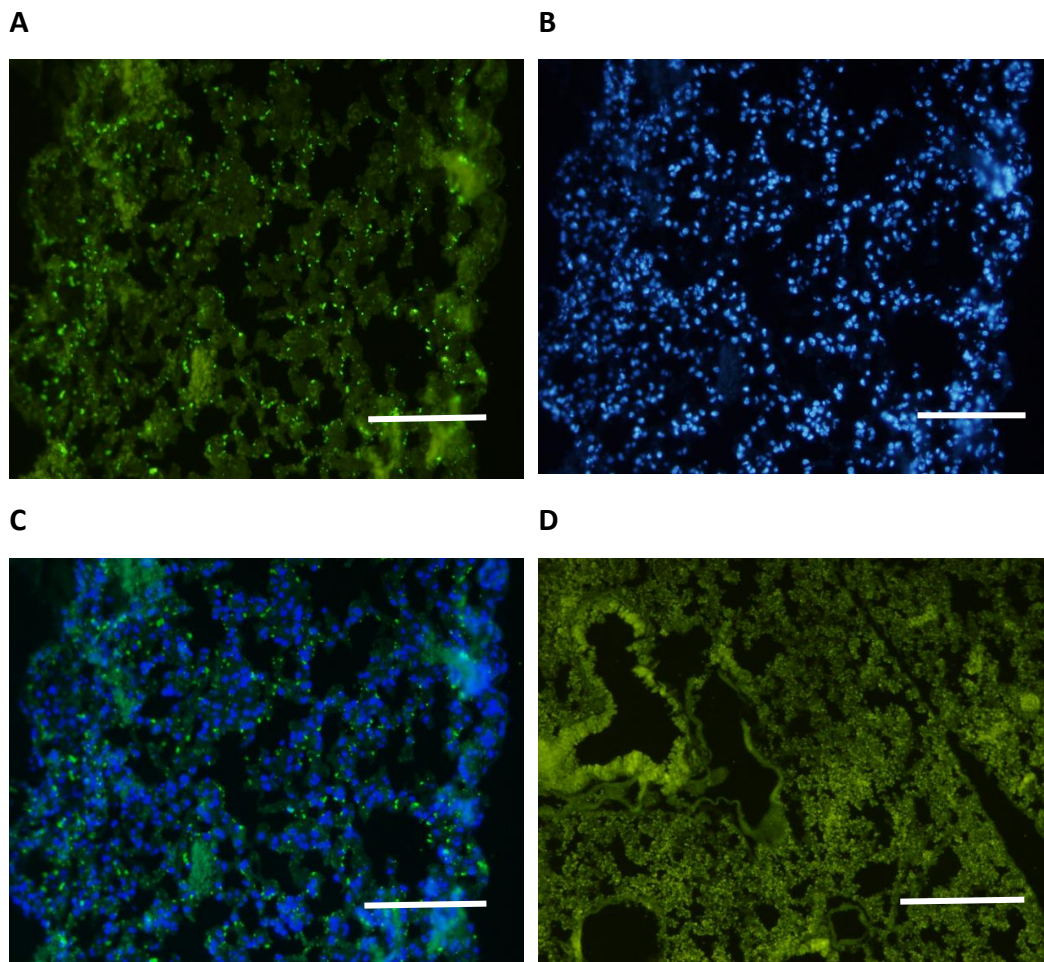


**Figure 4.27. IHC Mouse lung with labelled SP-A with secondary at 1:2000. A. SP-A antibody (1:500) B. DAPI stain. C. Merged composite. D. Control image from non-contiguous section omitting primary antibody and using secondary at 1:4000. Magnification 10X; scale bar = 200  $\mu$ m.**

Even at higher power and higher concentration (1:500) and with the contrast provided by DAPI stain (Fig 4.28C), the SP-A signal is most likely to be extracellular.

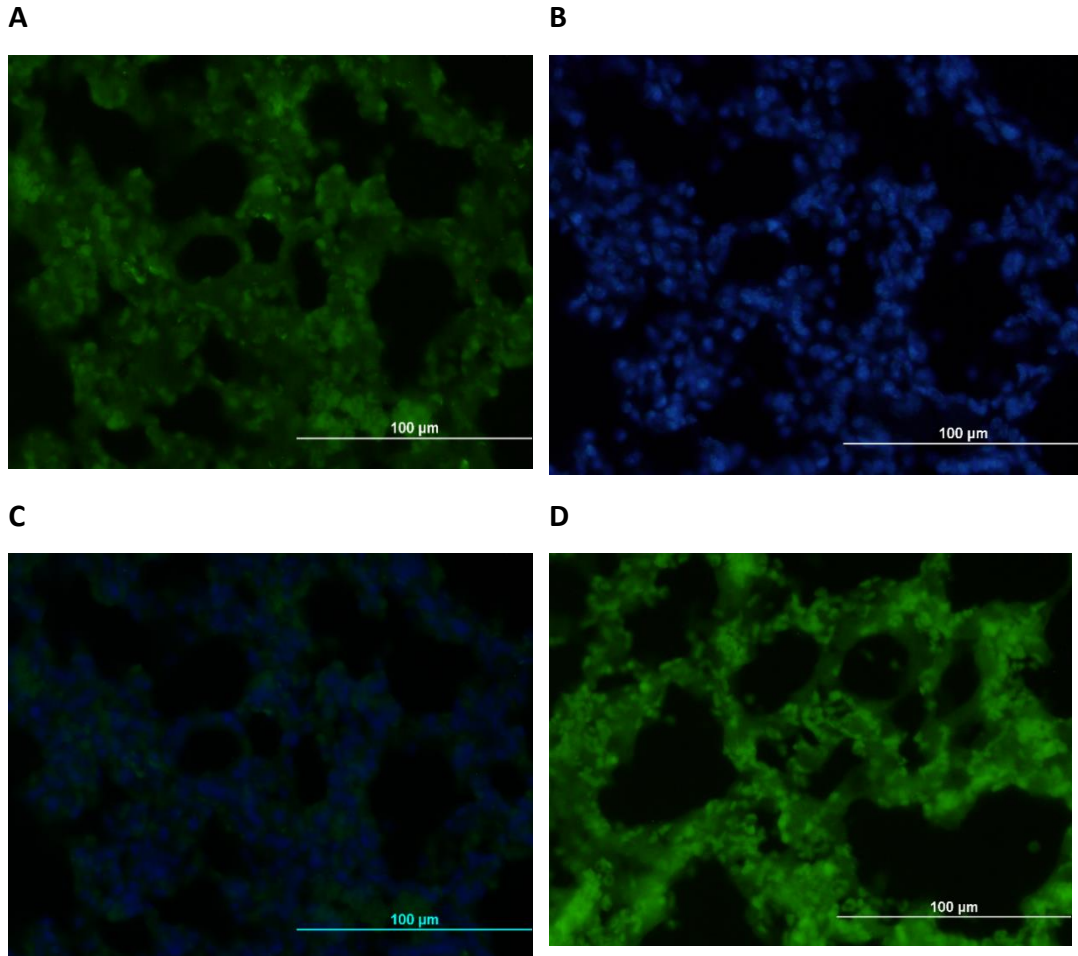
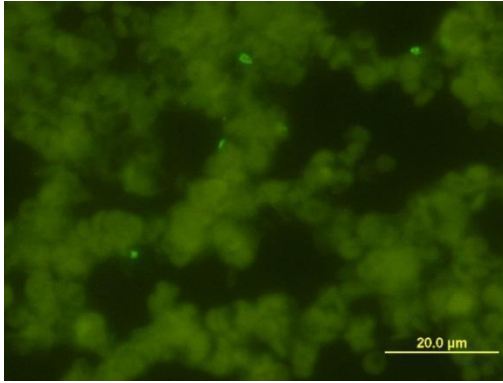


**Figure 4.28. IHC of Mouse lung. A. SP-A primary Ab (1:500) and secondary Ab applied at 1:4000. B. DAPI nuclear stain. C. Merged. D. shows a non-contiguous control section with omitted primary antibody. Magnification X20. Scale bar = 100  $\mu$ M.**

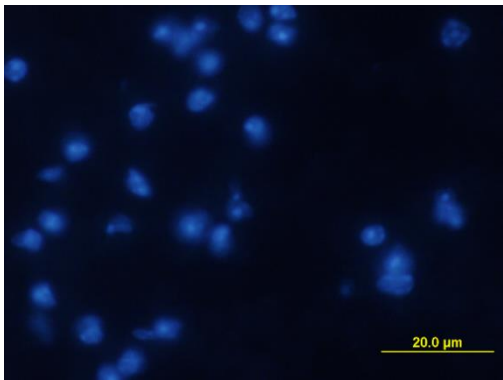
Furthermore, the rounded appearance of the extracellular signal probably reflects the presence of SP-A within secreted tubular myelin which may revert to a rolled up sheet during processing whereas in life it spreads out with the surfactant complex over the inside walls of expanding alveoli.

At this stage of investigation, examination at higher power (100X magnification) with oil immersion failed to confirm the presence of intracellular SP-A signal in mouse lung. The spots seen on Figure 4.29A and C are extracellular.

**A**



**B**



**C**

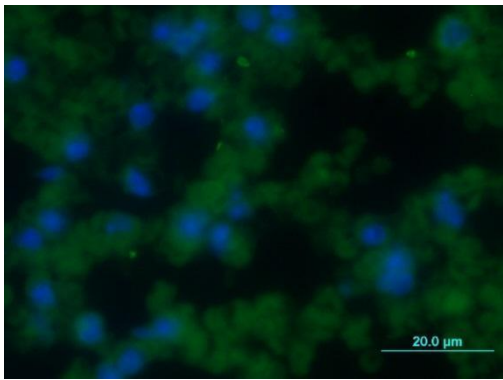
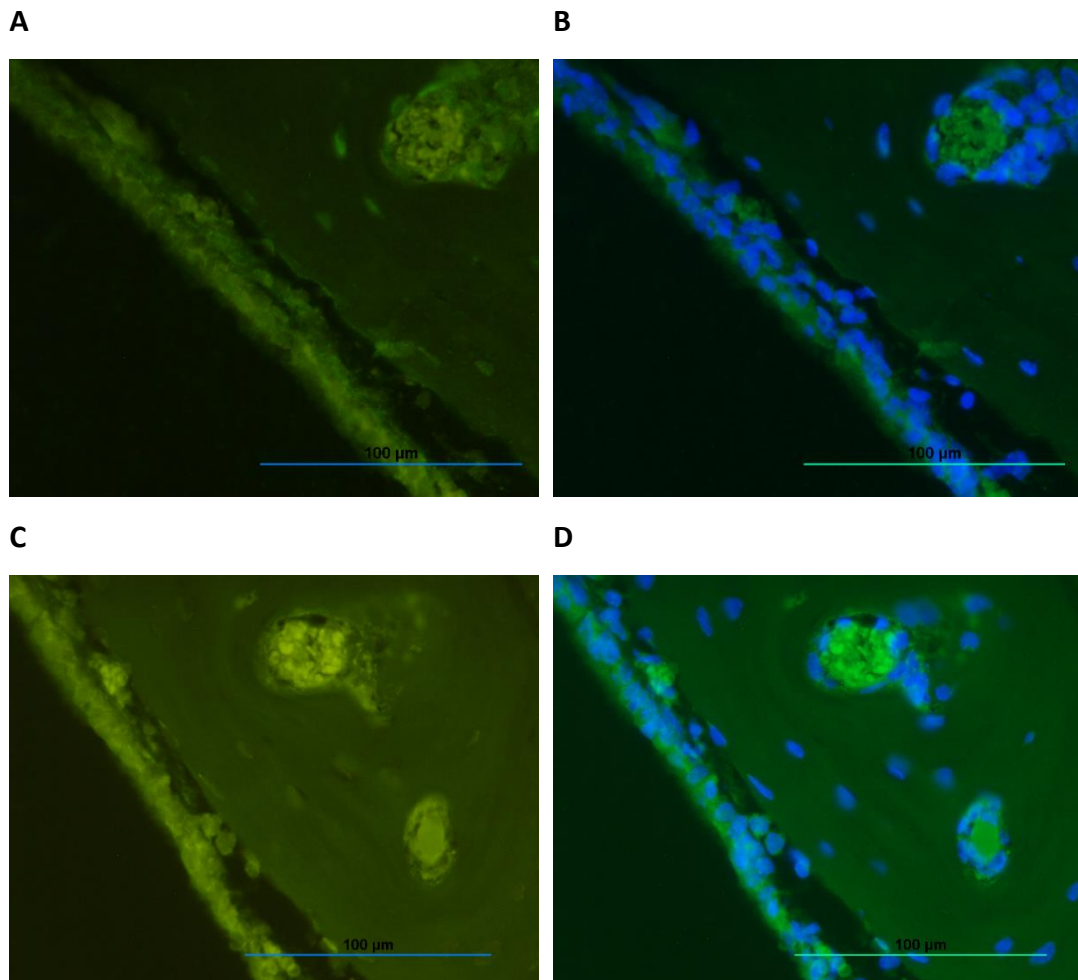


**Figure 4.29. IHC of Mouse lung with SP-A. A. positive signal for SP-A at 1:500 with mainly extracellular distribution. B. DAPI stain. C. Merged composite. No control section was available. Magnification 100X, scale bar omitted.**

Apart from lack of intracellular signal in mouse lung alveoli, it is also interesting to note that there is no convincing signal within Clara cells of the upper airways despite clear extracellular signal in all positive sections at lower power.

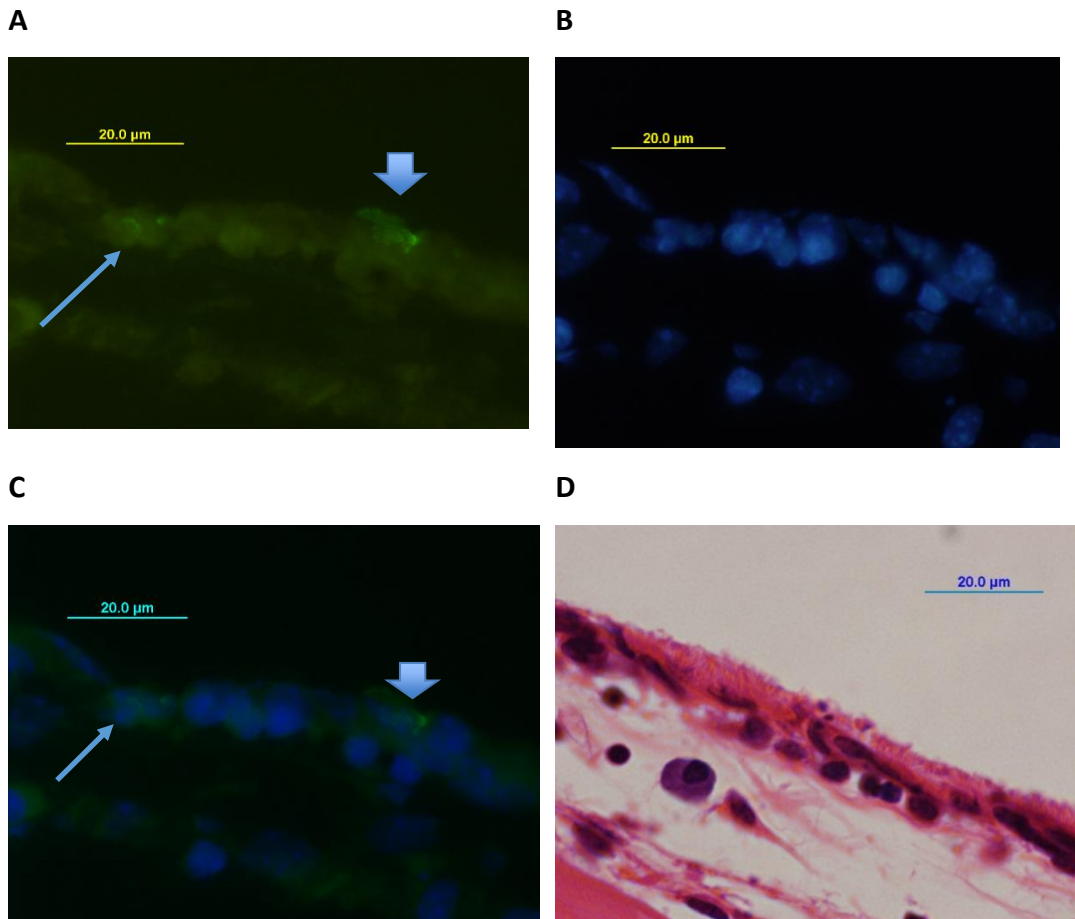
#### 4.2.8 SP-A in mouse middle ear

Figure 4.30 shows epithelium lining the bony cavity of the mouse middle ear. Within the bony wall, a nest of bone marrow cells is visible. SP-A fluorescence is evident as speckled signal within the epithelium in contrast to a more diffuse, robust signal within the cytoplasm of bone marrow cells. DAPI stain shows nuclei of connective tissue cells within the stromal layer deep to basement membrane.



**Figure 4.30. IHC of Mouse Ear. (A)** This figure shows the epithelium of the superomedial middle ear with SP-A antibody (1:50) at the highest concentration visible at 20X magnification. **(C)** Control images with primary antibody omitted showing no signal in primary or **(D)** composite image (20X magnification). Scale bar = 100 μM.

At higher 100X magnification with oil immersion (Figure 4.31), the intracellular signal can be confirmed by merging the primary image with the nuclear DAPI stain which reveals the signal as perinuclear. When the signal accumulates on the surface of the cell, it is difficult to say whether the secreted SP-A is simply adjacent to the cell or located within the sol or gel phase of mucoid secretion.



**Figure 4.31. IHC of Mouse Ear.** This figure shows epithelium of the inferomedial middle ear where there are some ciliated, low cuboidal cells with SP-A antibody (A) at the lower concentration 1:500 visible at 100X magnification with (B) DAPI stain, (C) composite image and (D) adjacent H&E section. The H&E shows that, in the middle ear, even flat cells may be ciliated. Some of the SP-A signal is accumulated on the cell surface (large arrow) and a tiny amount is seen in a perinuclear, intracellular location (small arrow). No control image available. Scale bar = 20  $\mu$ M.

However, one does get an impression of cilia at higher magnification (100X) when cell nuclei are observed superficial to the cytoplasmic layer as in the image below (Fig 4.32). These nuclei could be free macrophages or, perhaps more likely, extruded nuclei of epithelial apoptosis. Such an apoptotic nucleus can be seen in the H&E stain below (Fig 4.32D).

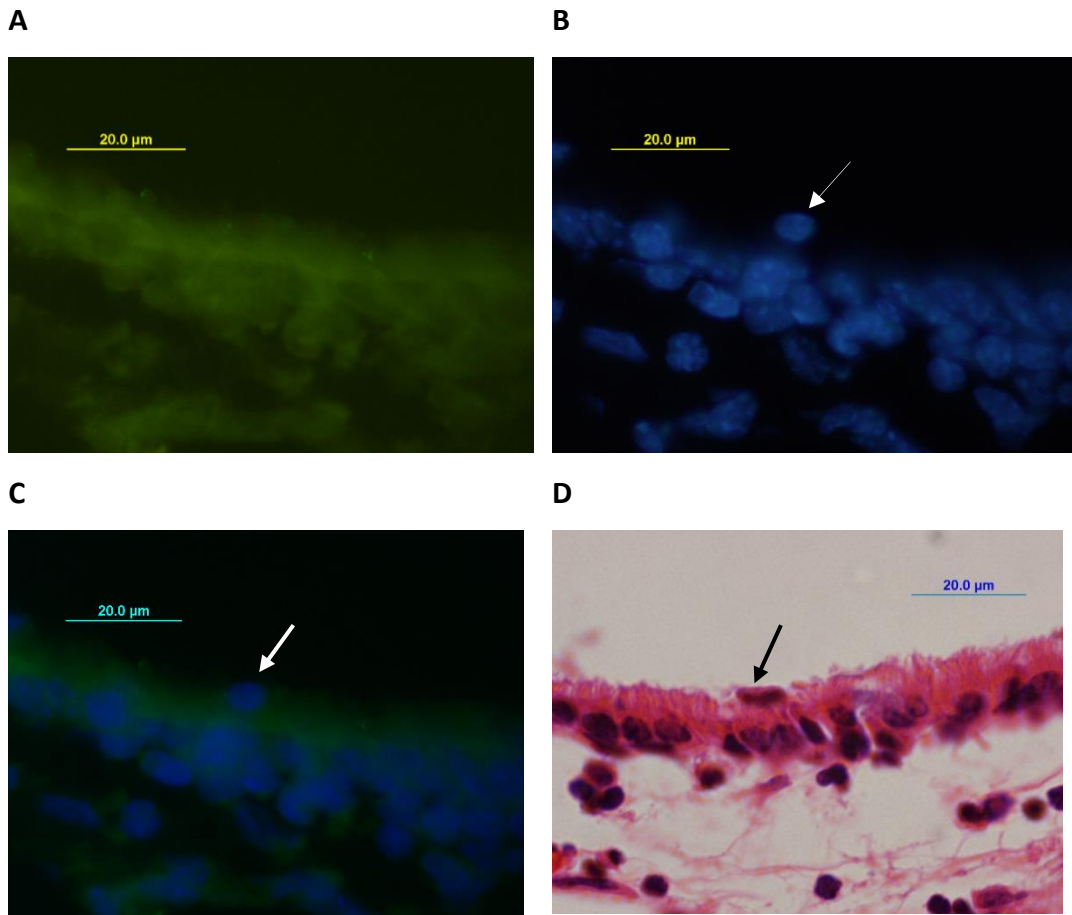


**Figure 4.32. IHC of Mouse Ear.** This figure shows ciliated, low cuboidal epithelium of the medial wall of middle ear with SP-A antibody (A) at the lower concentration 1:500. The SP-A signal is visible at 100X magnification with (B) DAPI stain in the composite image (C) although the signal is mainly situated in the ciliary layer of epithelium rather than intracellular. D. Adjacent H&E section shows typical ciliated, low cuboidal epithelium of middle ear adjacent to Eustachian tube. Scale bar = 20  $\mu$ M.

#### **4.2.9 SP-A in bone marrow nests above mouse middle ear**

The most convincing signal for SP-A within the cytoplasm of any cells of the middle ear is to be found within the surrounding bone marrow nests. For orientation purposes, the control images below in Figure 4.33 shows bone marrow cells in nests adjacent to the middle ear space. Cells in bone marrow are variable in size and morphology.

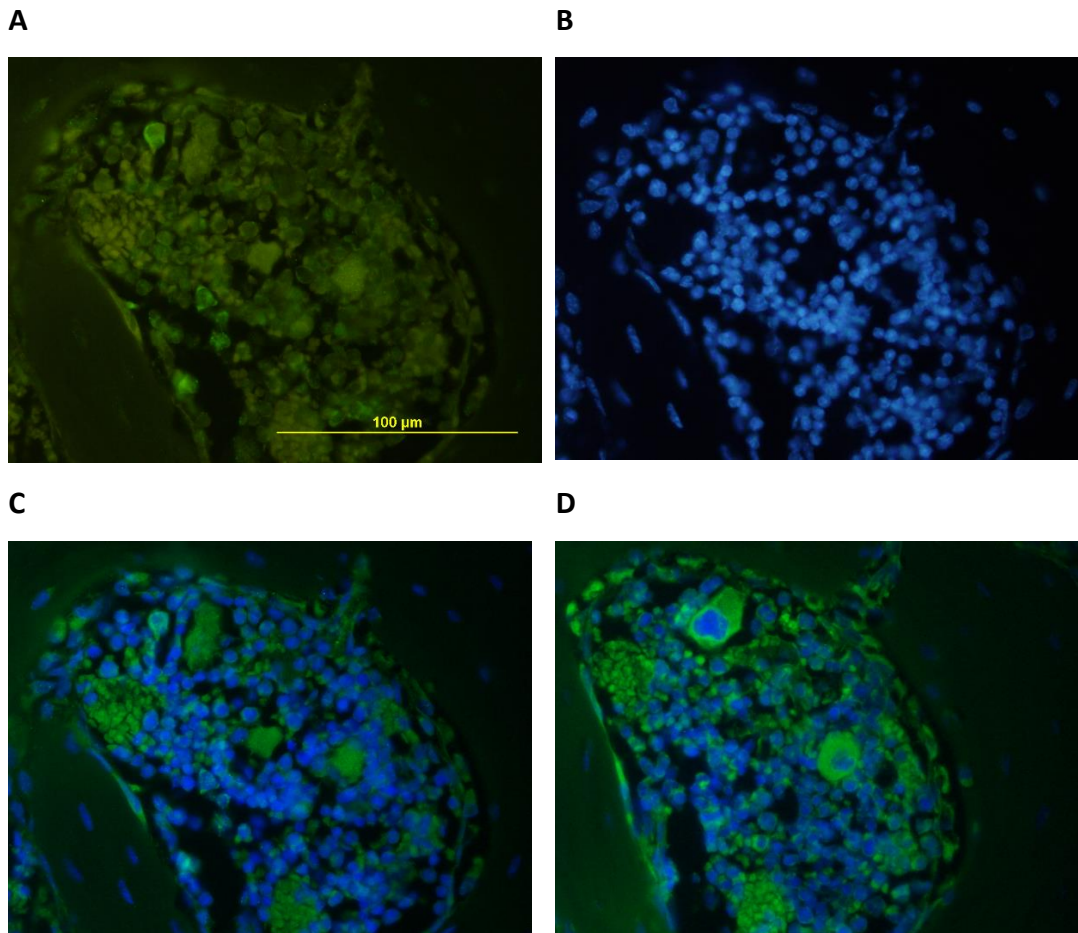


**Figure 4.33. IHC of Mouse Ear.** Figure A shows bone marrow cells labelled with SP-A in a bone marrow nest above the roof of the middle ear. It shows apple-green SP-A signal above background, B. is a DAPI stain and C. is a merged image which results in significant discoloration of primary antibody signal. The merging program gives an enhanced intensity to background fluorescence. D. shows control bone marrow cells without primary antibody giving diffuse background signal in cell cytoplasm. Scale bar = 100 $\mu$ m.

SP-A signal is generally clearer in bone marrow cells than in middle ear epithelium. This makes bone marrow cells a useful positive control adjacent to middle ear epithelium even though it is not clear what type of bone marrow cell – myeloid or lymphoid - contains SP-A protein. Below is Spa 1:500 signal in the bone marrow adjacent to middle ear (Figure 3.34).

The signal in bone marrow in this image shows some signal adjacent to nuclei. There is a faint, stippled signal within the bone marrow which is also in the epithelium of the middle ear as well as in the bone communication channel.

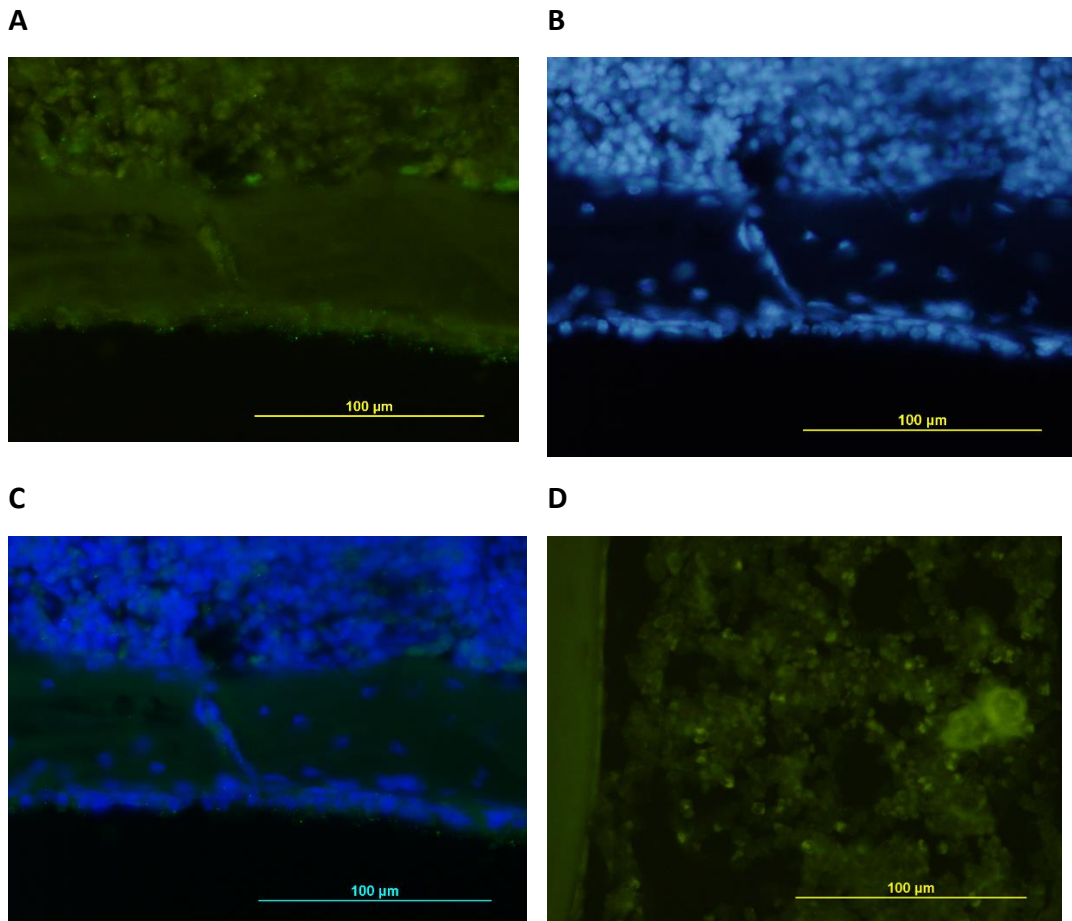


**Figure 4.34. IHC of Mouse Ear.** This figure shows bone marrow cells labelled with SP-A in a bone marrow collection above the roof of the middle ear. A. apple-green signal above background, B. DAPI stain and C. is a merged image which results in significant discoloration of primary antibody signal. D. control bone marrow from non-contiguous section of same specimen showing no signal. Scale bar = 100 µM.

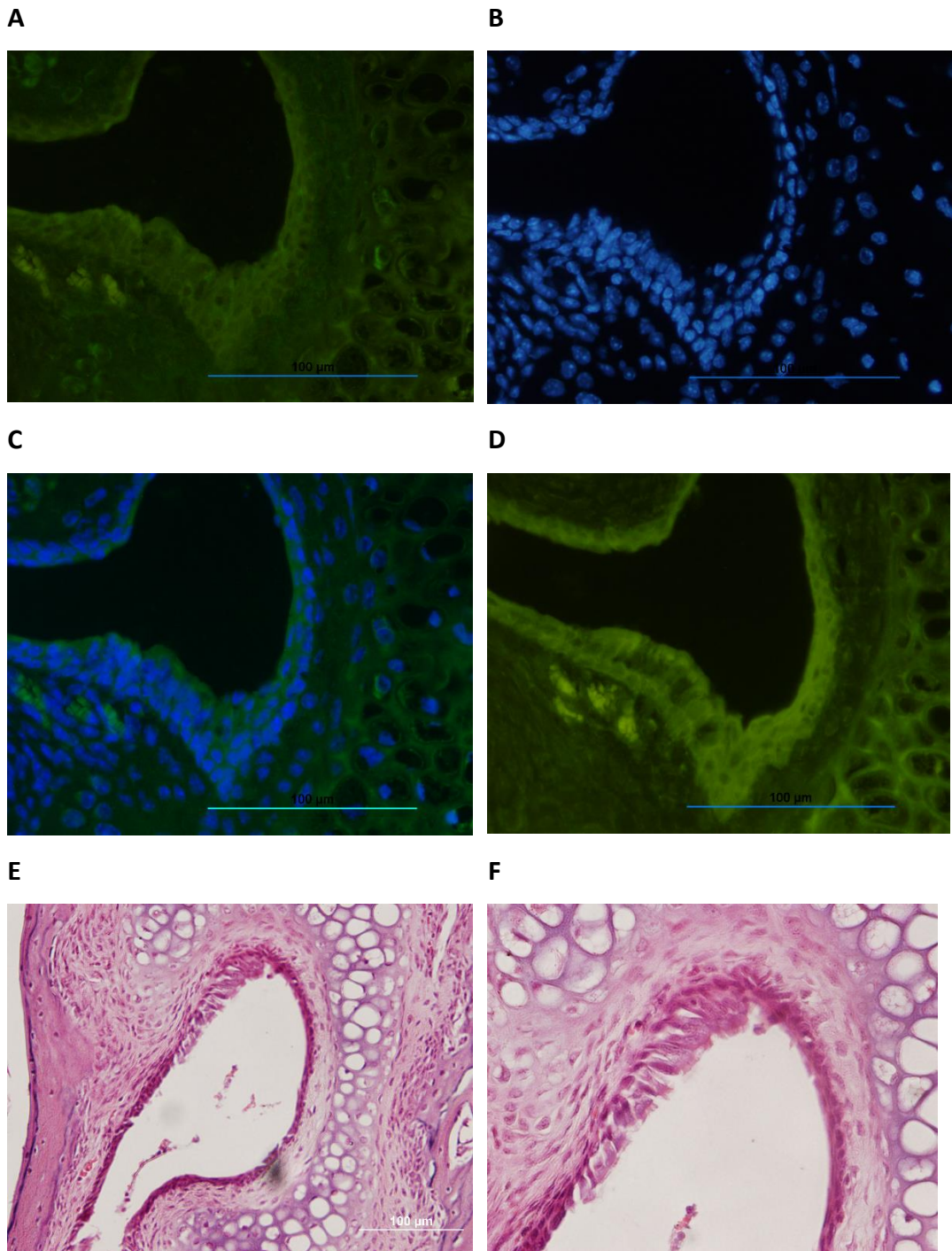
#### 4.2.10 SP-A signal in the mouse Eustachian tube

Figure 4.36 shows a coronal H&E section of the middle ear space. Note that the Eustachian tube is supported by cartilage and is superomedial to the main middle ear chamber. This results shows the relationship of the nasopharyngeal end of the Eustachian tube which lies above and medial to the middle ear cavity. A higher magnification of this region is shown in Figure 4.35 using IHC.



**Figure 4.35. Panoramic view of middle ear space and adjacent Eustachian tube cartilage (et), bone marrow niche (bm) and middle ear space (me). Magnification 2.5X. Scale bar =2 mm.**

Closer examination of the Eustachian tube epithelium confirms that there are mainly tall ciliated cells with some flat squamous cells as reported in previous studies (Lim, 1974). At high concentration (1:50), SP-A protein is expressed in the epithelium of the Eustachian tube within the intracellular compartment (see Figure 4.36).



**Figure 4.36.** IHC of mouse coronal section of left Eustachian tube (nasopharyngeal end) adjacent to its supporting cartilage. A. Primary SP-A at 1:50 showing signal in apical areas of epithelium as well as some chondrocytes of the Eustachian tube. B. DAPI stain. C. Merged. D. Control image. Magnification 40X. Scale bar = 100 μM. E. H&E of similar segment of Eustachian tube at 20X showing surrounding cartilage. F. H&E showing variation in epithelium from tall ciliated to flat squamous. Magnification 40X, scale bar omitted.

A more convincing result of epithelial debris containing SP-A is seen in Figure 4.37A at the “exit” to the middle ear, that is, the medial opening of the Eustachian tube. The DAPI stain reveals nuclear debris as well as intact nuclei with positive SP-A signal in the cytoplasm which probably represent free macrophages engulfing “used” SP-A or, alternatively, apoptosed cells containing SP-A (Figure 4.37C.)

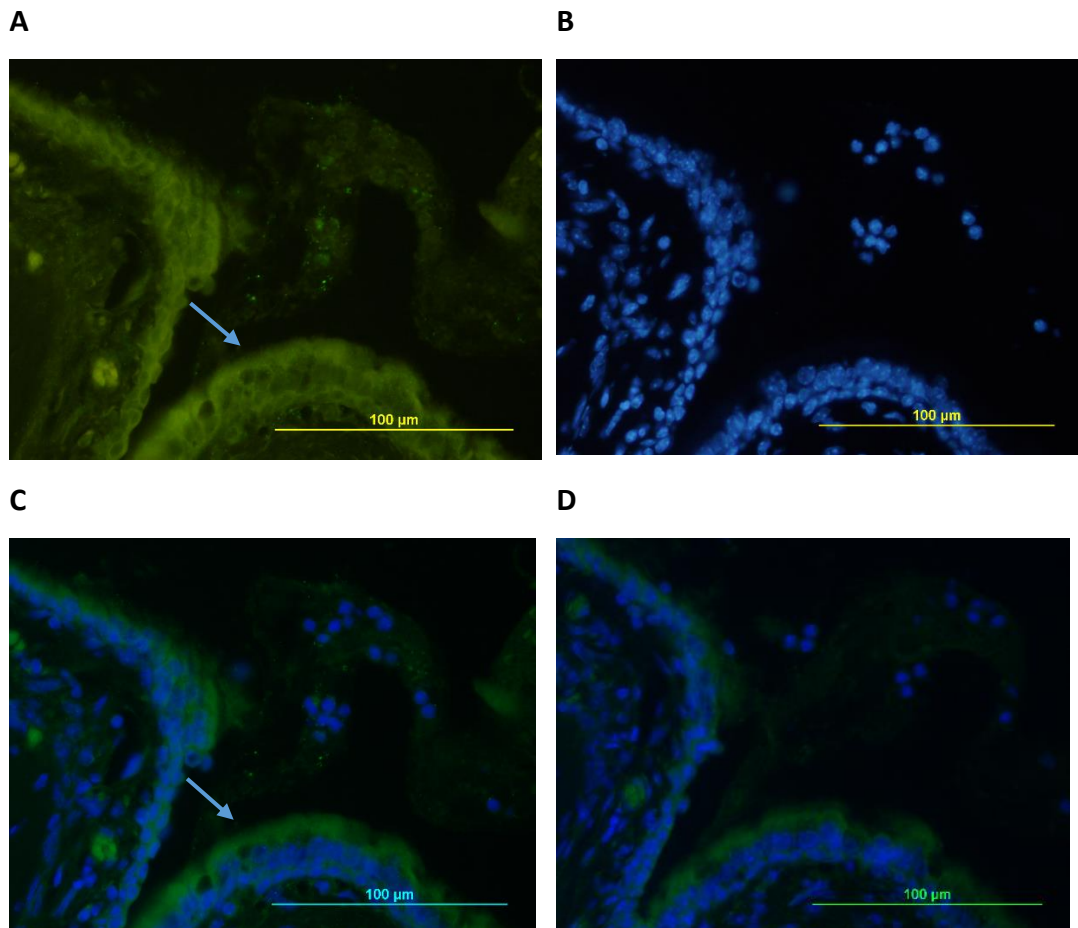


**Figure 4.37. IHC of Rat Coronal section of left Eustachian tube (tympanic end) adjacent to its supporting cartilage. A. Primary SP-A at 1:500 showing speckled signal in free cellular debris within middle ear space. There is also some intracellular perinuclear speckling within ciliated epithelium (arrow). B. DAPI stain. C. Merged. D. control image - omitting primary antibody. Magnification 40X. Scale bar = 100 μM.**

#### **4.2.11 Cytokeratins in mouse middle ear**

In general there was little if any convincing signal for cytokeratins in the mouse middle ear. CK18 was positive in some cells both ciliated and non-ciliated. Controls were done only in the CK18 specimens. CK7 showed only faint signal in some middle ear cells. CK19 was negative.

In summary, results depicted in this chapter demonstrate the following key points:

1. That SP-A protein can be demonstrated in rat lung alveolar spaces both intracellularly and extracellularly.
2. The most convincing signal for SP-A protein in rat lung tissue can be observed in the Clara cells of the airways making Clara cells an excellent positive control partly because of their large size and contiguity with each other.
3. The same cannot be said for mouse lung i.e., SP-A signal is only present in the extracellular location and seems conspicuous by its absence from Clara cells.
4. That SP-A protein is present within the air spaces of both the mouse lung and the mouse middle ear, although the cell of origin in the middle ear remains unclear.
5. That the strongest intracellular signal for SP-A protein is within some cells of the bone marrow nests adjacent to the middle ear.
6. That there are communications in the mouse temporal bones between bone marrow spaces and the adjacent middle ear cavity.
7. That cytokeratins are useful in distinguishing cell types within rat lung (type I versus type II alveolocytes). The role of cytokeratins for identifying specific cell types lining the middle ear cavity remains to be determined.

### **4.3 Western blotting**

#### **4.3.1 Protein concentrations using the Bradford assay**

A Bradford assay was carried out on four adult mouse lungs (C57/B6 strain) in order to provide an estimate of the total protein concentration. The Bradford assay was performed using four mouse lungs to provide six lung samples (L1, L2, L3, L3A, L4, L4A). From these six samples, lungs 1, 2, 3 measured average readings of 2 mg/mL, 7 mg/mL and 4 mg/mL, respectively. The remaining lungs (3A, 4, 4A) were too concentrated to give measurements within the standard curve range.

#### **4.3.2 Protein yield and quality using a Coomassie blue stained polyacrylamide gel**

A 12% commercial polyacrylamide gel was used to determine the quality and yield using Coomassie blue staining. Following gel electrophoresis, the greatest concentration of protein was found in two lung samples (L3A and L4A), ranging from 120 to 15 kDa as seen in Figure 4.38. All samples showed protein in bands at just above 60 kDa and another band at 10-15 kDa.

In regard to the protein of interest, the band above 60kDa is a region where one might encounter dimers of SP-A which typically weigh 66 kDa. The band at 10-15 kDa may represent degenerate protein debris present within both lung and middle ear.

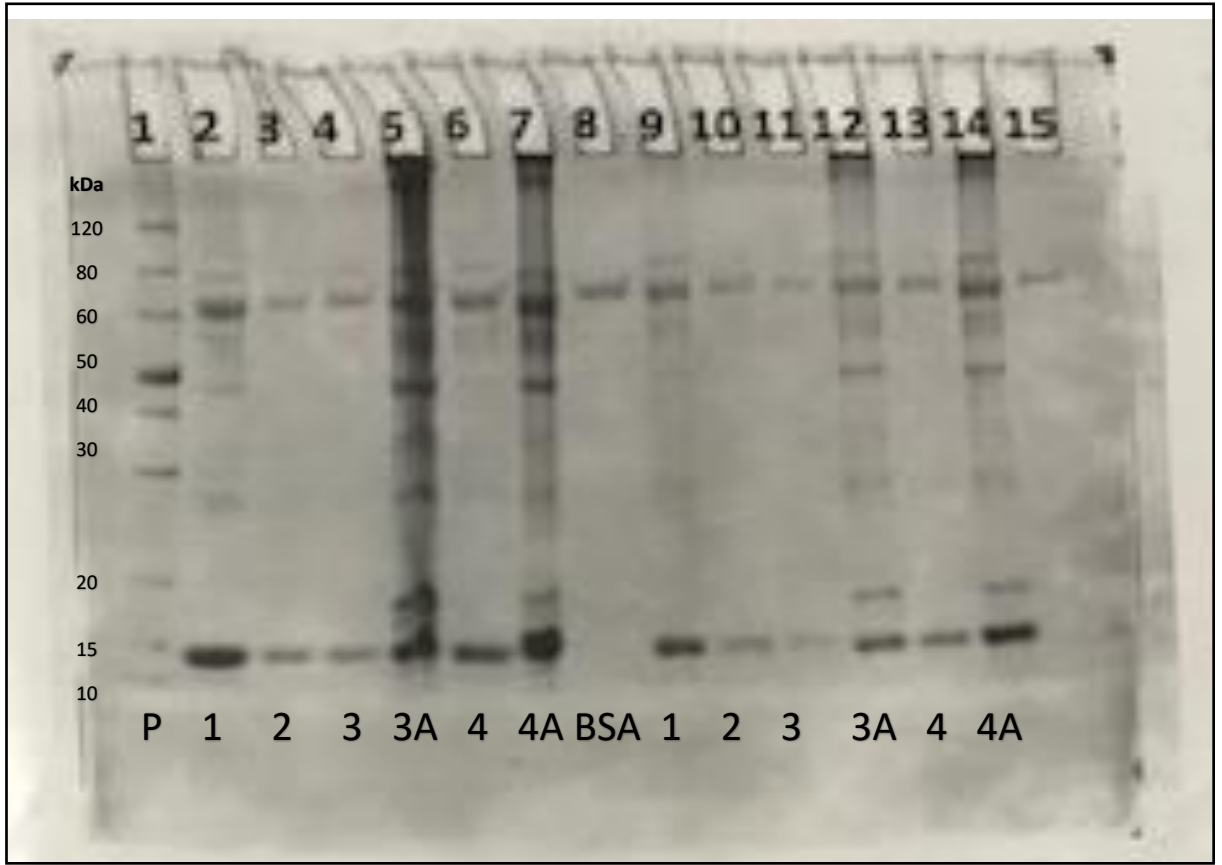


**Figure 4.38.** Coomassie blue stained 12% pre-cast polyacrylamide gel of mouse lung protein lysates. Lane 1: PAGE ladder (P). Lanes 2-7: Four partial mouse lungs from animal 1, animal 2, animal 3 (3, 3A), and animal 4 (4, 4A). Lane 8: BSA (1 mg/mL). Lanes 9-14: replicate loading samples as reported in Lanes 2-7.

Next, two lungs with lysates that represent the lowest and highest estimated protein concentration (lung 1 and lung 3A) were serially diluted, electrophoresed and stained with Coomassie blue. Figure 4.39 shows the increasing intensity of the six serially diluted six samples (a-f) on a 12% polyacrylamide gel. It was noted that not all of the serially diluted samples resulted in observable protein bands. Thus, it was decided to test all of these diluted samples for western blot analysis and then make a recommendation on what concentration(s) are suitable to use to ensure optimal signal strength and equal loading between samples (Figure 4.41).

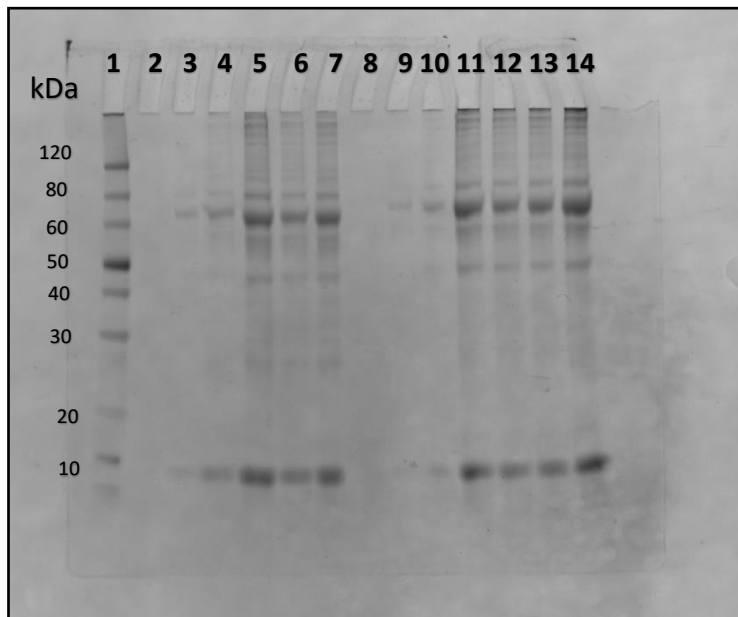


**Figure 4.39. Coomassie blue stained 12% pre-cast polyacrylamide gel of gradient mouse lung protein lysates (a-f) from animals 1 and 3A. Lane 1: PAGE ladder. Lanes 2-7: increasing concentration of mouse lung lysate from animal 3A (a-f). Lanes 8-14: increasing concentration of mouse lung lysate from animal 1. Lanes 7 and 14 represent the maximum protein concentration (f) available to add to the 4X Laemmli dye.**

We then assessed lysate samples of processed mouse middle ears in comparison to other tissues including lung, brain, kidney, liver, spleen. Because middle ear tissue is smaller in mass and volume than most other organs, four paired middle ears (8 middle ears) were used to provide an adequate tissue load. The resulting gel below (Figure 4.40) showed robust concentrations for middle ear comparable to other tissues. The intensity of the staining is more intense than Figures 4.39 and 4.38 as an electric stain blotter was used. The molecular size range of the protein lysates from the six mouse organs is from 120 to 20 kDa.

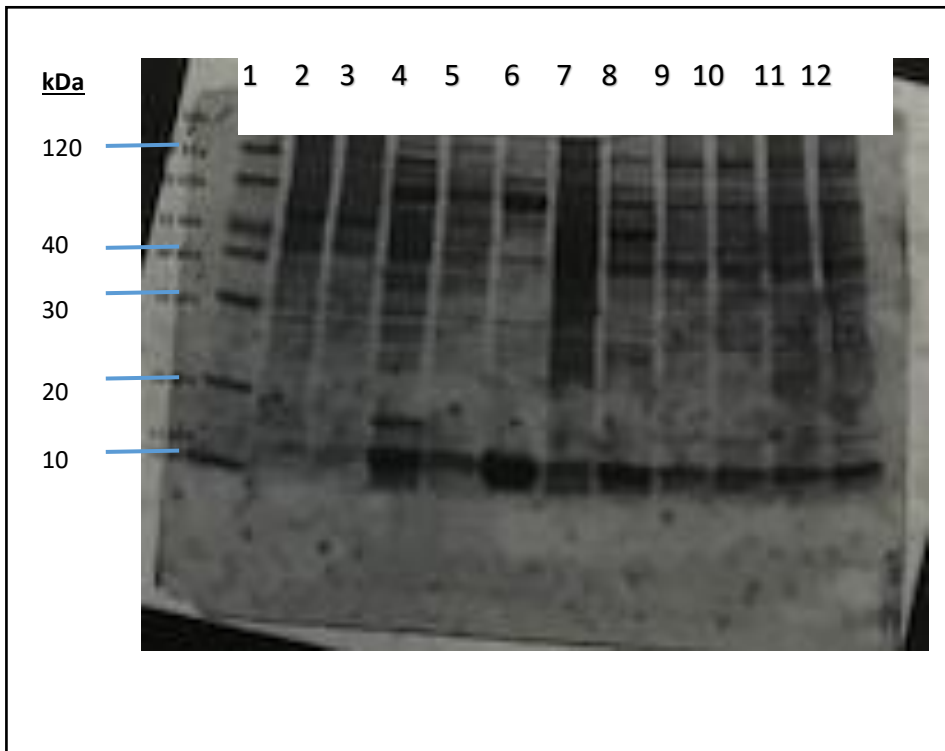


**Figure 4.40.** Coomassie blue stained 16% pre-cast polyacrylamide gel of mouse protein lysates from six mouse organs. Lane 1: PAGE ladder (P). Lane 2: brain 1, Lane 3: brain 2, Lane 4: kidney, Lane 5: liver, Lane 6: lung (1f and 4f), Lane 7: spleen, Lane 8: paired middle ears 1, 2, 3, 4.

### 4.3.3 Western blot for lung

Having established adequate equal loading protein lysates in both middle ear and lung, we moved onto western blotting to validate the antibodies used for IHC and demonstrate their specificity with antigen recognition with respect to the known protein molecular weight. We selected two lung samples with serial dilution (1 and 4) and ran these on a gel (12% in MOPS buffer) and performed a western blot with SP-A protein with an antibody concentration of 1:1000. No bands of the expected size were observed (data not shown). The experiment was repeated using antibody to SP-A at a concentration of 1:500 and a very faint band was seen in Figure 4.41 in two lung samples (Lanes 6, 7, 14 and 15). The band is just below the 30 kDa western ladder band. The membrane was stripped but failed to recognise any reprobing with another antibody such as GAPDH. Thus, we repeated the experiment.



**Figure 4.41. Western blot of 12% polyacrylamide gel of gradient mouse lung protein lysates from Animals 1 and 4 using SP-A antibody at 1:500 concentration. Lane 1: PAGE ladder. Lanes 2-7: increasing concentration of mouse lung lysate from animal 1. Lane 8: Western Ladder. Lanes 9-14: increasing concentration of mouse lung lysate from animal 4. Faint bands are visible at increased concentrations better seen in animal 1 (arrow). SP-A antibody = 1:500.**

Figure 4.42 shows the western blot results of mouse lysate from two lung samples tested with three antibodies. With the issues encountered in western blot optimisation, the first antibody probed was GADPH (1:2000) as it serves as a good positive control. A band of the expected size was observed, 35k Da. Next, we stripped the membrane and applied CK19 antibody and a band of the expected size was observed, 44 kDa. Then, the membrane was stripped and reprobed with 1:200 SP-A antibody. A band of the expected size was observed, 35 kDa. Finally, the membrane was stripped and reprobed with 1:2000 CK18 antibody. A band of the expected size was observed, 47 kDa

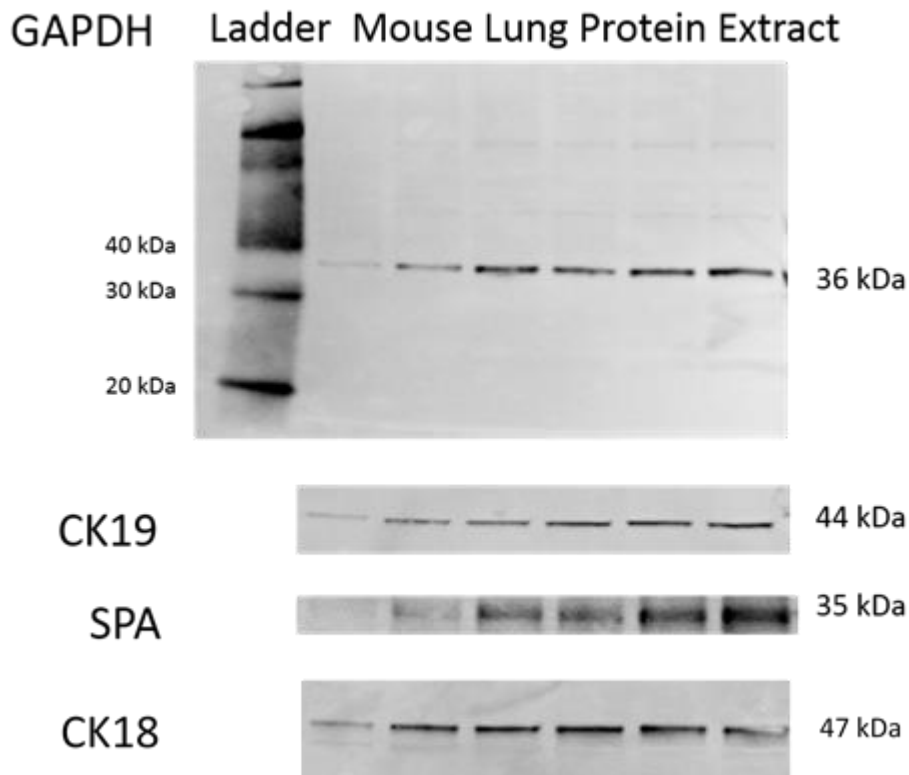


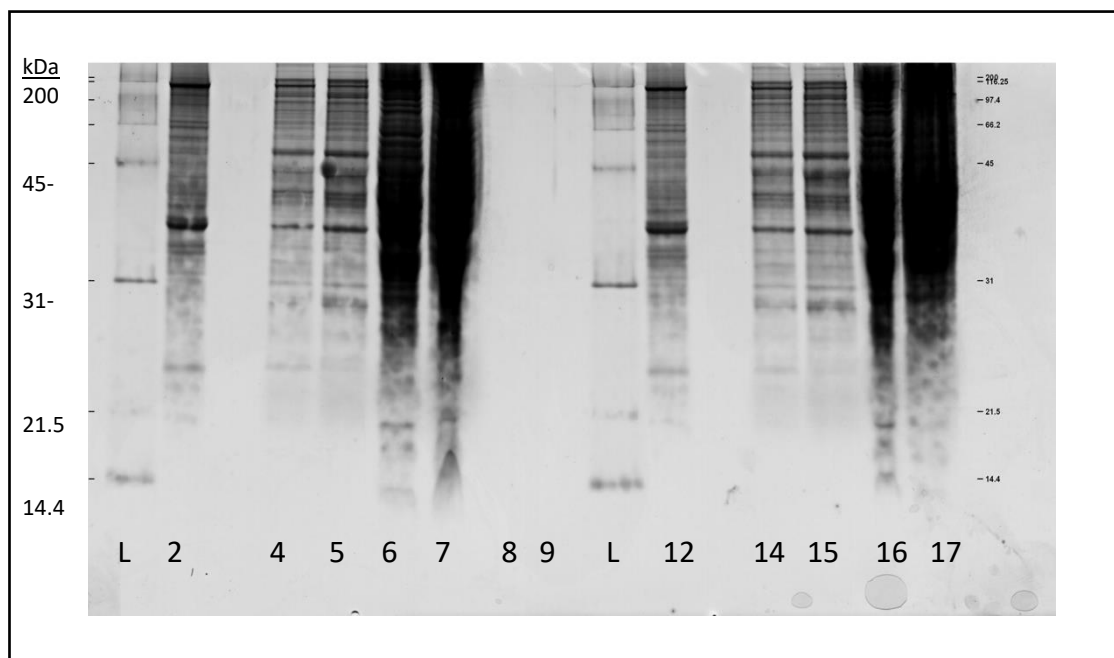
**Figure 4.42. Western blot of 12% polyacrylamide gel of gradient mouse lung protein lysates from animals 1 and 4 using three antibodies. Lane 1: PAGE ladder. Lanes 2-7: increasing concentration of mouse lung lysate from animal 2 (BALBc). GAPDH at 36 kDa; CK19 at 44 kDa; surfactant A (SP-A) at 35 kDa and CK18 at 47 kDa.**

No signal was detected from mouse middle ear (data not shown). In order to increase the protein load from mouse middle ear to improve western antigen detection, we acquired 20 pairs of mouse middle ears (16 male BALBc, 4 female C57/ B6; source Agresearch Ruakura) in an attempt to pool enough tissue sample of middle ear. Initially, 4 pairs of mouse ears were dissected by separating middle ear bullae and cochleae from the temporal bones using a dissecting microscope Nikon SMZ800. The temporal bones were perforated with a 25 gauge needle to allow penetration of phosphatase inhibitor solution (PhosSTOP, Roche, 04906837001) and RIPA lysis buffer ([cshprotocols.cshlp.org/RIPA\\_lys\\_bu](http://cshprotocols.cshlp.org/RIPA_lys_bu)). Middle ear epithelium was separated by enzyme dissection using trypsin (Gibco Life Technologies, EDTA-Trypsin 0.25% dissociation reagent).

Having acquired new antibodies to five proteins (SP-A, CK7, CK8, CK18, CK19), we began a new series of experiments to validate the new batch. The aim was to use more concentrated amounts of primary tissue from pooled middle ears so that

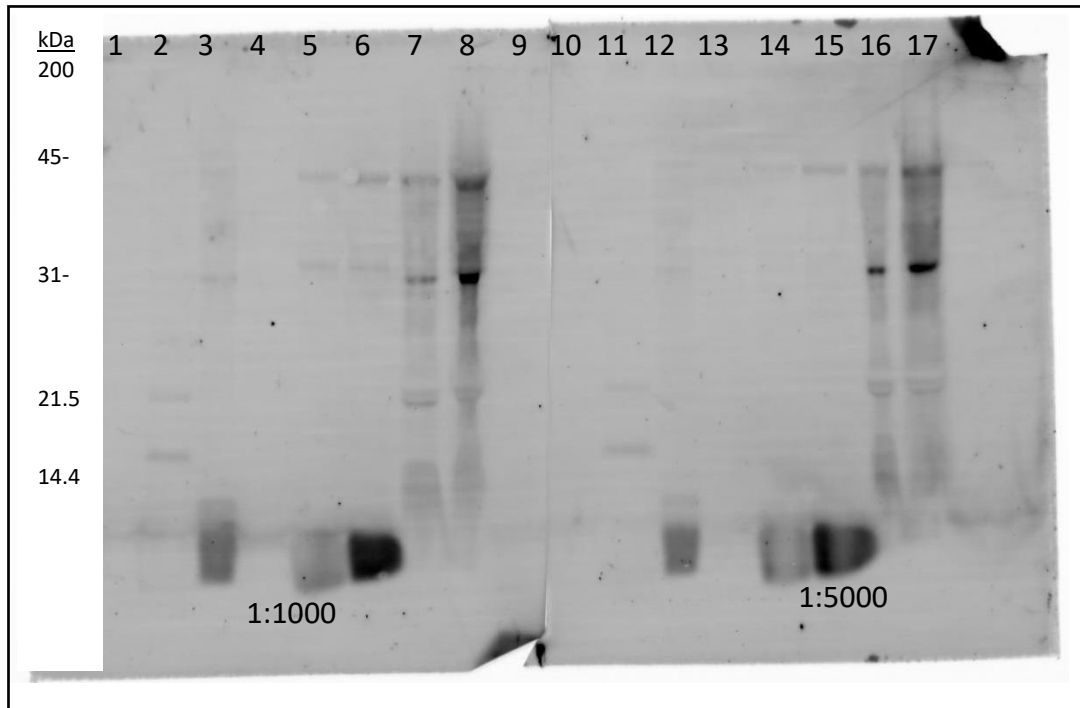
there would be enough tissue load to allow adequate comparison with lung. However, difficulties were encountered in the transfer of protein on the gel to the PVDF membrane. In a further attempt to identify why there has been lack of transfer from gel to membrane by repeating the study using equipment and resources kindly provided by MS3 Solutions Ltd. A new series of lung, middle ear and kidney protein lysates were also prepared.

Figure 4.43, shows the Coomassie stain of a electrophoresed 12% Bis-Tris Criterion™ Precast Gel where 12 samples had be transferred to a PVDF membrane including the ladder. Protein transfer was successful for mouse middle ear (25-200 kDa), lung (14-200 kDa) and kidney lysates (14-200 kDa).



**Figure 4.43. Coomassie blue stained 12% gel showing retention of mouse protein from middle ear (Lanes 2, 12), lung (Lanes 6, 7, 14, 15) and kidney (Lanes 7, 8, 16, 17). L = Ladder. This**

Next, the PVDF membrane underwent blocking in 3% salmon albumin in TBST and was then divided into two pieces to allow two different antibody concentrations. These were incubated overnight in primary SP-A antibody diluted to 1:1000 and 1:5000 respectively in 5 mL TBST with 0.1% bovine serum albumin. A secondary fluorescent antibody was applied (CY3 Goat anti-rabbit, 532nm) and the membrane developed on BioRad ChemiDoc™ MP Imaging System. The resulting image is seen in Figure 4.44 below.



**Figure 4.44. PVDF membrane showing SP-A signal in mouse kidney and corresponding faint bands in mouse middle ear and lung. SP-A 1:1000; Middle ear (Lane 2), lung (Lane 6, 7) and kidney (Lanes 7, 8). SP-A 1:5000; Middle ear (Lane 12), lung (Lanes 14, 15) and kidney (Lanes 16, 17).**

These results are in agreement with Figure 4.41 where a faint band was observed for SP-A in mouse lung when 1:500 primary antibody concentration is used. However, there is evidence of a  $\approx 29$  kDa band in mouse middle ear and  $\approx 35$  kDa band in kidney. There is also a higher band of  $\approx 45$  kDa, possibly a dimer. However, the literature refers to dimers in the 50-66 kDa (Bourbon & Chailley-Heu, 2001; Vieira, 2017). Of interest, a band is observed at 1:5000 SP-A antibody concentration in the kidney but not the lung or ear but the protein lysates have not been optimised for equal loading. The kidney sample is very concentrated and was thus diluted for subsequent studies.

#### 4.3.4 Signals for middle ear

Pooled, concentrated, middle ear tissues generated positive signal on western blotting for SP-A and CK18. The signal for the middle ear is approximately at 35 kDa. It is noted that this band is higher than the previous western (Figure 4.44) but a higher protein lysate concentration was loaded. The signal for SP-A in lung 1 shows a broad signal in the range 29-35 KDa and lung 2 shows a signal in keeping with the 29 KDa end of the range for SP-A. CK18 shows a strong signal in lung at 45 kDa and a broad signal in the middle ear also at 45 kDa.

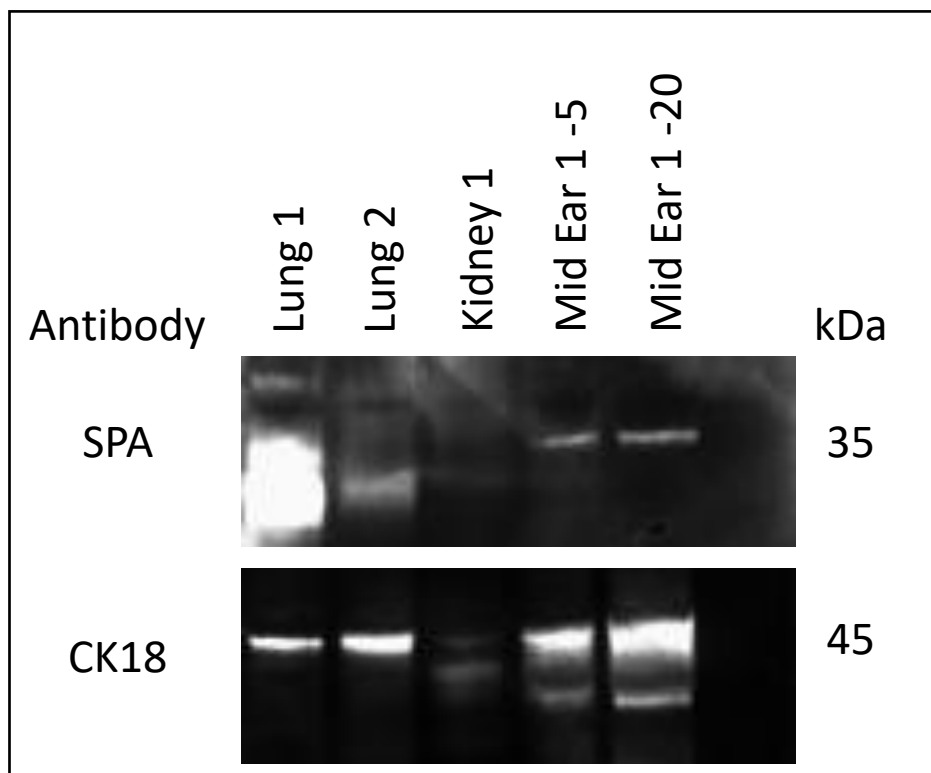


**Figure 4.45.** Western blot showing bands at approximately 35 kDa consistent with SP-A protein. Lung 1 is a fresh lung sample, Lung 2 is stored sample. Kidney is negative possibly due to deterioration in storage. Middle ear 1 is 5  $\mu$ L load and Middle ear 2 is 20  $\mu$ L. SP-A = 1:1000.

Antibody to CK 7 did generate bands in the middle ear and lung but we were unable to verify the exact level of the bands due to poor contrast with the dark background of the membrane image.

Two house-keeping antibodies – GAPDH and  $\alpha$ -tubulin - were applied to the membrane. GAPDH did not give a signal. A further stripping of the membrane was followed by application of  $\alpha$ -tubulin which also failed to give a signal.

## 5 Chapter 5

### Discussion

---

#### 5.1 Introduction

The project began with an attempt to develop an animal model of middle ear infection whose purpose was to assess the cellular debris which accumulates in the middle ear during infection. Using intraperitoneal injections of lipopolysaccharide (LPS), mice readily develop lung inflammation. We anticipated a similar natural inflammatory response in the middle ear, it being a part of the upper respiratory tract. LPS was administered to 6 mice (C57/B6) resulting in a clinically obvious response of shivering at 6 hours post-injection reflecting fever. One animal died within 4 hours of LPS injection. The temporal bones were harvested and processed for histological evaluation but failed to show any significant inflammatory response in the middle ear on H&E staining (data not shown). Because of this apparent lack of response, this model was abandoned. The direction of this investigation turned towards the location and distribution of respiratory cell types in untreated rodents using antibodies to SP-A and CKs in the middle ear.

During the course of this study, many challenges were encountered with embedding, sectioning, and high background. Therefore, the quality of sections sometimes meant that a matching control slide immediately adjacent to the test slide was not available. Efforts were undertaken to reduce high background by optimising the fixation time, blocking time, use of different blocking buffers, Sudan Black B and antigen revival time and buffer pH (data not shown). The preparation of mouse heads involved fine-tuning of the decalcification process as well as accurate orientation of the sections to allow permeation of the paraffin into air spaces of the middle ear. Both coronal and axial sections of middle ear proved to have their advantages. Coronal sectioning provided a good cross-section of the Eustachian tube as well as the epitympanum (attic), the location of early middle ear inflammation.

Examination of isolated lining of the middle ear was somewhat difficult in the mouse because the lining epithelium is too thin to be accurately dissected from bone. Identification of cells containing surfactant proved difficult initially due to poor decalcification resulting in disorganised sections. We then tried rat middle ear because the rat middle ear cavity is larger than mouse, the supporting stroma is thicker and harvesting the rat mucosa is thus easier. Initially we laid the mucosa on glass slides for wholemount labelling which gave some idea of the pattern of the arrangement of capillary vessels but was not useful for SP-A labelling because cell margins are not distinct on wholemount (data not shown). We then attempted frozen sections which succeeded in labelling of one cytokeratin (data not shown). The disadvantage of removing mucosa from the bony cavity is that it separated the epithelium of interest from its specific anatomical location within the rat middle ear. Overall, this study successfully developed a decalcification, fixation, embedding, H&E and IHC protocol for adult mouse temporal bones.

## **5.2 Extrapolating data from lung to middle ear**

This study has demonstrated that SP-A is present within the temporal bones of two strains of mice. It is present within some cells which make up the adjacent nests of bone marrow and also as free protein within the air spaces of the middle ear and Eustachian tube. What has not been established is whether any of the epithelial cells lining the middle ear cavity produces SP-A. At this stage, it has not been possible to confirm the existence of cells in the murine middle ear cavity proper which are analogous to type II alveolocytes of lung.

### **5.2.1 H&E staining**

Basic histology by H&E staining confirmed various structural and morphological aspects of rat and mouse lung before moving onto mouse middle ear. H&E staining confirmed the general observation that middle ear epithelium is generally ciliated on the floor of the middle ear and is flatter and non-ciliated on the roof of the middle ear. Although the middle ear is a bone-encased structure, an interesting feature is the presence of flatter epithelium covering its superior

surface. In general, the “ceiling” of all mammalian middle ear is considered for gas exchange which is partly reflected in its proximity to capillaries due to the thinner connective tissue stroma compared to taller cells. Flat cells are also found overlying mobile areas such as the tympanic membrane, ossicles and middle ear muscles. Tissue movement beneath any epithelium facilitates its natural apoptosis and this may be an area for future investigation as it relates to the apoptosed epithelial debris present within the normal middle ear.

### **5.2.2 H&E reveals communications from the middle ear cavity to the bone marrow**

An unexpected finding in two strains of mice (BALBc and C57/B6) was the presence of communications within the bone encasing the middle ear passing from the middle ear space to the surrounding nests of bone marrow. These communications were observed in axial rather than coronal sections. It is likely that this is present in other strains of mice. These communications could be called “micro-foramina” (plural of “foramen”). They differ from much longer lymphatic channels found in long bones called canaliculi (Clarke, 2008) and also from the large foramina within the skull base for the passage of cranial nerves e.g., foramen ovale, jugular foramen.

Such communications have not been reported in standard textbooks or papers on human temporal bone (Anson, 1984; Wang et al., 2006); nor in papers on human temporal bone marrow pathology (Li et al., 1994); nor through methods such as CT scanning of temporal bones (Ahmad, 2014). Some studies identified marrow even within the tiny ossicles of the middle ear but did not identify communications (Whyte-Orozco, 2007). Embryologically the middle ear chamber develops by pneumatisation of the mastoid. Initially the foetal middle ear space is filled with mesenchyme whose cells gradually disperse as the middle ear space pneumatises (Anson & Donaldson, 1981). The mesenchymal cells differentiate into mature connective tissue forming tenuous adhesions which suspend the middle ear ossicles. Literature referring to the bone marrow surrounding the air spaces does not refer to communications between the two (Koc et al., 2004).

There are reports of communications between the bone marrow of human temporal bones and middle ear mesenchyme which occurs in the foetal stage and continues into early infancy (Linthicum, 1994; Whyte-Orozco, 2007). However, these communications are continuations of connective tissue rather than patent passages with a definite bony margin. Both authors used CD15 antibodies to mark cells simultaneously in bone marrow and in the middle ear mesenchyme. These structures probably atrophy and perhaps give rise to the very thin, tenuous adhesions present in the attic spaces of the middle ear. Other studies examining the cochleae of small animals did not seem to encounter such structures (Hardie, 2004). Studies on developmental endochondral ossification make no mention of such communications in the temporal bone (Long, 2013; Mansour et al., 2013).

In summary, these communications deserve more investigation because they can be considered a part of the murine middle ear. In mice they can be assessed using axial sections and this approach could be applied to rat and other species including human. It would also be possible to study their development using rodent embryos. At least in mice, one can say that the middle ear includes its own supply of immune cells from its connected – not just adjacent – bone marrow.

### **5.3 Immunohistochemistry**

IHC revealed the strongest presence of SP-A protein within cells of the most remote part of the middle ear – the adjacent bone marrow spaces. The next strongest signal is seen amidst cellular debris at the entrance to the middle ear and the Eustachian tube opening. Some SP-A has been identified in relation to middle ear epithelium, more on the luminal surface of flat or cuboidal cells but occasionally seen within the apical surface of cuboidal or tall cells. These observations suggest that SP-A is produced in bone marrow and distributed to the middle ear either as a secretion or within cells which make their way from the bone marrow to the middle ear chamber.

IHC also helped to identify SP-A protein within cellular debris adjacent to the Eustachian tube at its nasopharyngeal opening. Since some SP-A signal was also noted on the surface of middle ear epithelium, it is likely that some of the debris in the nasopharynx has its origin in the middle ear and is not just from the nasopharynx. Whether this SP-A protein originates in middle ear epithelium or bone marrow remains unclear but there is material for a project to investigate the circulation of surfactant within the middle ear.

Poor signal to antigen staining may have been due to protein cross-linkage secondary to PFA fixation although fixation was restricted to 2 hours immersion. This may explain why so little signal to SP-A antigen and to some of the CKs was found.

Also, one limitation of the study was the lack of enough sequential sections to search conclusively for positive SP-A protein signal. This was partly due to technical issues with the microtome and some inconsistent sectioning.

For the purpose of providing negative controls for IHC of mouse tissues, the primary antibody was omitted as well as application of 5% goat serum to reduce background fluorescence. A better method for achieving a more conclusive negative control involves application of a pre-immune serum usually from the same species in which the secondary antibody was raised to the control slide (Ivell et al., 2014; Hewitt et al, 2014).

Exactly how SP-A protein and surfactant are dispersed throughout the middle ear remains unclear. One possibility is that SP-A-containing cells are matured in bone marrow, pass along micro-foramina, insinuate themselves into the lining epithelium of the middle ear and secrete surfactant and SP-A. The adjacent bone marrow may also provide the macrophages normally present within the middle ear. These may have a role similar to free pulmonary macrophages – collection of cell debris and recycling of surfactant including its component SP-A. Alternatively, the middle ear may receive its supply of SP-A-containing cells from mesenchymal stem cells of bone marrow via the blood stream.

IHC also gave some interesting results in regard to cytokeratin distribution in that CK18 and CK19 showed positive signal in various regions of the middle ear but did not seem to localise themselves to any particular cell type. Ideally IHC would have enabled co-localisation of SP-A protein and CK8 and CK18 within lung initially and then in middle ear pointing towards a more functional characterisation of middle ear epithelium.

A final aspect of SP-A protein labelling was the observation that SP-A is common to middle ear bone marrow, Eustachian tube openings, type II alveolocytes and Clara cells of the bronchial tree. Clara cells and type II cells have an important feature in common: both are a non-ciliated, progenitor cell for many of the other cell types adjacent to them although the Clara cell can produce also ciliated cells in the lung whereas the type II cell can only divide into a type I cell and another type II cell. Rather than search for a type II alveolocyte equivalent within the middle ear, perhaps the mouse middle ear has a Clara cell equivalent which acts as progenitor for all other cell types. In any case, SP-A within a cell in the upper or lower respiratory tract implies progenitor potential for that cell.

#### **5.4 Antibody validation**

Western blotting is essential for validation of antibodies used in IHC studies. Commercial pre-cast gels have advantages of consistency in their composition although it is difficult to ascertain whether they are made up of stacking and resolving components or are simply the resolving type alone. The concentration of the gel must be appropriate to the molecular weight of the protein. Home-made gels are cheaper but are time consuming to prepare and have less refrigeration life-span.

Western blotting enabled validation of the SP-A as well as CK18 and CK19 from lung and middle ear. Bands of expected antigen size were observed. This method only localises proteins to tissues but does not localise the SP-A to cell types or to specific locations within the temporal bone. Additional antibody cell markers at

different wavelengths are required for co-localisation studies with access to higher magnification such as the confocal microscope. In addition, mass spectrophotometry could also be used to further identify proteins in the lysate. This would involve separating proteins through gel electrophoresis and with further fractionation into component peptides to be analysed finally by spectrometry (Wang and Wilson, 2013). Future studies, could also use RNA transcriptome analysis at the cell level and as more technologies become cheaper, dual fluorescence detection of protein and RNA.

## **5.5 Future directions**

The micro-foramina found in the mouse middle ears provide a direct access from the bone marrow nests to the middle ear cavity. Free SP-A is present at the other extreme i.e., the Eustachian tube opening. A much more detailed study would be required to demonstrate any direct movement of such cells from bone marrow to middle ear. There is also some data from IHC staining to confirm SP-A signal within the cells lining at least one communicating foramen (see Figure 4.34 above).

It is worthwhile doing further histological and IHC study of the epithelium of the middle ear using rodent models to further identify and characterise micro-foramina. Rat offers relatively abundant middle ear epithelium which is easier to remove and keep intact by dissection. Mouse offers easier identification of cells in relation to their anatomical location because at least two sections of mouse head can be fitted onto one glass slide, facilitating comparison of a test section, a control section and an H&E slide for orientation.

Another aspect of SP-A protein is to examine whether surfactant and surfactant protein production may be more concentrated in the more crowded spaces of the middle ear such as the attic (epitympanum) where there are delicate mucosal folds which suspend the malleus and incus. These areas are subject to collapse in humans as they are adjacent to the “slack” pars flaccida of the tympanic membrane. SP-A and surfactant may have a role in preventing collapse

of this particular region of the middle ear. This also raises the question of whether there may be pressure-receptor cells in this region.

One other aspect for future investigation is the pattern of cellular turnover in the middle ear. In general, simple epithelium such as middle ear mucosa sheds by apoptosis. In the lateral tympanic membrane, replacement of epithelium occurs in part due to cell migration. This may also occur in the epithelium on the middle ear surface of the tympanic membrane and possibly in the middle ear itself. This can be investigated using proliferation markers such as bromodeoxyuridine and apoptosis markers such as TUNEL-labelling. This could be of relevance to the upper middle ear – the epitympanum - where inflammatory disease has its most severe effects in narrow compartments partly due to accumulation of cellular debris.

A final area for investigation is the identification and characterisation of gas-exchange cells within the middle ear. Several genetic markers for type I alveolocytes have already been found such as *Aquaporin AQP5* (Chen et al., 2004). An interesting protein target present in type I cells but not type II cells is caveolin I (Campbell et al., 1999).

In conclusion, there is much more to be learnt about the relevance of surfactant proteins to the mammalian middle ear. As part of the upper respiratory tract, the Eustachian tube leading to the middle ear is a first port of call for viral and bacterial assault on the upper airway and surfactant proteins are an important part of the innate immune system. The SP-A positive bone marrow “buds” connected to the mouse middle ear may also be present in other rodents and possibly other mammals including humans. Further work on this may lead to a better understanding of middle ear infection and methods of both treatment and prevention.

## References

---

- Ahmad, N. & Wright, A. (2014). Three dimensional temporal bone reconstruction from histological sections. *The Journal of Laryngology and Otology*, 128 (5): 416-420.
- Akiyama, J., Hoffman, A., Brown, C., Allen, L., Edmondson, J., Poulain, F., Hawgood, S. (2002). Tissue distribution of surfactant proteins A and D in the mouse. *The Journal of Histochemistry and Cytochemistry* 50:993-996.
- Albiin, N., Hellström, S., Stenfors, L.E., Cerne, A. (1986). Middle ear mucosa in rats and humans. *Ann Otol Rhinol Laryngol Suppl.* Sep-Oct; 126:2-15.
- Anson, B.J., Donaldson, J.A. (1981). *Surgical Anatomy of the Temporal Bone*. Philadelphia: Saunders.
- Ars, B., Ars-Piret, N. (1997). Morpho-functional partition of the middle ear cleft. *Acta Otorhinolaryngol Belg.* 51: 181-184.
- Barnett, C. M. E. (2007). *Association of Single Nucleotide Polymorphisms in Surfactant Protein A and D with Otitis Media* (MSc dissertation, The University of Waikato).
- Bass, J.J., Wilkinson, D.J., Rankin, D., Phillips, B.E., Szewczyk, N.J., Atherton, P.J. (2017). An overview of technical considerations for western blotting applications to physiological research. *Scandinavian Journal of Medicine and Science in Sports.* 27: 4-25.
- Bourbon, J. R. & Chailley-Heu, B. (2001). Surfactant proteins in the digestive tract, mesentery, and other organs: evolutionary significance. *Comparative Biochemistry and Physiology - Part A: Molecular & Integrative Physiology*, 129(1), 151-161.
- Brémond, G. & Coquin, A. (1972) Ultrastructure of normal and pathological middle ear mucosa. *Journal of laryngology and otology* 86 (5): 457-472.
- Broekaert, D., Cornille, A., Eto, H., Leigh, I., Ramaekers, F., Van Muijen, G., Coucke, P., De Bersaques, J., Kluyskens P., Gillis, E. (1988) A comparative immunohistochemical study of cytokeratin and vimentin expression in middle ear mucosa and cholesteatoma and in epidermis. *Virchows Archiv A Pathological Anatomy and Histopathology.* 413:39-51.
- Broekaert, D. & Boedts, D. (1993). The proliferative capacity of the keratinizing annular epithelium. *Acta Otolaryngol (Stockh).* 113:345-348.
- Broekaert D., Coucke P., Leperque S. et al (1992). Immunohistochemical analysis of the cytokeratin expression in middle ear cholesteatoma and related epithelial tissues. *Ann Otol Rhinol Laryngol.* 101:931-938.

- Buchwalow, I. B. & Böcker, W. (2010) *Immunohistochemistry: Basics and Methods*. New York: Springer Verlag.
- Campbell, L., Hollins, A.J., Al-Eid, A., Newman, G.R., von Ruhland, C., Gumbleton, M. (1999). Caveolin1 expression and caveolae biogenesis during cell transdifferentiation in lung alveolar epithelial primary cultures. *Biochem Biophys Res Commun*. 262, 744-751.
- Chen, Z., Jin, N., Nasaraju, T., Chen, J., McFarland, L.R., Scott, M., Liu, L. Identification of novel markers for alveolar type I and type II cells. (2004). *Biochem Biophys Res Commun*. 319 (3), 774-780.
- Cho, A., Suzuki, S., Hatakeyama, J., Haruyama, N., Kulkarni, A.B. (2010). A method for rapid demineralization of teeth and bones. *Open Dentistry J* 4:223–229.
- Clarke, B. (2008) Normal bone anatomy and physiology. *Clin J Am Soc Nephrol* 3: S131-S139.
- Creuwels, L.A.J.M., van Golde, L.M.G., Haagsman, H.P (1997). The pulmonary surfactant system: biochemical and clinical aspects. *Lung*. 171: 1-39.
- Crouch, E., Hartshorn, K., Ofek, I. (2000). Collectins and pulmonary innate immunity. *Immunology Reviews*. 173: 52-65.
- Dutton, J. M., Goss, K., Khubchandani, K. R., Shah, C. D., Smith, R. J., Snyder, J. M. (1999). Surfactant protein A in rabbit sinus and middle ear mucosa. *Ann Otol Rhinol Laryngol*. 108 (10): 915-924.
- Floros, J., & Hoover, R. R. (1998). Genetics of the hydrophilic surfactant proteins A and D. *Biochimica et Biophysica Acta (BBA) - Molecular Basis of Disease*. 1408(2-3), 312-322.
- Forrester-Gauntlett, B.K.E. (2013). *Developmental gene expression profile of Vmo1 in the mouse auditory system* (MScR dissertation, University of Waikato).
- GeneCards (2019). The human gene database. Retrieved on 2.10.2019 from URL <https://www.genecards.org/cgi-bin/carddisp.pl?gene=SFTPA1&keywords=surfactant,a>.
- Glasser, S.W., Burhans, M.S., Korfhagen, T. R., Na,C.L., Sly, P. D., Ross, G. F., Ikegami, M., Whitsett, J. A (2001). Altered stability of pulmonary surfactant in Sp-C-deficient mice. *Proceedings of the National Academy of Sciences*. (98):11: 6366-6371.
- Gobran L.I., Rooney, S.A. (2004). Pulmonary surfactant secretion in briefly cultured mouse type II cells. *American Journal of Physiology of Lung, Cellular Molecular Physiology*. 286: L331–L336.

- Grace, A., Kwok, P., Hawke, M. (2007). Surfactant in middle ear effusions. *Otolaryngology Head and Neck Surgery*. 96:336-340.
- Gribben B, et al. (2012). The incidence of acute otitis media in New Zealand children under five years of age in the primary care setting. *J Prim Health Care*. 4(3):205-12.
- Haczku A. (2008). Protective role of the lung collectins surfactant protein A and surfactant protein D in airway inflammation. *J Allergy Clin Immunol*. 122(5):861-79.
- Hardie N.A., MacDonald, G., Rubel, E.W. (2004). A new method for imaging and 3D reconstruction of mammalian cochlea by fluorescent confocal microscopy. *Brain Res*. 1000: 200–1.
- Hawgood, S. & Clement, J.A. (1990). Pulmonary surfactant and its apoproteins. *J Clin Invest*. Jul; 86(1): 1–6.
- Head, J.F., Mealy, T.R., McCormack, F.X., Seaton, B.A. (2003). Crystal structure of trimeric carbohydrate region and neck domains of surfactant protein A. *The Journal of Biological Chemistry*, 278(44): 43254-43260.
- Helms, M.N., Jain, L., Self, J.L., Eaton, D.C. (2008). Redox regulation of epithelial sodium channels examined in alveolar type 1 and 2 cells patch-clamped in lung slice tissue. *The Journal of Biological Chemistry* 283:22875-22883.
- Hewitt, S. M., Baskin, D. G., Frevert, C. W., Stahl, W. L., & Rosa-Molinar, E. (2014). Controls for immunohistochemistry: the Histochemical Society's standards of practice for validation of immunohistochemical assays. *The journal of histochemistry and cytochemistry: official journal of the Histochemistry Society*, 62(10), 693–697.
- Hills, B.A., Bryan-Brown, C.W. (1983). Role of surfactant in the lung and other organs. *Critical Care Medicine*, 11(12): 951-956.
- Hirano S. (1996). Migratory responses of PMN after intraperitoneal and intratracheal administration of lipopolysaccharide. *Am J Physiol Lung Cell Mol Physiol*. 270:L836-L845.
- Huang, K., Kang, X.O., Wang, X., Wu, S., Xiao, J., Li, Z., Wu, X., Zhang, W. (2015). Conversion of bone marrow mesenchymal stem cells into type II alveolar epithelial cells reduces pulmonary fibrosis by decreasing oxidative stress in rats. *Molecular Medicine Reports*, 11: 1685-1692.
- Human Protein Atlas (2019). Retrieved on 13/12/2019 from URL <https://www.proteinatlas.org/ENSG00000122852-SFTPA/tissue>.
- Irvin, C. G., & Bates, J. H. (2003). Measuring the lung function in the mouse: the challenge of size. *Respiratory research*, 4(1), 4.

- Ivell, R., Teerds, K., & Hoffman, G. E. (2014). Proper application of antibodies for immunohistochemical detection: antibody crimes and how to prevent them. *Endocrinology*, 155(3), 676–687.
- Jang, C.H., Cho, Y.B., Oh, S.E., Choi, J.U., Park, H., Choi, C.H. (2010). Effect of Nebulised Bovine Surfactant for Experimental Otitis Media with effusion. *Clinical and Experimental Otorhinolaryngology*, 3 (1): 13-17.
- Johansson, J., Curstedt, T. (1997). Molecular structures and interactions of pulmonary surfactant components Eur. J. Biochem. 244, 675-693.
- Kasper, M. & Singh, G. (1995). Epithelial lung cell marker: current tools for cell typing. *Histology and Histopathology* (10): 155-169.
- Kasper M. (1993). Heterogeneity in the immunolocalization of cytokeratin-specific monoclonal antibodies in the rat lung: evaluation of three different alveolar epithelial cell types. *Histochemistry*. 100 (1): 65-71.
- Ketko, A.K., Lin, C., Moore, B.B., LeVine, A.M. (2013) Surfactant protein A binds flagellin enhancing phagocytosis and IL-1 $\beta$ . *PLoS One* 8(12): e82680.
- Kim S. J., Jung, H. H. (2005) Expression of Clara cell secretory protein in experimental otitis media in the rat, *Acta Oto-Laryngologica*, 125:1, 43-47.
- King, R.J., Simon, D., Horowitz, P.M. (1989). Aspects of secondary and quaternary structure of surfactant A protein from canine lung. *Biochimica et Biophysica Acta (BBA) - Lipids and Lipid Metabolism*, 1001 (3): 294-301.
- Kobayashi K., Kataura, A., Ohtani, S., Saito, T., Akino, T. (1992). Presence of an 80 kilodalton protein, cross-reacted with monoclonal antibodies to pulmonary surfactant A, in the human middle ear. *Ann Otol Rhinol Laryngol* 101(6): 491-495.
- Koc, A., Karaaslan, O., Koc, T. (2004). Mastoid air cell system, *Otoscope*, 4:144-154.
- Kolble, K., Mole, S.E., Kaluz, S., Reid, K.B.M. (1993) Assignment of the human pulmonary Surfactant D protein gene (SFTP4) to 10q22-q23 close to the surfactant protein A gene cluster. *Genomics*, 17: 294-298.
- Kotton, D.N. & Fine, A. (2008). Lung stem cells. *Cell Tissue Res* 331: 145-156.
- LeVine, A.M., Whitsett, J.A., Gwozdz, J.A. (2000). Distinct effects of Surfactant protein A or D deficiency during bacterial infection of the lung. *The Journal of Immunology*, 165(7): 3934-3940.
- Li, L., Guo, X., Olszewski, E., Fan, Z., Ai, Y., Han, Y., Xu, L., Li, J., Wang, H. (2015). Expression of surfactant protein–A during LPS-induced otitis media with effusion in mice. *Otolaryngology–Head and Neck Surgery*. 153(3) 433–439.

- Li, W., Schachern, P.A., Morizono, T., Paparella, M. (1994). The temporal bone in multiple myeloma. *Laryngoscope*. 104 (6, part 1): 675-680.
- Liang, J., Michaels, L., & Wright, A. (2003). Immunohistochemical Characterization of the epidermoid formation in the middle ear. *Laryngoscope*, 113(6), 1007-1014.
- Lim, D.J. (1974). Functional morphology of the lining membrane of the middle ear and Eustachian tube: an overview. *Ann Otol Rhinol Laryngol*. Mar-Apr, 83: Suppl 11: 5-26.
- Lim, D.J., Bluestone, C.D., Casselbrandt, M. (2003). *Recent Advances in Otitis Media. Proceedings of the Eighth International Symposium*, © B.C. Decker Inc., ISBN 1-55009-279-0.
- Linthicum, F.H., Tian, Q., Slattery, W. (1997). Marrow-mesenchyme connections in the fetal and newborn tympanum. *Annals of Otology, Rhinology and Laryngology* 106 (6): 466-470.
- Long, F. & Ornitz, D.M. (2013). Development of the Endochondral Skeleton in *Perspectives in Biology*. Editors: Patrick P.L. Tam, W. James Nelson, and Janet Rossant. © Cold Spring Harbor Laboratory Press.
- Luo, W., Yi, H., Taylor J., Li J., Chi, F., Todd N.W., Lin, X., Ren, D., Chen, P. (2017). Cilia distribution and polarity in the epithelial lining of the mouse middle ear cavity. *Nature Scientific Reports*. 7, Article number: 45870
- MacArthur, C.J., Trune, D.R., Mouse models of otitis media. (2006). *Current Opinion In Otolaryngology & Head And Neck Surgery*. 14 (5): 341-6.
- Marin, L. (1991) Chapter 2, "The Type II Pneumocyte" in *Pulmonary Surfactant: Biochemical, Functional, Regulatory and Clinical Concepts*. J. Bourbon Editor, © CRC Press Inc., ISBN 0-8493-6924-X.
- Mansour, S., Magnan, J., Haidar, H., Nicolas, K., Louryan, S. (2013). In Chapter 1 The Temporal Bone in *Comprehensive and Clinical Anatomy of the Middle Ear*. © Springer publications, pp 1-5.
- McCormack, F.X. (1998). Structure, processing and properties of surfactant protein A. *Biochim Biophys Acta*. 1408(2-3):109-31.
- McElroy M.C., Kasper, M. (2004). The use of alveolar epithelial type I cell selective markers to investigate lung injury and repair. *Eur Res J*. 24: 664-673.
- McGuire, J.F. (2002). Surfactant in the middle ear and eustachian tube: a review. *Int J Pediatr Otorhinolaryngol*; 66:1-15.

- Merchant SN, Nadol JB Jr (eds): (2010). Schuknecht's Pathology of the Ear, 3<sup>rd</sup> edition. Shelton, People's Medical Publishing House, vol 942, pp 142-147.
- Mills, N., Best E.J., Murdoch, D., Souter, M., Anderson, T., Salkeld, L., Ahmad, Z., Mahadevan, M., Barber, C., Brown, C., Walker, C., Walls, T. (2015). What is behind the ear drum? The microbiology of otitis media and the nasopharyngeal flora in children in the era of pneumococcal vaccination. *Journal of Pediatrics and Child Health* 51 (3), 300-306.
- Mulay, A., Akram, K. M., Williams, D., Armes, H., Russell, C., Hood, D., Bingle, C. D. (2016). An *in vitro* model of murine middle ear epithelium. *Disease Models & Mechanisms*, 9(11), 1405–1417.
- Mulder, J.J.S., Kuijpers, W., Peters, T.A., Tonnaer, E.L.G.M., Ramaekers F.C.S. (1998). Development of the tubotympanum in the rat, *The Laryngoscope*, 108:1846-1852.
- Nayak, A., Dodagatta-Marri, E., Tsolaki, A.G., Kishore, U. (2012). An insight into the diverse roles of surfactant proteins SP-A and SP-D in innate and adaptive immunity. *Frontiers in Immunology*. (3): 131: 1-21.
- NCBI Gene online database (2019). ). Retrieved on 13.12.2019 from <https://www.ncbi.nlm.nih.gov/gene?Db=gene&Cmd=DetailsSearch&Term=407213>.
- NCBI SMARTBLAST online database (2019). Retrieved on 12.12.2019 from <https://blast.ncbi.nlm.nih.gov/smartblast>.
- NCBI (2019). National Center for Biotechnology Information. Retrieved on 2.10.2019 from <https://www.ncbi.nlm.nih.gov>.
- Nunn's Applied Respiratory Physiology (2017) Elsevier. Editor Lumb, A.B. Eighth Edition, ISBN 9780702062940.
- New Zealand District Health Board (2004). *Otitis media in children: referral guidelines for primary care management*.
- Ochs, M., Johnen, G., Müller, K-M., Wahlers, T., Hawgood, S., J. Richter, J. and Brasch, F. (2002). Intracellular and intraalveolar localization of surfactant protein A (SP-A) in the parenchymal region of the human lung. *American Journal of Respiratory Cellular and Molecular Biology*. Vol 26, pp 91-98.
- Panaanen, R., Sormunen, R., Glumoff, V., van Eijk, M., Hallman, M. (2001). Surfactant proteins A and D in Eustachian tube epithelium. *American Journal of Physiology – Lung Cellular and Molecular Physiology*, 281 (3): L660-L667.

- Passali, D., Zavattini, G. (1987). Multicenter study on the treatment of secretory otitis media with Ambroxol. Importance of a surface-tension lowering substance. *Respiration*. 51: 52-59.
- Perez-Gil, J. (2008). Structure of pulmonary surfactant membranes and films: The role of proteins and lipid-protein interactions. *Biochimica et Biophysica Acta*. 1778 (7-8): 1676-1695.
- Popov, B.V., Serikov, V.B., Petrov, N.S., Isuzova, T.I., Gupta, N., Matthay, M.A. (2007). Lung epithelial cells induce endodermal differentiation in mouse mesenchyme bone marrow stem cells by paracrine mechanisms. *Tissue Engineering*. 13 (10): 2441-2450.
- Rannels, D., & Rannels, S.R. (1989). Influence of the extracellular matrix on type 2 cell differentiation. *Chest*. (96)165-173.
- Reynolds, S. D., Giangreco, A., Power, J. H., & Stripp, B. R. (2000). Neuroepithelial bodies of pulmonary airways serve as a reservoir of progenitor cells capable of epithelial regeneration. *The American journal of pathology*, 156(1), 269–278.
- Reynolds, S.D., Malkinson, A.M. Clara cell: (2010). Progenitor for the bronchiolar epithelium. *International Journal Biochemistry Cell Biology*. 42(1): 1-4.
- Sano, H., Kuroki, Y. (2005). The lung collectins, SP-A and SP-D, modulate pulmonary innate immunity. *Molecular Immunology* 42: 279-287.
- Schraml, B. U., & Sousa, C. R. E. (2015). Defining dendritic cells. *Current Opinion in Immunology*, 32, 13–20.
- Shepherd, V. L. (2002). Pulmonary surfactant protein D: a novel link between innate and adaptive immunity. *American Journal of Physiology-Lung Cellular and Molecular Physiology*, 282(3), L516-517.
- Taylor, S., Marchisio, P., Vergison, A., Harriague, J., Hausdorff, W. P., & Haggard, M. (2012). Impact of pneumococcal conjugate vaccination on otitis media: a systematic review. *Clinical infectious diseases: an official publication of the Infectious Diseases Society of America*, 54(12), 1765–1773.
- Tesfaigzi, Y. (2006). Roles of apoptosis in airway epithelia. *American Journal of Respiratory Cell and Molecular Biology*. 34(5): 537-547.
- Thompson, A., & Tucker, A.S. (2013). Dual origin of the epithelium of the mammalian middle ear. *Science*. 339: 1453-1456.

- Thornton, R.B., Wiertsema, S.P, Kirkham, L-A.S., Rigby, P.J., Vijayasekaran, S., Coates, H.L. (2013) Neutrophil extracellular traps and bacterial biofilms in middle ear effusion of children with recurrent acute otitis media. – a potential treatment target. *PLoS ONE* 8(2): e53837.
- UCSC Genome Browser: Kent, W.J., Sugnet, C.W., Furey, T.S., Roskin, K.M., Pringle, T.H., Zahler, A.M., Haussler, D. The human genome browser at UCSC. Retrieved on 7.10.19 from <https://genome.ucsc.edu/>.
- Uhlén, M., Fagerberg, L., Hallström, B.M., Lindskog, C., Oksvold, P., Mardinoglu, A., Sivertsson, Å., Kampf, C., Sjöstedt, E., Asplund, A., Olsson, I., Edlund, K., Lundberg, E., Navani, S., Szigartyo, C.A., Odeberg, J., Djureinovic, D., Takanen, J.O., Hober, S., Alm, T., Edqvist, P.H., Berling, H., Tegel, H., Mulder, J., Rockberg, J., Nilsson, P., Schwenk, J.M., Hamsten, M., von Feilitzen, K., Forsberg, M., Persson, L., Johansson, F., Zwahlen, M., von Heijne, G., Nielsen, J., Pontén, F. (2015). Tissue-based map of the human proteome. *Science*. 347(6220):1260419.
- Van Rozendaal, B.A.W.M., van Golde, L.M.G., Haagsman, H.P. (2001). Localization and functions of SP-A and SP-D at mucosal surfaces. *Pediatric Pathology and Molecular Medicine*. 20: 319-339.
- Verdaguer, J. M., Trinidad, A., González-García, J. Á., García-Berrocal, J. R., Ramírez-Camacho, R. (2006) Spontaneous otitis media in Wistar rats: an overlooked pathology in otological research. *Lab Animal* 35:10, 40-44.
- Vieira, F., Kung, J.W., Bhatti, F. (2017). Structure, genetics and function of the pulmonary associated proteins A and D: the extra-pulmonary role of these type C lectins. *Ann Anat*. 211:184-201.
- Wang, H., Northrop, C., Burgess, B., Liberman, M. C., & Merchant, S. N. (2006). Three-dimensional virtual model of the human temporal bone: a stand-alone, downloadable teaching tool. *Otology & neurotology*, 27(4), 452–457.
- Wang, P., & Wilson, S. R. (2013). Mass spectrometry-based protein identification by integrating de novo sequencing with database searching. *BMC bioinformatics*, 14 Suppl 2(Suppl 2), S24.
- Ware, L. B. Modeling human lung disease in animals. (2008). *Am J Physiol Lung Cell Mol Physiol* 294: L149–L150.
- Whyte-Orozco, J.R., Cisneros Gimeno, A.I., Pérez Sanz, R., Yus Gotor, C., Gañet Solé, J. F., Sarrat Torres, M. A. (2007). Connections between bone marrow and mesenchyme of the middle ear. *Acta Otorrinolaringologica* (English Edition), 58(1): 4-6.

- Wong, C.J., Akiyama, J., Allen, L., and Hawgood, S. (1996). Localisation and developmental expression of surfactant proteins D and A in the respiratory tract of the mouse. *Pediatric Research* 39, 930–93.
- Xiao, H., Li, D.X., Liu, M. (2012). Knowledge translation: airway epithelial migration and respiratory diseases. *Cell.Mol.Life Sci.* 69: 4149-4162.
- Yang S., Milla C., Panoskaltsis-Mortari, A., Hawgood, S., Blazar, B.R., Haddad, I.Y. (2002). Surfactant protein A decreases lung injury and mortality after murine marrow transplantation. *Am J Respir Cell Mol Biol.*(3):297-305.
- Young, B., Woodford, P., O'Dowd, G. (2014). Wheater's Functional Histology, A Text and Colour Atlas, 6<sup>th</sup> Edition, © Elsevier, Churchill-Livingstone.

# Appendices

---

## APPENDIX 1

### Solutions and Buffers

#### 6X Agarose gel loading buffer

Ingredients	Quantity
Glycerol	3 mL
Bromophenol Blue	25 mg
Xylene Cyanol	20 µL

Make up to 500mL with sterile mQH2O

#### Antigen revival buffer – Sodium citrate buffer

Ingredients	Quantity
Tri-sodium citrate (dehydrate)	1.47g
Tween 20	250µl

Make up to 500mL with sterile mQH2O and autoclave

#### Blocking solution for Immunohistochemistry

Ingredients	Quantity
Goat serum	200µL
1X PBS	1mL

#### Blocking solution for western blot

Ingredients	Quantity
Dye reagent concentrate	1 part
mQH2O	1 part

#### Bradford reagent

Ingredients	Quantity
Dye reagent concentrate	1 part
mQH2O	1 part

Filter through Whatman #1 filter paper to remove particulates.

#### 0.5M EDTA pH 8.0

Ingredients	Quantity
EDTA	93.05 g

Make up to 500mL with sterile mQH2O and autoclave.

#### 4 X Laemmli dye

Ingredients	Quantity
10% SDS	4 mL/0.8g
Glycerol 100%	4 mL
1 M Tris pH 6.8	2.4 mL
Bromophenol blue 0.01%	200µL final conc. 0.02%
H <sub>2</sub> O	2.6 mL

Just before use, take 475µL of 2X dye and add 25µL β-mercapto-ethanol.

#### 1 X MOPS running buffer

Ingredients	Quantity
Tris base	6.06 g
MOPS	10.46 g
SDS	1 g
EDTA	0.4 g

Make up to 1 L with de-ionised water.

#### 4% Paraformaldehyde (PFA)

Ingredients	Quantity
PFA	4.0 g (use 10 g for 10%)

Make up to 100mL with sterile mQH<sub>2</sub>O and autoclave.

#### 1X PBS – phosphate buffered saline pH 7-7.4

Ingredients	Quantity
NaCl	8g
KCl	0.25g
KH <sub>2</sub> PO <sub>4</sub>	0.2g
Na <sub>2</sub> HPO <sub>4</sub>	1.15g

Make up to 1L with mQH<sub>2</sub>O.

#### 1X PBS-T – phosphate buffered saline + Tween 20, pH 7-7.4

Ingredients	Quantity
NaCl	8g
KCl	0.25g
KH <sub>2</sub> PO <sub>4</sub>	0.2g
Na <sub>2</sub> HPO <sub>4</sub>	1.15g
Tween 20	0.5 mL

Make up to 1L with mQH<sub>2</sub>O.

### Ponceau S Stain

Ingredients	Quantity
mQH <sub>2</sub> O	10mL
glacial acetic acid	0.3mL
Ponceau S	<b>0.033 g</b>

Make up to 30 mL with mQH<sub>2</sub>O.

1. After electrophoresis, immerse the blotted membrane in a sufficient amount of Ponceau S Staining Solution and stain for 5 minutes.
2. After staining, immerse the membrane in an aqueous solution containing 5% acetic acid (v/v) for 5 minutes, change the aqueous solution, and immerse the membrane for another 5 minutes.
3. Transfer the membrane into water for two washes of 5 minutes each.

### 10 X Complete Protease inhibitor Cocktail (PIC)

Ingredients	Quantity
1 X PBS	1 mL
PIC tablet	1 tablet

### RIPA Buffer

Ingredients	Quantity
1M NaCl	1.5 mL
1% Nonidet P-40	0.1 mL
0.5% Sodium deoxycholate	0.05 mL
1% SDS	0.01 mL
50 mM Tris	5 mL

Make up to 10 mL with mQH<sub>2</sub>O. Aliquot and store at -20°C.

### 1 X TBS

Ingredients	Quantity
Tris 1 M	50 mL
NaCl 5 M	30 mL

Make up to 1 L with sterile mQH<sub>2</sub>O and autoclave.

### 1 X TBS-T

Ingredients	Quantity
TSB solution	999 mL
Tween-20	1 mL

Make up to 1 L with sterile mQH<sub>2</sub>O and autoclave.

## APPENDIX 2

### Chemicals and Consumables

Product	Supplier	Catalogue number
<b>Consumables</b>		
Blades for microtome	Thermo Fisher Scientific	MX35 Ultra
Coverslips	Thermo Fisher Scientific	FSHMNJ-500-010G
Falcon tubes sterile 15 mL	Thermo Fisher Scientific	LBSCN8CT15
Falcon tubes sterile 50 mL	Thermo Fisher Scientific	LBSCN8CT50
membrane nitrocellulose	Genscript WestClear™	LO 0224A60
membrane PVDF 0.45 µm	Amersham Hybond-P	RPN2020F
Paper Filter	Thermo Fisher Scientific	LBS0001.070
Pipette bulbs	Thermo Fisher Scientific	C-P24820-60
Pipette tips 1 mL	Interlab, NZ	LC1057-965
Pipette tips 500 µL	Interlab, NZ	LC1059-965
pipettes sterile disposable	Ray Lab, NZ	RL200CS01
plate 96 well round	Thermo Fisher Scientific	NUN145397
<b>Chemicals</b>		
Ethanol ETOH	Sigma-Aldrich NZ	E 7023
Isopropanol	Sigma- Aldrich NZ	563935
Methanol MeOH	Sigma- Aldrich NZ	M1770
Neoclear (xylene analogue)	Stoddart	8052-41-3
Paraformaldehyde	Sigma- Aldrich NZ	158127
Sucrose C <sub>12</sub> H <sub>22</sub> O <sub>11</sub>	Biolab	AJA530-5KG

### Electrophoresis Equipment and Enzymes

Equipment	Supplier	Specifications
100 base pair ladder	Genscript	M 102 R 500 µL
PAGE Master Protein Standard Plus	Genscript	MM1397-500
Spectrophotometer	Thermo 56 Fisher Scientific Multiskan™ GO	
i-Bright analyser	Invitrogen	FL1000

## APPENDIX 3

### Example of Bradford Assay Results

Protein Sample	Average (mg/mL)	Standard Deviation
Lung 1	3.8841	3.0612
Lung 2	4.5126	1.3058
Lung 3	6.9743	0.8973
Lung 3A	NaN	NaN
Lung 4	8.1005	0.7257
Lung 4A	4.5650	3.3351

NaN = underdetermined as reading is above the BSA standards used.